

Aus dem Bereich Physiologie
Theoretische Medizin und Biowissenschaften
der Medizinischen Fakultät
der Universität des Saarlandes, Homburg/Saar

**Astroglial GABA_B receptor deletion attenuates epileptic
network function *in vivo***

Dissertation

zur Erlangung des Grades eines Doktors der Naturwissenschaften

**der Medizinischen Fakultät
der UNIVERSITÄT DES SAARLANDES**

2021

vorgelegt von: Laura Christel Caudal

geb. am: 06.11.1991 in Trier

Date of oral examination: 14.01.2022

Dean of the faculty: **Univ.-Prof. Dr. med. Michael D. Menger**

Examinants:

Prof. Dr. Frank Kirchhoff
University of Saarland

Dr. Etienne Audinat
University of Montpellier

Prof. Dr. med. Frank Schmitz
University of Saarland

Prof. Dr. Michael Wegner
Friedrich-Alexander-University Erlangen-Nürnberg



This project has received funding from the European Union's Horizon 2020 research and innovation programme under the Marie Skłodowska Curie grant agreement No 722053.

Eidesstattliche Erklärung

Ich erkläre hiermit an Eides statt, dass ich die vorliegende Arbeit ohne unzulässige Hilfe Dritter und ohne Benutzung anderer als der angegebenen Hilfsmittel angefertigt habe. Die aus anderen Quellen direkt oder indirekt übernommenen Daten und Konzepte sind unter Angabe der Quelle gekennzeichnet.

Bei der Auswahl und Auswertung folgenden Materials haben mir die nachstehend aufgeführten Personen in der jeweils beschriebenen Weise

unentgeltlich

entgeltlich geholfen:

- Arne Blickle hat im Rahmen seiner Masterarbeit die ektopische Rekombination der GLAST-Cre^{ERT2} Mauslinie quantifiziert (Suppl. figure 8)

Weitere Personen waren an der inhaltlich-materiellen Erstellung der vorliegenden Arbeit nicht beteiligt. Insbesondere habe ich nicht die entgeltliche Hilfe von Vermittlungs- bzw. Beratungsdiensten (Promotionsberaterinnen/Promotionsberater oder anderer Personen) in Anspruch genommen. Außer den Angegebenen hat niemand von mir unmittelbar oder mittelbar geldwerte Leistungen für Arbeiten erhalten, die im Zusammenhang mit dem Inhalt der vorgelegten Dissertation stehen.

Die Arbeit wurde bisher weder im Inland noch im Ausland in gleicher oder in ähnlicher Form in einem anderen Verfahren zur Erlangung des Doktorgrades einer anderen Prüfungsbehörde vorgelegt.

Ich versichere an Eides statt, dass ich nach bestem Wissen die Wahrheit gesagt und nichts verschwiegen habe.

Die Bedeutung der eidesstattlichen Erklärung und die strafrechtlichen Folgen einer unrichtigen oder unvollständigen eidesstattlichen Erklärung sind mir bekannt.

Ort, Datum

Unterschrift der/des Promovierenden

*“Todo ser humano puede ser, si se lo propone,
escultor de su propio cerebro”*

*“Every human being can be, if it so desires,
the sculptor of its own brain”*

Adapted from Santiago Ramon y Cajal, Reglas y consejos sobre investigación biológica (1899)

CONTENT

Eidesstattliche Erklärung	I
List of abbreviations	VII
List of figures	IX
List of supplementary figures	X
List of tables	XI
1. ABSTRACT.....	1
2. GRAPHICAL ABSTRACT	2
3. ZUSAMMENFASSUNG	3
4. INTRODUCTION	5
4.1. Astrocytes: identity and housekeeping duties	5
4.2. Multipartite synapse and gliotransmission.....	7
4.3. Astroglial Ca²⁺ signaling	10
4.4. The epilepsies.....	13
4.4.1. Temporal lobe epilepsy (TLE).....	14
4.4.2. Experimental TLE models	16
4.5. An astroglial focus on epilepsy.....	18
4.5.1. Astroglial network function in epileptogenesis	18
4.5.2. The role of astroglial Ca ²⁺ signaling and gliotransmission in epilepsy	19
4.5.3. Relevance of GABAergic signaling in epilepsy	20
4.5.4. Astroglial GABAergic signaling at the interface of excitation and inhibition	21
5. AIMS OF THE STUDY	25

6.	MATERIALS AND METHODS.....	27
6.2.	Materials	27
6.2.1.	Reagents	27
6.2.2.	Consumables and kits.....	27
6.2.3.	Devices	27
6.2.4.	LCP surface electrodes for ECoG recording.....	28
6.2.5.	Buffers and aqueous solutions	29
6.2.6.	Enzymes	31
6.2.7.	Drugs	31
6.2.8.	Antibodies	31
6.2.8.1.	Primary antibodies	31
6.2.8.2.	Secondary antibodies	32
6.2.9.	Dyes	32
6.2.10.	Primers	33
6.2.11.	Genetically modified mouse lines.....	34
6.2.11.1.	Tamoxifen-inducible DNA recombination	34
6.2.11.2.	Astrocyte-specific GABA _B receptor deletion and GCaMP3 reporter expression	35
6.2.12.	Software	35
6.2.13.	Graphical elements.....	35
6.3.	Methods	36
6.3.1.	General	36
6.3.1.1.	Genotyping	36
6.3.1.2.	Tamoxifen treatment	36
6.3.1.3.	Whole body perfusion fixation	36
6.3.2.	Immunohistochemistry.....	37
6.3.3.	Surgeries and downstream in vivo procedures	37
6.3.3.1.	Intracortical kainate injection	37
6.3.3.2.	EEG-transmitter implant and recording	38
6.3.3.3.	ECoG electrode implant for combined in vivo 2P-LSM	38
6.3.3.4.	Awake imaging	39
6.3.4.	Microscopy and ECoG recordings.....	39
6.3.4.1.	In vivo two photon laser-scanning microscopy setup.....	39
6.3.4.2.	ECoG recording synchronized with in vivo 2P-LSM.....	39
6.3.4.3.	Automated epifluorescence microscopy on fixed brain slices	39
6.3.5.	Data analysis.....	41
6.3.5.1.	Telemetric EEG data.....	41

6.3.5.2.	Analysis of Ca ²⁺ imaging and ECoG with MSparkles	41
6.3.5.3.	Immunohistochemical data.....	45
6.3.5.4.	Statistics	45
6.3.6.	Mouse administration and veterinary licenses.....	45
7.	RESULTS	47
7.2.	Adaptation of the unilateral intracortical kainate injection model of temporal lobe epilepsy.....	47
7.2.1.	Optimized injection procedure	47
7.2.2.	Generalizing seizures spread to contralateral cortical areas and evoke stereotypical astroglial Ca ²⁺ waves	49
7.2.3.	Cortical astroglial Ca ²⁺ signaling is enhanced during kainate-evoked epileptiform activity in vivo	51
7.3.	Astroglial GABA_BR loss induces anti-epileptic phenotype	54
7.4.	The role of GABA_BR-dependent astroglial Ca²⁺ signaling in generalized epileptic network function.....	58
7.4.1.	Basic Ca ²⁺ signal properties are not affected by astroglial GABA _B R deletion prior to kainate or saline injection	58
7.4.2.	Astroglial Ca ²⁺ signal properties are amplified in GABA _B R cKOs during status epilepticus and depressed in controls during the latent period	60
7.4.3.	Ca ²⁺ signal architecture is differentially modulated in control and GABA _B R cKO during the latent phase	63
7.4.4.	Stereotypical Ca ²⁺ waves during epileptiform activity are delayed in GABA _B R cKO	65
7.4.5.	Development of regular epileptiform activity is disturbed in GABA _B R cKO	69
7.5.	GABA_BR loss attenuates histopathological hallmarks of TLE.....	71
7.5.1.	Chronic hippocampal astro- and microgliosis is diminished in GABA _B R cKO mice.....	71
7.5.2.	Granule cell dispersion incidence is reduced in GABA _B R cKO	74

8.	DISCUSSION	77
8.1.	Anti-epileptic effect of astroglial GABA_BR deletion during progression of TLE.....	78
8.1.1.	GABA _B R mutant mice display reduced γ -power but unchanged global astroglial Ca ²⁺ dynamics during baseline.....	78
8.1.2.	Loss of astroglial GABA _B Rs reduces acute seizure burden and delays stereotypical astroglial Ca ²⁺ waves during status epilepticus.....	79
8.1.3.	Astroglial GABA _B R deletion confers resilience against Ca ²⁺ signal depression during the latent phase	83
8.1.4.	Chronic histopathological features of TLE are attenuated in GABA _B R deficient mice.....	84
8.1.5.	Potential roles of inflammation and microglia-astrocyte cooperation in TLE	86
8.2.	The adapted intracortical kainate model of TLE displays reduced acute seizure burden and provides genuine baseline recordings	87
8.3.	Technical aspects of employing genetically modified mice	91
8.3.1.	Emergence of anti-epileptic effect requires prolonged receptor deletion period.....	91
8.3.2.	Glutamate transporter activity and radial glia recombination in the GLAST-Cre ^{ERT2} driver line.....	92
8.3.3.	GCaMP3 is adequate to study astroglial Ca ²⁺ dynamics on a global scale	93
9.	CONCLUSION AND OUTLOOK	95
10.	APPENDIX: SUPPLEMENTARY FIGURES	97
11.	REFERENCES	107
12.	ACKNOWLEDGEMENT	123
13.	CURRICULUM VITAE AND LIST OF PUBLICATIONS	125

List of abbreviations

2P	2 Photon
AED	anti-epileptic drug
AMPA	α -amino-3-hydroxy-5-methyl-4-isoxazolpropionat
bp	base pair
BSA	bovine serum albumin
cAMP	cyclic adenosine monophosphate
cKO	conditional knock out
cl	contralateral
CNS	central nervous system
Cre	Cre-DNA recombinase
ctrl	control
ctx	cortex
Cx43	connexin 43
DAPI	4',6-Diamidin-2-phenylindol
DNA	deoxyribonucleic acid
dpE	days post electrode
dpi	days post injection
dpKA	days post kainate
ECoG	electrocorticography
EDTA	ethylenediaminetetraacetic acid
EEG	electroencephalography
ERT2	mutant human oestrogen receptor ligand-binding domain
f.c.	final concentration
fl	flanked by loxP sites
FOV	field of view
g	centrifugal force
GABA	γ -amino butyric acid
GABA _{BR1}	GABA _B receptor subunit 1
GCD	granule cell dispersion
GFP	green fluorescent protein
GPCR	G-protein-coupled receptor
HS	horse serum
HSP	heat shock protein

i.p.	intraperitoneal
IHC	immunohistochemistry
Il	ipsilateral
KA	kainate; kainic acid
kDa	kilo Dalton
KI	knock in
LoxP	locus of crossover of the bacteriophage P1
lsl	fl/stop/fl
LSM	laser scanning microscopy
mc	monoclonal
mRNA	messenger ribonucleic acid
NMDA	N-methyl-D-aspartate
OPC	oligodendrocyte precursor cell
p	p-value
pA	poly-A sequence
pc	polyclonal
px	pixel
RNA	ribonucleic acid
ROI	region of interest
RT	room temperature
s.c.	subcutaneous
Sal	saline
SE	<i>status epilepticus</i>
SNARE	soluble <i>N</i> -ethylmaleimide-sensitive factor attachment protein receptors
SRS	spontaneously recurrent seizures
TAq	<i>Thermophilus aquaticus</i>
TAM	tamoxifen
TgH	transgenic mouse generated via homologous recombination
Tris	tris(hydroxymethyl)aminoethane
UV	ultraviolet light
wpi	weeks post injection
WPRE	woodchuck hepatitis Virus posttranscriptional regulatory element
wt	wild type

The dimensions of this thesis are consistent with the International System of Units (SI).

List of figures

Figure 1	Astroglial populations in cortex and hippocampus	6
Figure 2	Astroglial Ca ²⁺ signaling and gliotransmission pathways	8
Figure 3	Hippocampal sclerosis with granule cell dispersion in the unilateral intracortical kainate model of TLE	15
Figure 4	GABA _A receptive astrocytes at the interface of excitation and inhibition	22
Figure 5	Experimental design	40
Figure 6	Analysis of epileptiform and synchronous Ca ²⁺ events	44
Figure 7	Fluorescence intensity measurement and granule cell dispersion (GCD) assessment	45
Figure 8	Unilateral intracortical saline injection induces an acute lesion but neither electrographic seizures nor histopathological hallmarks of TLE	48
Figure 9	Synchronized ECoG recording and <i>in vivo</i> 2P Ca ²⁺ imaging revealed the generation of stereotypical astroglial Ca ²⁺ waves in the cortex during seizures	50
Figure 10	Kainate but not saline injection acutely enhanced general Ca ²⁺ signal characteristics	53
Figure 11	Astroglial GABA _B R loss reduces seizure burden and γ band power	57
Figure 12	General Ca ²⁺ signal properties do not differ between control and GABA _B R cKO during baseline	59
Figure 13	Ca ²⁺ signal dimensions are acutely enhanced in GABA _B R cKOs and reduced in controls during the latent phase	60
Figure 14	Ca ²⁺ signal architecture is altered during epileptogenesis	64
Figure 15	Stereotypical Ca ²⁺ waves associated with epileptiform activity in the cortex are delayed in GABA _B R cKOs	66
Figure 16	GABA _B R cKOs develop atypical epileptiform activity	70
Figure 17	Chronic activation of hippocampal astrocytes and microglia is attenuated in GABA _B R cKO	72
Figure 18	Astroglial GABA _B R cKO reduces occurrence but not severity of granule cell dispersion	74
Figure 19	Putative mechanisms contributing to anti-epileptic effects of astroglial GABA _B R deletion	81

List of supplementary figures

Suppl. figure 1	Controls and GABA _B R cKOs display similar Ca ²⁺ dynamics in baseline conditions.....	97
Suppl. figure 2	Basic Ca ²⁺ signal properties during SE do not differ between controls and GABA _B R cKOs, irrespective of tamoxifen protocol.....	98
Suppl. figure 3	Chronic ipsilateral activation of cortical astrocytes is reduced in GABA _B R cKO.....	100
Suppl. figure 4	Overview of individual Ca ²⁺ signals during baseline and kainate-induced SE four weeks post tamoxifen.....	101
Suppl. figure 5	Overview of individual Ca ²⁺ signals at various time points post saline injection in the prolonged receptor deletion protocol.....	102
Suppl. figure 6	Overview of individual Ca ²⁺ signals at various time points post kainate injection in the prolonged receptor deletion protocol.....	103
Suppl. figure 7	LCP cortical surface electrodes are long-term biocompatible <i>in vivo</i>	104
Suppl. figure 8	Unspecific recombination of mature neurons in the GLAST-Cre ^{ERT2} line is negligible in cortex and hippocampus four weeks post kainate.....	105

List of tables

Table 1	Most commonly used <i>in vivo</i> models of temporal lobe epilepsy.....	17
Table 2	List of devices	27
Table 3	Primary antibodies for immunohistochemistry	31
Table 4	Secondary antibodies for immunohistochemistry	32
Table 5	Dyes	32
Table 6	Genotyping primers	33
Table 7	Single transgenic mouse lines.....	34
Table 8	AxioScan.Z1 filter sets	40
Table 9	Seizure detection parameters in Neuroscore	41
Table 10	Ca ²⁺ signal analysis parameters in MSparkles	42
Table 11	ECoG analysis parameters in MSparkles.....	43

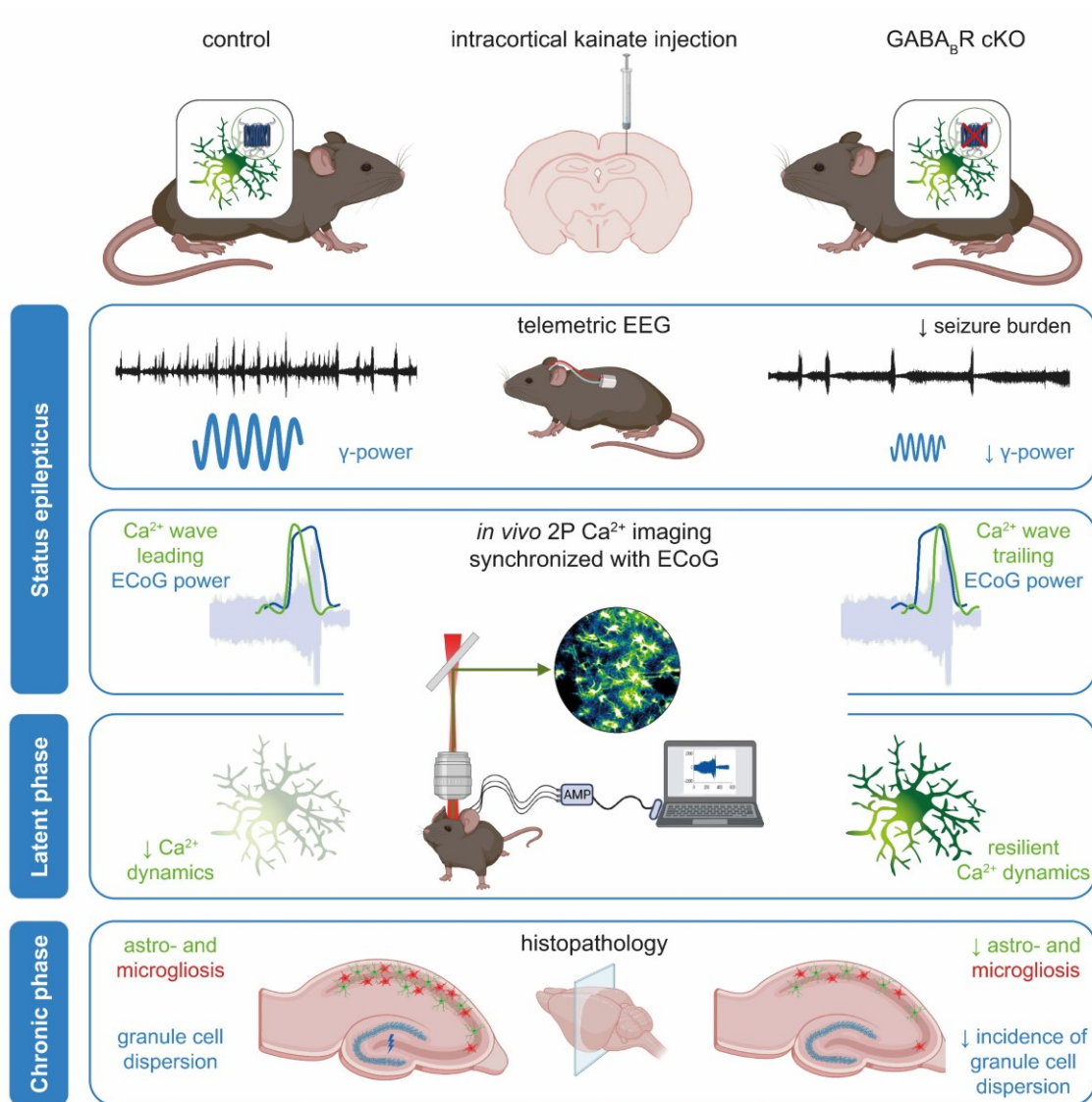
1. ABSTRACT

Temporal lobe epilepsy is a neurological condition characterized by erratically recurrent seizures. To date, anti-epileptic drug treatment is unsatisfactory, since more than one-third of patients remain drug resistant and require neurosurgical intervention. Thus, progress in the field demands investigation of basic underlying mechanisms to identify new therapeutic targets. Epilepsy is linked to the disruption of the excitation-inhibition balance in the brain. Therefore, astrocytes arise as key elements in this neurological disorder, due to their essential functions at the interface of excitation and inhibition. More specifically, astroglial γ -aminobutyric acid receptor type B (GABA_B receptor)-signaling, involving intracellular calcium rises and subsequent gliotransmitter release, crucially modulates network excitability. Hence, we investigated the contribution of the astroglial GABA_B receptor to pathological network function in an adapted mouse model of temporal lobe epilepsy. To this end, we performed EEG telemetry, *in vivo* two-photon calcium-imaging and histopathological analysis in transgenic mice with astrocyte-specific GABA_B receptor deletion and expression of the calcium sensor GCaMP3.

Astroglial GABA_B receptor loss had an overall anti-epileptic effect. During *status epilepticus* (acute phase), GABA_B receptor-deficient mice experienced 70 % less seizures than controls and displayed a significant reduction in γ -band power, even before seizure induction. Concomitantly, astrocytes displayed large stereotypical Ca²⁺ waves during generalized epileptiform activity in the cortex. In GABA_B receptor mutant mice, the calcium waves were delayed compared to controls. In addition, GABA_B receptor deficient animals developed atypical epileptiform activity, lacking correlations between basic epileptiform event and calcium wave characteristics. These data suggest a promoting role for astroglial calcium signals during epileptiform events, restricted by GABA_B receptor deletion. During the latent phase, astroglial calcium dynamics of mutant mice were resilient against the global depression observed in controls. Finally, in the early chronic phase (four weeks post kainate), GABA_B receptor loss attenuated histopathological hallmarks. Specifically, GABA_B receptor mutant mice displayed diminished astro- and microgliosis as well as reduced incidence of granule cell dispersion, without impacting its severity.

In conclusion, astroglial GABA_B receptor-dependent signaling endorses the development and maintenance of epileptic network function *in vivo* and thereby constitutes an attractive target for future research in the epilepsy field.

2. GRAPHICAL ABSTRACT



3. ZUSAMMENFASSUNG

Temporallappenepilepsie ist eine neurologische Erkrankung, welche durch unberechenbare, wiederkehrende Anfälle gekennzeichnet ist. Gegenwärtig ist die Behandlung mit Antiepileptika unbefriedigend, da mehr als ein Drittel der Patienten medikamentenresistent ist und einen neurochirurgischen Eingriff benötigt. Die Erforschung der grundlegenden Mechanismen ist daher elementar, um neue therapeutische Ziele zu identifizieren. Epilepsie basiert auf der Störung des Erregungs-Inhibitions-Gleichgewichts im Gehirn. In diesem Zusammenhang spielen Astrozyten aufgrund ihrer essentiellen Funktionen an der Schnittstelle von Erregung und Hemmung eine Schlüsselrolle bei dieser neurologischen Störung. Genauer wird die Erregbarkeit des neuronalen Netzwerks durch astrogliale γ -Aminobuttersäure-Rezeptor Typ B (GABA_B-Rezeptor) - Signalübertragung, über einen intrazellulären Calcium-Anstieg und die anschließende Freisetzung von Gliotransmittern, moduliert. In dieser Arbeit untersuchten wir den Beitrag des astroglialen GABA_B-Rezeptors zur pathologischen Netzwerkfunktion in einem adaptierten Mausmodell der Temporallappenepilepsie. Dazu wurden EEG-Telemetrie, *in vivo* Zwei-Photonen-Mikroskopie der Calcium-Signale und histopathologische Analysen in transgenen Mäusen mit Astrozyten-spezifischer GABA_B-Rezeptor Deletion und Expression des Calcium-Sensors GCaMP3 durchgeführt.

Ein astroglialer GABA_B-Rezeptor Verlust hatte einen globalen anti-epileptischen Effekt. Während des *Status epilepticus* (akute Phase) erlebten GABA_B-Rezeptor-defiziente Mäuse 70 % weniger Anfälle als ihre Kontrollen und zeigten eine Reduktion der γ -Band-Leistung, sogar vor der Anfallsinduktion durch Kainat. Gleichzeitig zeigten Astrozyten große stereotype Calcium-Wellen während generalisierter epileptiformer Aktivität im Cortex. In GABA_B-Rezeptor-defizienten Mäusen waren die Calcium-Wellen verzögert. Darüber hinaus entwickelten GABA_B-Rezeptor-defiziente Tiere atypische epileptiforme Aktivität, wobei Korrelationen zwischen epileptiformen Ereignissen und Calcium-Wellen Charakteristika entfielen. Diese Daten legen eine fördernde Rolle für astrogliale Calcium-Signale während epileptiformer Ereignisse nahe, welche durch die GABA_B-Rezeptor Deletion gemindert wurde. In der latenten Phase hat sich die astrogliale Calcium-Dynamik von GABA_B-Rezeptor-defizienten Mäusen als widerstandsfähig gegen die globale Depression erwiesen, welche in Kontrollen beobachtet wurde.

Schließlich führte der GABA_B- Rezeptor Verlust in der frühen chronischen Phase (vier Wochen nach Kainat) zu signifikant abgeschwächten histopathologischen Merkmalen. GABA_B-Rezeptor-defiziente Mäuse zeigten eine verringerte Astro- und Mikrogliose sowie eine verringerte Inzidenz der Körnerzelldispersion, ohne sich auf deren Schweregrad auszuwirken.

Zusammenfassend unterstützt die astrogliale GABA_B-Rezeptor abhängige Signalübertragung die Entwicklung und Aufrechterhaltung der epileptischen Netzwerkfunktion *in vivo* und stellt somit ein attraktives Ziel für die zukünftige Forschung im Bereich der Epilepsie dar.

4. INTRODUCTION

Astrocytes (Michael von Lenhossék, 1895) are classified as glial cells, a major cell type in the central nervous system (CNS), besides neurons. Glial cells further comprise microglia, acting as CNS resident immune cells (Río-Hortega, 1932; Kettenmann et al., 2013), myelinating oligodendrocytes (Río-Hortega, 1928), as well as NG2-glia (Dimou and Gallo, 2015) and ependymal cells (Del Bigio, 2010). In vertebrates, roughly half of the brain is constituted by glial cells, while around 20-40 % of total mammalian brain cells are astrocytes (Pelvig et al., 2008; Azevedo et al., 2009; Jahn et al., 2018). Although these numbers are subjected to inter-regional and inter-species variations (Herculano-Houzel, 2014), it is worth mentioning that all CNS areas are populated by astroglia (Sofroniew and Vinters, 2010). Given this wide distribution of astrocytes, it is readily conceivable that they form a highly **heterogenous** population - in morphology as well as in function (Matyash and Kettenmann, 2010; Zhang and Barres, 2010; Khakh and Sofroniew, 2015; Xin and Bonci, 2018; Pestana et al., 2020).

4.1. Astrocytes: identity and housekeeping duties

The long-established basic **morphological distinction** between protoplasmic and fibrous astrocytes (Andriezen, 1893) is still valid nowadays (Sofroniew and Vinters, 2010; Verkhratsky and Nedergaard, 2018). Protoplasmic astrocytes mainly reside in gray matter and are characterized by up to ten primary processes, diverging into sophisticated spongiform arborizations that do not essentially overlap with neighbouring astrocytes. This generic description can however be challenged even within the same anatomical structure, such as the hippocampal CA1 area, where protoplasmic astrocytes can also appear rather elongated (Bushong et al., 2002; Halassa et al., 2007b; Seifert and Steinhäuser, 2018) (Figure 1). Fibrous astrocytes, aligned with axon bundles in white matter, do not exhibit domain organization and have longer but less terminal processes, compared to protoplasmic astrocytes (Köhler et al., 2019). This non-exhaustive classification can be complemented by **specialized cells** of the astroglial family: cerebellar Bergmann glia, retinal Müller cells, ventricular tanycytes and radial glia, the latter being particularly important due to their neurogenic potential (Doetsch, 2003; Malatesta et al., 2003; Anthony et al., 2004; Denise et al., 2004). Thereby, the family of astroglia can be sub-classified according to anatomo-morphological criteria, cellular markers and genetic profiling (Verkhratsky and Nedergaard, 2018).

Widely accepted, not necessarily overlapping, **astroglial markers** (Figure 1) include the glial fibrillary acidic protein (GFAP) (Bignami et al., 1972; Nolte et al., 2001), the glutamate transporter EAAT-1 (GLAST) (Shibata et al., 1997; Jungblut et al., 2012), the Ca²⁺-binding protein S100B (Ogata and Kosaka, 2002), the milk fat globule epidermal growth factor 8 (MFGE8) (Zeisel et al., 2015), connexin 43 (Dermietzel et al., 1991), glutamine synthetase (GS) (Derouiche and Frotscher, 1991), aldehyde dehydrogenase 1 (ALDH1L1) (Yang et al., 2011) and the water channel aquaporin-4 (Nielsen et al., 1997) (for review see (Verkhratsky and Nedergaard, 2018).

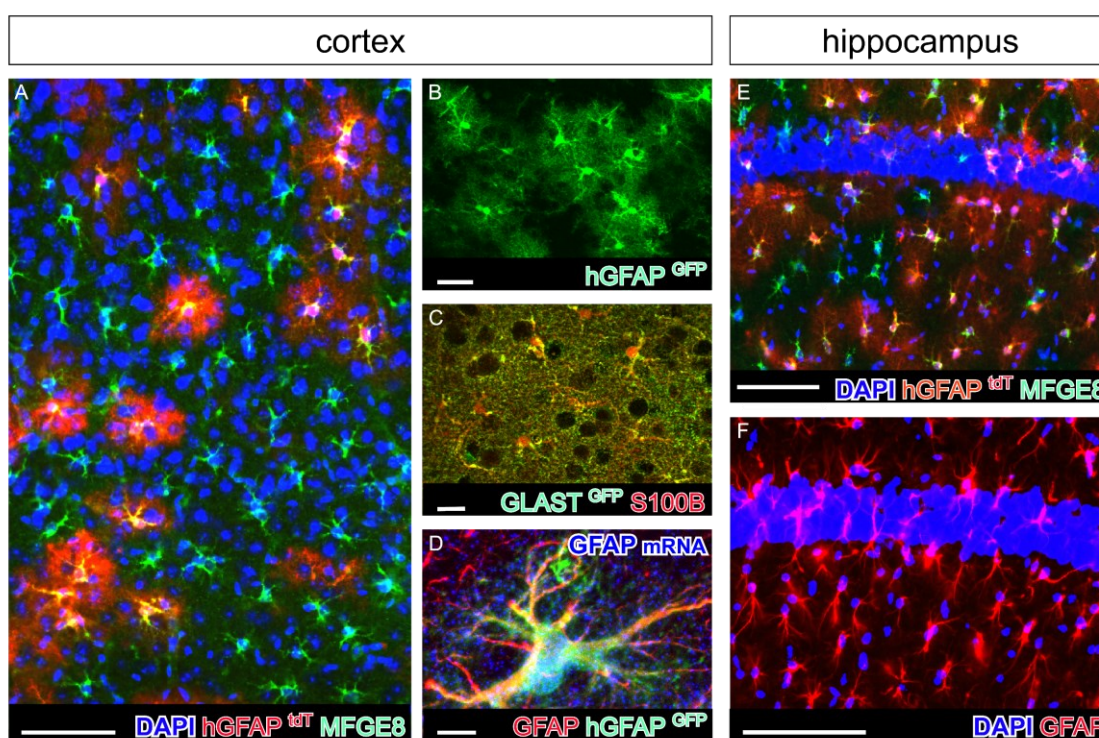


Figure 1 Astroglial populations in cortex and hippocampus

A Cortical astrocytes labelled via td tomato (tdT) reporter expression in GFAP-CreERT2 x R26-tdTomato mice co-stained with milk fat globule-EGF factor 8 (MFGE-8). MFGE-8⁺/tdT⁺ positive astrocytes are often found near blood vessels. Scale bar = 50 μ m. **B** Transgenic expression of eGFP under the human GFAP promoter labels cortical protoplasmic astrocytes with spongiform appearance. Scale bar = 50 μ m. **C** Expression of S100B is largely overlapping with GLAST expression, revealing the meshwork of fine processes (gliapil). GFP staining against GCaMP3 labels GLAST⁺ astrocytes in GLAST-CreERT2 x R26-GCaMP3 mice. Scale bar = 20 μ m. **D** Activated astrocytes (hGFAP-GFP) become hypertrophic and upregulate GFAP. In addition, GFAP mRNA is visualized by fluorescence *in situ* hybridization. Scale bar = 10 μ m. **E** Hippocampal astrocytes express high GFAP (GFAP-CreERT2 x R26-tdTomato) levels in physiological conditions, co-labelled by MFGE-8. CA1 region, scale bar = 100 μ m. **F** In contrast to transgenic expression of a fluorescent protein under the human GFAP promoter (E), GFAP immunostaining reveals fusiform protoplasmic astrocytes in the hippocampal CA1 region. Scale bar = 100 μ m.

Along the same lines, great effort is dedicated to revealing **molecular signatures** of neural cell types throughout the CNS, applying transcriptomic approaches (Cahoy et al., 2008; Zhang et al., 2014; Tasic et al., 2018).

Pioneer gliologists of the 19th and early 20th century, such as S. Ramón y Cajal, C. Golgi, R. Virchow, M. von Lenhossék and C. L. Schleich identified glial cells as brain glue (attributed to R. Virchow, “γλία” (glia), glue; Oxford English Dictionary) and postulated homeostatic support functions. Indeed, presently, a plethora of essential **homeostatic functions** in the CNS are known to be assumed by astroglia (for review see (Allen and Barres, 2009; Mederos et al., 2018; Verkhratsky and Nedergaard, 2018). These functions comprise metabolic support (Rouach et al., 2008; Bélanger et al., 2011; Oheim et al., 2017; Marina et al., 2018), regulation of blood-brain barrier as well as blood flow (Attwell et al., 2010; MacVicar and Newman, 2015), K⁺ buffering (Seifert et al., 2009; Beckner, 2020), regulation of extracellular volume (Simard and Nedergaard, 2004; Nagelhus and Ottersen, 2013), neurotransmitter homeostasis (Walls et al., 2015; Boddum et al., 2016; Murphy-Royal et al., 2017; Mahmoud et al., 2019), as well as synaptogenesis and synaptic remodelling (Allen and Eroglu, 2017). Fulfilment of these functions is crucially determined by the astrocytes’ **interlacement with synapses** (Figure 2) (Ventura and Harris, 1999; Perea et al., 2009; Heller and Rusakov, 2017) and **vasculature** (Abbott et al., 2006), combined with the expression of a vast assortment of transmitter receptors, channels, transporters, and the ability to form interconnected networks through **gap junction coupling** (Figure 2 A) (Giaume et al., 2010).

4.2. Multipartite synapse and gliotransmission

The tight association and functional interaction of perisynaptic astroglial processes (PAPs), pre-synaptic terminals, post-synaptic neurons, extracellular matrix (ECM) components and microglial processes is commonly termed **multi-partite synapse** (Araque et al., 1999; Halassa et al., 2007a; Dityatev and Rusakov, 2011; Arizono et al., 2020) or astroglial cradle (Verkhratsky and Nedergaard, 2014) (Figure 2 A, B).

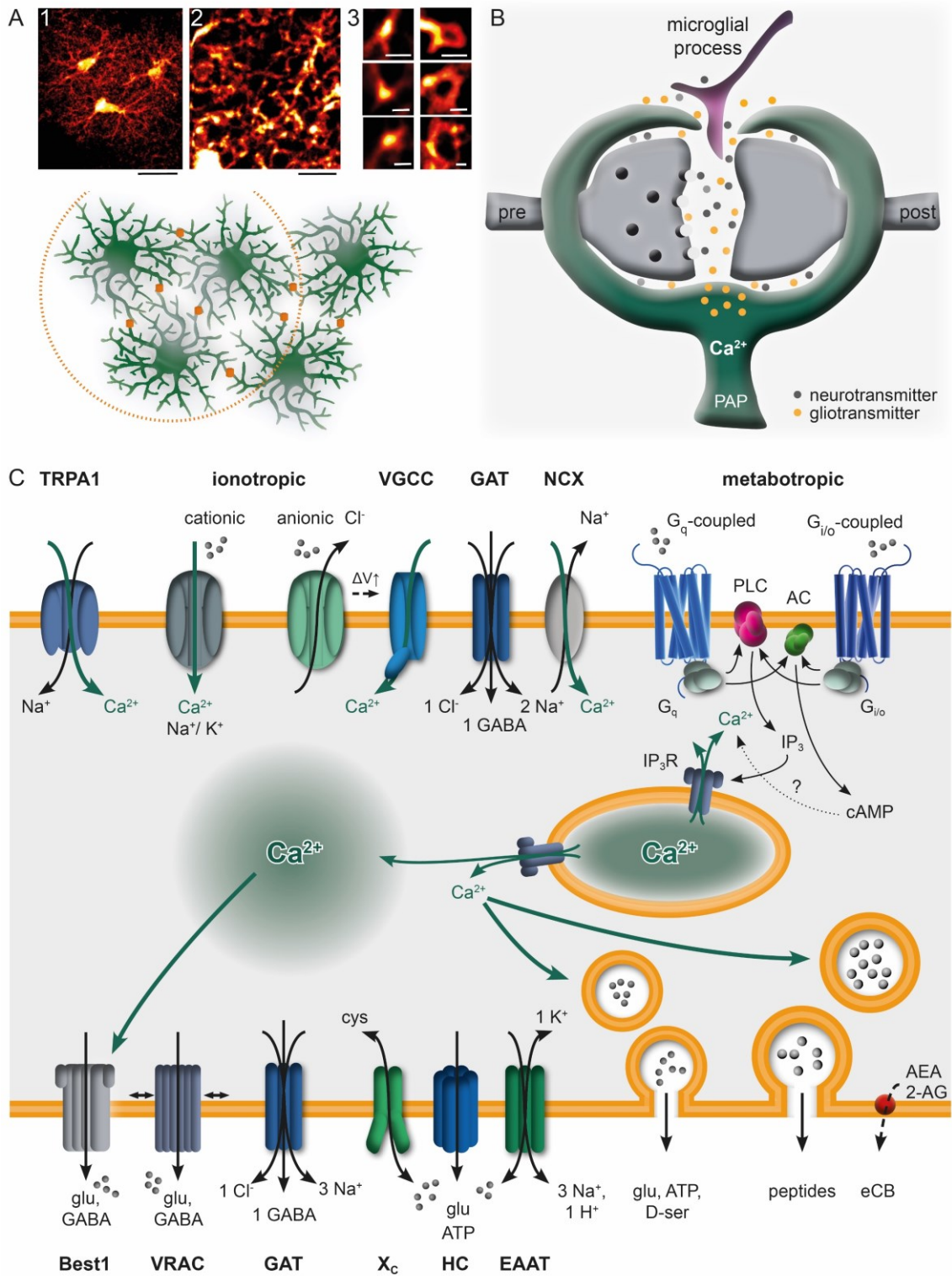
Cortical astrocytes contact 4-8 neuronal somata and up to 600 dendrites (Halassa et al., 2007b) and hippocampal astroglia are associated to ~140.000 synapses, contacting several hundred dendrites (Bushong et al., 2002). Despite these multiple contact sites, their basically non-overlapping distribution alludes to functional characteristics described as “astromeres” (Freeman and Rowitch, 2013) or “synaptic islands” (Halassa et al., 2007b). The essence of these terms implies that astrocytes are organized in regionally distinct, specialized domains, including a distinct subset of neuronal communication partners. On a higher level, those functional domains are interconnected via gap junctions, forming the astroglial syncytium (Figure 2 A).

Embedded in this context, astrocytes arise as **decisive elements in CNS function**, beyond their homeostatic roles. Their sophisticated equipment with **transmitter receptors and secretion mechanisms** (Figure 2 C) (Parpura et al., 1994; Bezzi et al., 2004; Perea and Araque, 2007; Verkhratsky et al., 2016) enables astrocytes to sense and actively participate in synaptic transmission.

Figure 2 Astroglial Ca²⁺ signaling and gliotransmission pathways

A Individual astrocytes occupy essentially non-overlapping areas and form a syncytium via gap junction coupling (orange icons, scheme). **A 1-3** Exemplary astroglial perisynaptic structures in the dentate gyrus, scale bar 1 = 20 μm (2P-LSM), 2 = 5 μm (2P-LSM), 3 = 500 nm (2P-STED). Modified from Arizono et al., 2020, reproduction permitted under the Creative Commons attribution 4.0 international license. **B** Multipartite synapse including perisynaptic astroglial processes (PAPs) and microglial processes as building block of neuron-glia interaction. **C** Astrocytes are equipped with a plethora of transporters, voltage-gated ion channels as well as ionotropic and metabotropic transmitter receptors mediating intracellular Ca²⁺ rises either originating from the extracellular space or released from internal stores. Ionotropic receptors include cationic NMDAR, AMPAR, P2XR_{1/5}, P2XR₇ and nAChR, mediating Ca²⁺, Na⁺ and K⁺ influx, as well as anionic GABA_AR and GlyR inducing Cl⁻ efflux. Metabotropic receptors are mainly coupled to G_{i/o} (mGluR_{2/3}, GABA_BR, adenosine receptors, β-adrenergic, 5-HT₇) and G_q-proteins (adenosine receptors, P2YR, mAChR, α-adrenergic, serotonergic, dopaminergic, histaminergic receptors). Intracellular Ca²⁺ rises induce vesicular release of various gliotransmitters and neuroactive molecules. However, main gliotransmitters can also be released through partially Ca²⁺ sensitive transporters and channels. Modified from Caudal et al., 2020.

2-AG, 2-arachidonoylglycerol; 5-HT, serotonergic receptor family; AC, adenylate cyclase; ADP/ATP, adenosine di/tri-phosphate; AEA, anandamide; AMPAR, α-amino-3-hydroxy-5-methyl-4-isoxazolepropionic acid receptor; Best1, bestrophin-1 channel; cAMP, cyclic AMP; cys, cysteine; D-ser, D-serine; EAAT, excitatory amino acid transporter; eCB, endocannabinoids; GABA, γ-aminobutyric acid; GAT, GABA transporter; glu, glutamate; GlyR, glycine receptor; HC, hemichannel; IP₃, inositol triphosphate; IP₃R, inositol triphosphate receptor; mAChR, muscarinic acetylcholine receptor; mGluR, metabotropic glutamate receptor family; nAChR, nicotinic acetylcholine receptor; NCX, Na⁺-Ca²⁺ exchanger; NMDAR, N-methyl-D-aspartate receptor; P2XR, ionotropic purinoceptors; P2YR, metabotropic purinoceptors; PLC, phospholipase C; TRPA1, transient receptor potential A1; VGCC,



This capacity is majorly based on the expression of **iono- and metabotropic receptors** to glutamate (Seifert and Steinhäuser, 1995; Lalo et al., 2006; Saab et al., 2012; Kirchhoff, 2017), GABA (MacVicar et al., 1989; Mariotti et al., 2016; Perea et al., 2016), ADP/ATP (Domercq et al., 2006; Verkhatsky et al., 2009; Orr et al., 2015), serotonin, (nor-) adrenaline (Paukert et al., 2014; Pankratov and Lalo, 2015), acetylcholine, dopamine, endocannabinoids (Navarrete and Araque, 2010; Scheller and Kirchhoff, 2016) and various neuromodulators. Stimulation of receptor subsets triggers intracellular signaling pathways leading to Ca^{2+} rises and subsequent gliotransmitter release, such as glutamate (Parpura et al., 1994; Kang et al., 1998; Angulo et al., 2004), ATP (Pascual et al., 2005; Serrano et al., 2006; Lalo et al., 2014; Covelo and Araque, 2018) and D-Serine (Henneberger et al., 2010).

Through this process, referred to as gliotransmission, **astrocytes exert complex effects on the neuronal network** (Perea and Araque, 2007; Di Castro et al., 2011; De Pittà et al., 2016). Of note, gliotransmitter release can also occur in non-vesicular (SNARE-independent) modes (Figure 2 C). Two essential gliotransmitters, glutamate and GABA, can be released through bestrophin-1 anion channels (Park et al., 2009; Lee et al., 2010), reverse operation of membrane transporters (Rossi et al., 2000; Cavelier and Attwell, 2005; Héja et al., 2009) and volume-regulated anion channels (VRAC) (Kimelberg et al., 1990; Le Meur et al., 2012). Glutamate release has also been shown to occur via TREK-1 two-pore domain potassium channels (Woo et al., 2012). Moreover, ATP and glutamate are released through connexin hemichannels or pannexons (Ye et al., 2003; Abudara et al., 2018).

4.3. Astroglial Ca^{2+} signaling

An essential part of the astrocytes' integrative function revolves around **intracellular Ca^{2+} dynamics**, being a main **activity indicator and mediator of gliotransmission** in astrocytes (Cornell-Bell et al., 1990; Hirase et al., 2004; Zorec et al., 2012; Guerra-Gomes et al., 2017). Ca^{2+} is a widely used secondary messenger in cell biology and its functional versatility ranges from vital heart contractions to apoptosis (Carafoli, 2002). To serve as informative signal however, Ca^{2+} dynamics require rigorous regulation. Resting cytoplasmic concentration is kept as low as 100-150 nM (presence of Ca^{2+} buffering proteins such as S100B), creating **electrochemical concentration gradients** with the extracellular space (~2mM Ca^{2+}) and intracellular organelles, such as the endoplasmic reticulum (ER) (0.6-0.8 mM) (Shigetomi et al., 2016).

Therefore, cytoplasmic Ca^{2+} elevations may originate from the extracellular space through ligand-gated channels (e.g. P2XR, NMDAR), voltage-gated Ca^{2+} channels and TRP channels (Shigetomi et al., 2011), in addition to other sources such as GABA or glutamate transporter activity (Figure 2 C). The GABA transporter GAT-3 for instance is involved in mediating Ca^{2+} signaling, eventually regulating neurotransmission via ATP/ADP release (Boddum et al., 2016; Matos et al., 2018). Moreover, Ca^{2+} can originate from **internal stores** such as the ER after GPCR-mediated signaling (Cornell-Bell et al., 1990; Porter and McCarthy, 1996; Zur Nieden and Deitmer, 2006) (amplified through Ca^{2+} -induced Ca^{2+} release (Golovina and Blaustein, 2000)) or mitochondria (Agarwal et al., 2017) (Figure 2 C). Finally, Ca^{2+} **extrusion** from the cytoplasm occurs towards the extracellular space via Na^{+} - Ca^{2+} exchangers (NCX) and plasma membrane Ca^{2+} ATPase (PMCA), and into organelles through sarco-endoplasmic reticulum Ca^{2+} ATPases (SERCA) or mitochondrial uniporter (MCU) (Shigetomi et al., 2016; Verkhratsky and Nedergaard, 2018) (Figure 2 C).

Astroglial Ca^{2+} signals are generally **classified** by the **compartment** in which they arise (soma vs gliapil), the **spreading area** of the signal (ultralocal microdomains vs multicellular events) and **dynamic characteristics** (propagating waves vs globally synchronized signals) (Fiacco and McCarthy, 2006; Araque et al., 2014; Khakh and Sofroniew, 2015; Semyanov, 2019). The **most confined** type of astroglial Ca^{2+} signals arises from highly localized microdomains ($0.07 - 0.7 \mu\text{m}^2$) in the fine, terminal astrocyte processes (Figure 2 A) (Shigetomi et al., 2010; Bindocci et al., 2017; Arizono et al., 2020). These signals partially depend on the GPCR/ IP_3 intracellular Ca^{2+} store release but also on ligand-gated ion channels and TRP channels (Malarkey et al., 2008; Shigetomi et al., 2011).

Importantly, a subset of these spatially confined signals is independent of neuronal activity and therefore intrinsic to astrocytes (Parri et al., 2001; Nett et al., 2002; Takata and Hirase, 2008; Hausteil et al., 2014). **Local** Ca^{2+} signals in **astrocyte processes**, driven by spontaneous synaptic transmitter release, cover an area of $\sim 4 \mu\text{m}$ and their duration spans from milliseconds to a couple of seconds (Di Castro et al., 2011). Longer lasting ($\sim 70\text{s}$), discrete Ca^{2+} twinkles have been visualized in cortical astrocyte processes *in vivo* (Kanemaru et al., 2014). **Regional** astroglial Ca^{2+} transients (“regional wave”), induced through action potential firing, are more robust ($> 10\mu\text{m}$, tens of seconds) and occur in primary branches, propagating to the somata (Di Castro et al., 2011; Hausteil et al., 2014). **Global** Ca^{2+} waves include the entirety of several astrocytes.

They display a velocity of 20 $\mu\text{m/s}$ on average and encompass a terrain of roughly 200 μm^2 (Cornell-Bell et al., 1990; Fujii et al., 2017). Such global Ca^{2+} waves can either be propagating or synchronized between astrocytes (“standing wave”).

Propagation of Ca^{2+} waves through the astroglial syncytium can occur via two different, though not mutually exclusive mechanisms (Bennett et al., 2003; Fiacco and McCarthy, 2006). Firstly, the intracellular messenger IP_3 can directly diffuse to neighbouring cells via gap junctions and induce Ca^{2+} release from internal stores. This propagation mode is characterized by comparatively higher velocity but relatively restrained, proximal spreading area (Kang and Othmer, 2009). The second propagation mode involves astroglial ATP release (Guthrie et al., 1999) through gap junction hemichannels, P2X receptors and volume-regulated anion channels (VRAC) (Fujii et al., 2017). Astrocyte-derived ATP (ADP if metabolized by ectonucleotidases) subsequently acts on iono- and metabotropic purinoceptors of neighbouring astrocytes and leads to further ATP release. This process is termed ATP-induced ATP-release and constitutes the basis for regenerative ATP release by astrocytes (Bennett et al., 2003; Anderson et al., 2004). Considering this mechanism, propagation of Ca^{2+} waves carried by ATP is comparatively slow, with greater spatial extent (Kang and Othmer, 2009; Fujii et al., 2017). A special type of Ca^{2+} signal, characteristic during **locomotion and startle responses** *in vivo*, covers the majority of cells within a single imaging area and is controlled by volumetric neuromodulator release (Ding et al., 2013; Paukert et al., 2014). Furthermore, a cerebellar Bergmann glia-specific classification of Ca^{2+} signals was proposed by Nimmerjahn and colleagues (Nimmerjahn et al., 2009). Overall, the observable variety of Ca^{2+} signals crucially depends on the experimental design (slices vs *in vivo*, 2D vs 3D) (Rusakov, 2015; Bindocci et al., 2017) and the use of anaesthetics (Nimmerjahn et al., 2009; Thrane et al., 2012). Recent data suggest that the localized Ca^{2+} signals originating in the gliapil (occupying ~75 % of the cell volume) are not only numerically dominant (vs somata) but also sensitive indicators of neuronal activity *in vivo*, due to their proximity to synapses (PAP) (Kanemaru et al., 2014; Bindocci et al., 2017). Concerning the **impact** of Ca^{2+} transients on the **network activity**, more localized signals are associated with homosynaptic modulation, while signals propagating to several branches and somata evoke the integrative vocation of astrocytes and mediate heterosynaptic or even larger, territorial synaptic modulation (Araque et al., 2014).

Decoding Ca^{2+} signals and their downstream effects is an ongoing task in glia research. Nevertheless, intracellular Ca^{2+} will presumably regulate gene expression, homeostatic functions, astrocyte morphology and the release of various molecules (signaling, synaptogenic, inflammatory), eventually impacting neuronal network activity (Delorenzo et al., 2005; Khakh and Sofroniew, 2015). These functionalities are not only the basis for physiological brain function but also confer a key role in neuropathologies, especially those with network dysfunction, such as epilepsy.

4.4. The epilepsies

Epilepsy, or more appropriately, the epilepsies form a highly diverse family of neurological syndromes with the common clinical symptom of **erratically recurrent seizures**, affecting about 1-2 % of the world population or an estimated 50-65 million people (Hesdorffer et al., 2011; Collaborators, 2019). Most of the epileptic syndromes are of **idiopathic origin**, i.e. without known cause, however perinatal brain damage, brain infections, brain trauma, stroke, as well as rare genetic mutations have been identified among the etiologies of epilepsy (Pandolfo, 2011; Goldberg and Coulter, 2013; Scheffer et al., 2017). Commonly, the initial **precipitating event** and the chronic condition of **recurrent seizures** are chronologically separated by a period designated as **latent phase**. This phase can last several years in humans and reflects the process of **epileptogenesis**, in the context of which a physiologically operating neural network progressively becomes permissive to seizures. The **classification** of epileptic syndromes suggested by the International League Against Epilepsy (ILAE) is primarily based on the seizure and epilepsy type, considering the onset, EEG features and behavioral symptoms such as loss of consciousness or convulsions, additionally combined with the determination of etiology (Scheffer et al., 2017).

Seizures can arise either from restricted areas of one hemisphere (focal), potentially spreading to other brain areas (secondarily generalizing) or starting in several brain areas of both hemispheres simultaneously (generalized) (Fisher et al., 2005; Scheffer et al., 2017). At the cellular level, seizures represent an aberrant hypersynchronous neuronal activity, promoted by a compromised **excitation/ inhibition (E/I) balance** in the brain. However, the anti-epileptic drugs (AED) designed to re-establish the E/I balance by aiming at neuronal targets have a merely symptomatic effect and fail in at least 30 % of patients.

Thus, it has become utterly clear, that the mechanisms underlying epilepsy are far from being understood and that there is an urgent need for new therapeutic targets, beyond primarily neuronal functions (Löscher and Schmidt, 2011; Crunelli et al., 2015).

4.4.1. Temporal lobe epilepsy (TLE)

Temporal lobe epilepsy is the most represented focal epileptic syndrome among adults, characterized by particular severity and drug-refractoriness. Up to 2/3 of patients experience pharmacologically intractable, potentially convulsive seizures, often leaving neurosurgical resection of epileptic foci as last resort (Asadi-Pooya et al., 2017). In TLE, focal seizures commonly arise from restricted areas of the hippocampus or neighbouring temporal structures and can secondarily generalize to other, even contralateral structures (Jobst et al., 2001; Trevelyan et al., 2006; Bedner et al., 2015). From a histopathological point of view, TLE displays a set of characteristic hallmarks observed in human tissue as well as experimental models, commonly termed **hippocampal sclerosis (HS)** (Figure 3).

HS describes the histopathological manifestation of glial scarring (gliosis) and **neuronal loss** generally but not exclusively occurring in the hippocampal CA1, CA3 region and dentate gyrus (Thom, 2014; Walker, 2015) (Figure 3 A, a2). Reactive **astrogliosis** is characterized by the upregulation of intermediate filaments such as the glial fibrillary acidic protein (GFAP), accompanied by cellular hypertrophy and proliferation, and has become a common factor in a plethora of neurological diseases (Sofroniew, 2014; Pekny et al., 2016; Robel, 2017). It is further accompanied by the **activation of microglia**. The role and impact of astrogliosis in epilepsy is still a matter of debate. Human studies on neurosurgical specimens confirmed that severe gliosis correlates with seizure burden and the extent of neuronal loss (Johnson et al., 2016; Hattingen et al., 2018). It has been further postulated, that astrogliosis itself is potentially epileptogenic. Experimental procedures causing astrogliosis isolated from other pathological insults, for example via induced adenosine deficiency (Li et al., 2012b), genetic manipulation of astroglial GFAP (Messing et al., 2012) or β 1-integrin (Robel et al., 2015), have induced spontaneous epileptiform activity. Vice versa, seizure activity does not necessarily entail astrogliosis, as seen in non-sclerotic contralateral hippocampi in guinea pig model of non-convulsive *status epilepticus* (Noè et al., 2019).

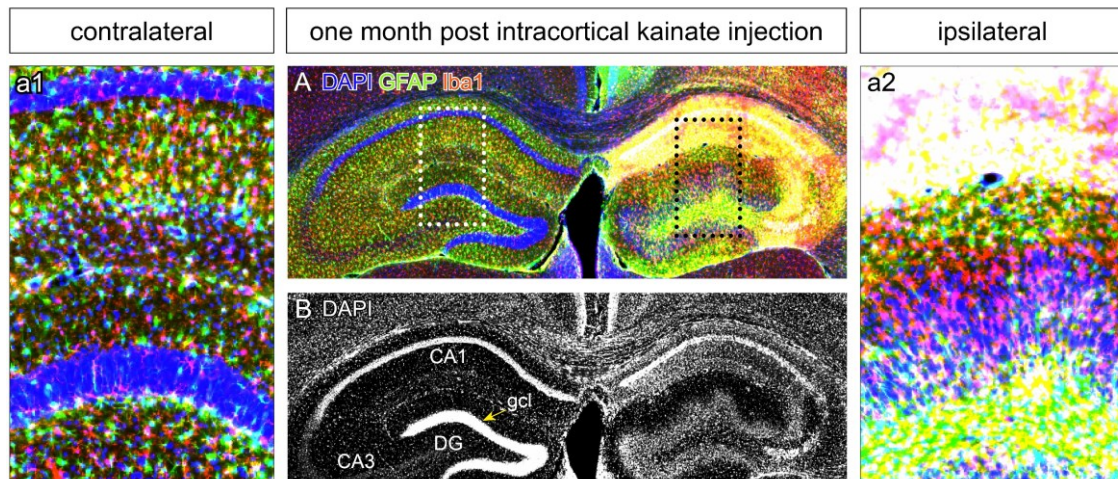


Figure 3 Hippocampal sclerosis with granule cell dispersion in the unilateral intracortical kainate model of TLE

A One month post kainate injection, the ipsilateral hippocampus (**a2**) presents extensive gliosis mediated by activated astrocytes (GFAP) and microglia (Iba1), accompanied by granule cell dispersion in the dentate gyrus. The contralateral hippocampus (**a1**) can present activated glial cells but is generally less affected in contrast to ipsilateral. **B** Granule cell dispersion is characterized by a loss of compact, layered cytoarchitecture of the granule cell layer in the sclerotic, ipsilateral hippocampus but remains intact in the contralateral side. CA: cornu ammonis, DG: dentate gyrus, gcl: granule cell layer. Scale bar in A, B = 500 μ m; in a1, a2 = 200 μ m.

About 40-50 % of TLE patients exhibit **granule cell dispersion** (GCD) in the dentate gyrus (Thom et al., 2005; Blümcke et al., 2009) (Figure 3 B). The pathological widening of the granule cell layer from ≤ 120 μ m to up to 400 μ m (Houser, 1990) was thought to be caused either by aberrant motility of newborn granule cells, generated by seizure-induced neurogenesis, or seizure-induced migration of mature granule cells. It is becoming increasingly clear, that GCD is independent of neurogenesis and rather caused by reelin deficiency, inducing migration of mature granule cells along a radially aligned glial scaffold (Fahrner et al., 2007; Haas and Frotscher, 2010). Reelin, an extracellular matrix protein synthesized and released by Cajal-Retzius cells, is known as essential migration signal in the development of the cortical plate (Frotscher et al., 2009). A further histopathological finding in the dentate gyrus is the **sprouting of mossy fibres** (granule cell axons), usually projecting through the polymorphic hippocampal layer to CA3 pyramidal cells. In epilepsy, the mossy fibre connections to the CA3 region are lost and subsequently these axons branch out to form recurrent excitatory connections with granule cell dendrites in the molecular layer (Represa et al., 1993; Buckmaster et al., 2002).

4.4.2. Experimental TLE models

Owing to the complexity and heterogeneity of epileptic syndromes, different aspects of the condition may be investigated in different models. In general, experimental TLE is studied in rodent model organisms such as rat, mouse and guinea pig. Mechanisms underlying seizure generation (ictogenesis) in hyperexcitable networks are commonly studied in **brain slice** preparations, where epileptiform activity is evoked via application of low Ca^{2+} and Mg^{2+} -free extracellular solutions (Trevelyan et al., 2006), pentylenetetrazole (PTZ) (Accardi et al., 2018) or other GABA receptor antagonists (e.g. penicillin, picrotoxin, bicuculline) (Khalilov et al., 2005; Pinto et al., 2005; Avoli and Jefferys, 2016). Other models induce hyperexcitability using the K^+ channel blocker 4-aminopyridine, sometimes in combination with NMDA application and low extracellular Mg^{2+} (Uva et al., 2009; Losi et al., 2016). These preparations however do not recapitulate characteristics of human TLE and are not suitable to study **epileptogenesis**, the process by which an initial trigger will elicit progressive changes in the network leading to chronic **spontaneously recurrent seizures** (SRS). To this end, ***in vivo* models** of TLE were developed (Table 1). The ideal model firstly reflects the acute phase *status epilepticus*, characterized by electrographic non-convulsive and convulsive seizures originating from limbic structures, potentially secondarily propagating to the neocortex (generalization). On electrographic recordings, seizures manifest by high amplitude spiking (up to 60 Hz) lasting for 20-60 s and are followed by post ictal depression after generalized seizures (Bedner et al., 2015). Secondly, after a latent period without seizure activity, SRS mark the initiation of the chronic phase. In parallel to this time course, hippocampal sclerosis (HS) including astrogliosis, neuronal loss and granule cell dispersion should develop. Available TLE models are widely based on the **systemic or intracerebral application of chemoconvulsants** such as pilocarpine (cholinomimetic), kainate (glutamate analogue) and pentylenetetrazole (PTZ, GABA_{A} antagonist) or **electrical stimulation** (Table 1). Kainate and pilocarpine models have the highest **homology** with the human condition, although systemic administration routes should be carefully considered due to extratemporal lesions (Lévesque et al., 2016). The kindling approach, either chemical or electrical, is based on repetitive, intermittent sub-threshold stimulation, eventually eliciting seizures (Dürmüller and Porsolt, 2003; Dhir, 2012). The advantage of these models is the predictability of seizures since they are induced by the experimenter. Thus, kindling models and maximal electroshock models (not specifically TLE model, but generalized seizures) are commonly employed in **drug discovery** (Castel-Branco et al., 2009; Barker-Haliski and Steve White, 2020). Nonetheless, a critical disadvantage is that these models do not produce SRS and neither replicate histopathological hallmarks.

From a technical point of view, *in vivo* electrographic activity is recorded with intracerebral or epidural electrodes, preferentially connected to telemetric systems and synchronized video footage (Weiergräber et al., 2005; Bedner et al., 2015; Puttachary et al., 2015). Behavioural aspects of convulsive seizures are then classified according to the Racine scale (Racine, 1972). The application however is highly heterogenous, since this scale is commonly adapted to the different experimental procedures (Sharma et al., 2018).

Trigger	Administration route	Characteristics	SE duration	Latency period	Mortality	Reference	
		seizures	histology				
<i>pilocarpine</i>	systemic (i.p.)	acute SRS	HS	terminated within 30- 90 min*	7-35 d	20-60 %	(Hamilton et al., 1997; Borges et al., 2003; Curia et al., 2008)
	intra-hippocampal				2-30 d	20-30 %	
<i>kainate</i>	systemic (i.p.)				10-30 d	17 %	(Lévesque and Avoli, 2013; Bedner et al., 2015; Puttachary et al., 2015; Sharma et al., 2018)
	intra-hippocampal	acute SRS	HS	1-7 h	5-30 d	12 %	
	intra-amygdaloid				10-40 d	55 %	
	intra-cortical				2-8 d	6 %	
repetitive subthreshold electrical stimulation	limbic structures, frequently intraamygdaloid	acute rarely SRS	-		-	-	(Löscher, 2002; Dürmüller and Porsolt, 2003; Chen et al., 2016)
subconvulsive doses of <i>PTZ</i>	systemic (i.p., subcutaneous)	acute	-	seizures elicited on demand	-	20-30 %	(da Silva et al., 1998; Hoeller et al., 2017; Shimada and Yamagata, 2018)

Table 1 Most commonly used *in vivo* models of temporal lobe epilepsy

d: days, h: hours, HS: hippocampal sclerosis, PTZ: pentylenetetrazole, SE: status epilepticus, SRS: spontaneously recurrent seizures. *administration of benzodiazepines, barbiturates and anti-convulsant drug cocktails.

4.5. An astroglial focus on epilepsy

4.5.1. Astroglial network function in epileptogenesis

The astroglial network, interconnected via gap junctions, enforces **anti- as well as pro-epileptic** functions. On one hand, neuronal excitability is decreased via K^+ redistribution and glutamate clearance (Wallraff et al., 2006; Pannasch et al., 2011) while on the other hand, providing energy endorses high level synaptic activity (Rouach et al., 2008). In epileptic conditions, astrocytes become reactive and their properties change radically (Bedner et al., 2015), entailing extensive consequences for neuronal function and epileptogenesis (Steinhäuser et al., 2016). **Glutamate homeostasis** is severely impaired in epilepsy (Coulter and Eid, 2012). Human studies found up to 10-fold increased glutamate levels close to epileptic foci (During and Spencer, 1993; Cavus et al., 2005), while astroglial glutamine synthetase expression was drastically diminished (Eid et al., 2004; van der Hel et al., 2005). The enzyme glutamine synthetase degrades glutamate to glutamine, an essential precursor in astroglial and neuronal GABA synthesis. Hence, failure of normal function leads to accumulation of extracellular glutamate and reduced neuronal GABA release (Ortinski et al., 2010), promoting hyperexcitability. The role of astroglial glutamate uptake through glutamate transporters (EAAT1, EAAT2) is controversially discussed in epilepsy. While some studies find reduced transporter expression by 20-40% (Sarac et al., 2009), others found physiological levels (Bjørnsen et al., 2007). Nonetheless, deletion of EAAT1 was shown to promote hyperexcitability (Jen et al., 2005). In addition, astroglial **K^+ buffering** is compromised in epilepsy as documented by the disturbance of K^+ uptake and changes in K^+ conductance (inwardly rectifying K^+ channels) in human sclerotic hippocampi (Hinterkeuser et al., 2000; Kivi et al., 2000; Bedner et al., 2015). In fact, hippocampal protein levels of Kir 4.1 have been shown to drop by approximately 50 % in human samples (Das et al., 2012). Moreover, astroglial **aquaporin** water channels influence neuronal excitability by modulation the extracellular space in terms of size and osmolarity (Binder et al., 2012). Together, these findings point to a dysfunctional astroglial network in epilepsy. Indeed, astrocytes of sclerotic hippocampi were shown to loose gap junction **coupling** at an early stage of epileptogenesis, before neuronal loss or spontaneous recurrent seizures appeared (Bedner et al., 2015). Therefore, astrocytes are considered to actively participate in the development and maintenance of epileptic network function. In support of the **causative roles**, Cx 43 deletion leading to coupling-deficient astrocytes promotes epileptiform activity in hippocampal slices (Wallraff et al., 2006; Pannasch et al., 2011) and exacerbate kainate-induced TLE *in vivo* (Deshpande et al., 2020).

4.5.2. The role of astroglial Ca²⁺ signaling and gliotransmission in epilepsy

Ca²⁺-dependent astroglial glutamatergic gliotransmission crucially modulates **neuronal excitability and synchronization** (Carmignoto and Haydon, 2012). Glutamate release from astrocytes activates neuronal extrasynaptic NMDA receptors, inducing typical slow inward currents (SIC), thereby driving neuronal excitation and favouring synchronous firing episodes (Parpura et al., 1994; Parri et al., 2001; Angulo et al., 2004; Fellin et al., 2004; Sasaki et al., 2014). Epileptiform network function has been associated with “hyperexcitable” astrocytes in terms of frequent Ca²⁺ oscillations (Tian et al., 2005a; Fellin et al., 2006). In rat entorhinal and temporal cortex, astroglial Ca²⁺ signals engage into **recurrent excitatory loops** with neurons *ex vivo*. Hence, by recruitment of a critical mass of synchronously firing neurons, astrocytes trigger and promote maintenance of focal, seizure-like discharges (Gómez-Gonzalo et al., 2010; Losi et al., 2016). Interestingly, the underlying mechanism not only depends on glutamatergic gliotransmission but is additionally regulated by (autocrine) astroglial purinergic signaling (Álvarez-Ferradas et al., 2015; Shen et al., 2017). Supporting the **pro-epileptic role** of astroglial Ca²⁺ signals, it was shown that substantial Ca²⁺ elevations in astrocytes precede neuronal epileptiform activity and promote kainate-induced hippocampal seizure spreading *in vivo* (Heuser et al., 2018). Thus, **Ca²⁺ signals** associated with **epileptiform activity** differ from the physiological state (Shigetomi et al., 2019) and may manifest in a **stereotypical fashion**. A prominent example is the large astroglial Ca²⁺ oscillations promoted by spreading depression (Wu et al., 2018). The fortuitous discovery of **spreading depression**, presently also termed **spreading depolarization** (Aristides A. P. Leão, 1944), exposed a propagating wave of flattened electrocorticographic activity in the seizing rabbit cortex (Teive et al., 2005). In fact, this propagating wave of exhaustive local depolarization reaches a velocity in the order of mm / min while shifting the extracellular potential by millivolts. During this episode, K⁺ and Ca²⁺ homeostasis is abruptly and critically corrupted by extracellular K⁺ levels rising up to 20-fold and massive Ca²⁺, Na⁺ as well as water influx into the cells. Intracellular Ca²⁺ rises in turn lead to the release of neuro- and gliotransmitters and together with excessive extracellular K⁺ levels, confer a regenerative character to the phenomenon. This integral membrane depolarization inhibits electrical activity until homeostasis is restored, hence the term spreading depression (Ayata and Lauritzen, 2015; Bernard, 2015; Seidel et al., 2016).

Spreading depolarization is not only associated with epilepsy (Fabricius et al., 2008; Bernard, 2015; Loonen et al., 2019) but also other CNS disorders such as stroke (Somjen, 2001; Dreier, 2011) and migraine (Charles and Baca, 2013). Moreover, *in vivo* studies of neuronal Ca²⁺ signals in the murine hippocampus after subcutaneous kainate administration identified epileptiform Ca²⁺ signals in CA1, CA3, dentate gyrus and entorhinal cortex. Two out of three **stereotypical wave forms** were shared by all hippocampal structures, suggesting an underlying **cellular specificity** rather than regional specificity (Zhang et al., 2019).

4.5.3. Relevance of GABAergic signaling in epilepsy

In the CNS, **E/I balance** is largely attached to **excitatory versus inhibitory** transmission and their representative neurotransmitters **glutamate and GABA**, respectively. Classically, it is assumed that in epilepsy, the E/I balance would tip in favour of excessive excitation and diminished inhibition, which is supported by the fact that a large proportion of anti-epileptic drugs (AED) next to blocking voltage-gated sodium channels, aims at decreasing excitatory transmission or increasing inhibition (Rogawski and Löscher, 2004). Moreover, the observations of up to 10-fold increased extracellular glutamate levels (During and Spencer, 1993) and special vulnerability of inhibitory hippocampal interneurons in epilepsy consolidate this point of view (Sanon et al., 2005; Huusko et al., 2015; Buckmaster et al., 2017; Upadhyaya et al., 2019). However, experimental evidence shows that seizures, of the absence type, can just as well be elicited by enhanced inhibitory transmission, e.g. through GABA transporter-1 malfunction leading to enhanced GABA_A receptor activity in thalamo-cortical neurons or application of the GABA_B receptor agonist γ -hydroxybutyric acid (GHB) (Cope et al., 2005; Cossart et al., 2005; Pirttimäki et al., 2013; Gobbo et al., 2021). Along the same lines, despite pronounced loss of inhibitory interneurons in the hippocampus, tonic GABA-mediated inhibition is preserved in epilepsy, likely attributable to compensatory mechanisms involving astroglial GABA overproduction and release through bestrophin-1 channels (Pavlov and Walker, 2013; Müller et al., 2020; Pandit et al., 2020).

Although AEDs target GABAergic transmission in the context of TLE or convulsive seizures in general, glutamatergic and purinergic signaling has received more scientific interest (Treiman, 2001; Crunelli and Carmignoto, 2013; Rassendren and Audinat, 2016; Steinhäuser et al., 2016; Nikolic et al., 2020). Especially **GABA_BR-mediated signaling** has been scarcely studied. While neuronal GABA_BR subunit 1 knock-out mice develop epileptic phenotypes ranging from spontaneous absence and tonic-clonic seizures (Schuler et al., 2001) to generalized epilepsy (Prosser et al., 2001), the function of astroglial GABA_BR signaling in epilepsy is unknown.

4.5.4. Astroglial GABAergic signaling at the interface of excitation and inhibition

Astrocytes are metabolically and functionally associated to the **interface of excitation and inhibition** in the CNS (Caudal et al., 2020). **Metabolically**, astrocytes are exclusive providers of glutamine, the only precursor of both major neurotransmitters governing excitation and inhibition, glutamate and GABA, respectively. Neurons are not capable of glutamine biosynthesis, due to a lack of the astrocyte-specific enzyme glutamine synthetase (GS). Moreover, astrocytes synthesize both glutamate and GABA (Angulo et al., 2008). In addition, extracellular GABA can be taken up by astrocytes through GABA-transporters (GAT-1, GAT-3). Astroglial GABA (taken up or endogenously produced) can then be released as gliotransmitter, together with the endogenously synthesized supplies. Aside from being GABAergic cells, astrocytes are also GABAceptive (Vélez-Fort et al., 2012; Yoon et al., 2012; Ishibashi et al., 2019) which is particularly interesting with respect to their **functional association** to multipartite synapses including GABAergic interneurons and glutamatergic circuits in cortical and hippocampal structures (Losi et al., 2014; Mariotti et al., 2016; Perea et al., 2016; Mederos and Perea, 2019). Astrocytes integrate interneuron activity (Mariotti et al., 2018) and can **transform inhibitory into excitatory signals**, thereby orchestrating fine-tuning of neuronal network activity (Perea et al., 2016; Covelo and Araque, 2018).

The GABAceptive nature of astrocytes manifests via the expression of ionotropic GABA_A and metabotropic GABA_B receptors (GABA_AR, GABA_BR) (Figure 4) (Zhang et al., 2014). **Ionotropic GABA_ARs** mediate Cl⁻ efflux-driven depolarization of the astroglial membrane (MacVicar et al., 1989; Fraser et al., 1994; Bernstein et al., 1996; Meier et al., 2008). Supposedly, astrocyte networks thereby buffer extracellular Cl⁻ to maintain GABAergic neurotransmission during excessive network activity (Kettenmann et al., 1987; Isomura et al., 2003; Egawa et al., 2013). **Metabotropic GABA_BRs** are G-protein-coupled, seven-transmembrane domain receptors (GPCR). Functional receptors are essentially composed of heterodimers with one GABA_{B1a} or GABA_{B1b} and one GABA_{B2} subunit (Marshall et al., 1999), while different auxiliary subunits have been described in neurons (Figure 4 B). Ligand binding and signal transduction are segregated between the B1 and B2 subunits. The GABA_{B1} subunit accommodates the GABA binding site within its Venus fly trap domain, whereas the GABA_{B2} subunit is linked to the heterotrimeric G-protein (Pin and Bettler, 2016). The exact intracellular cascade of the astroglial GABA_BR is still elusive.

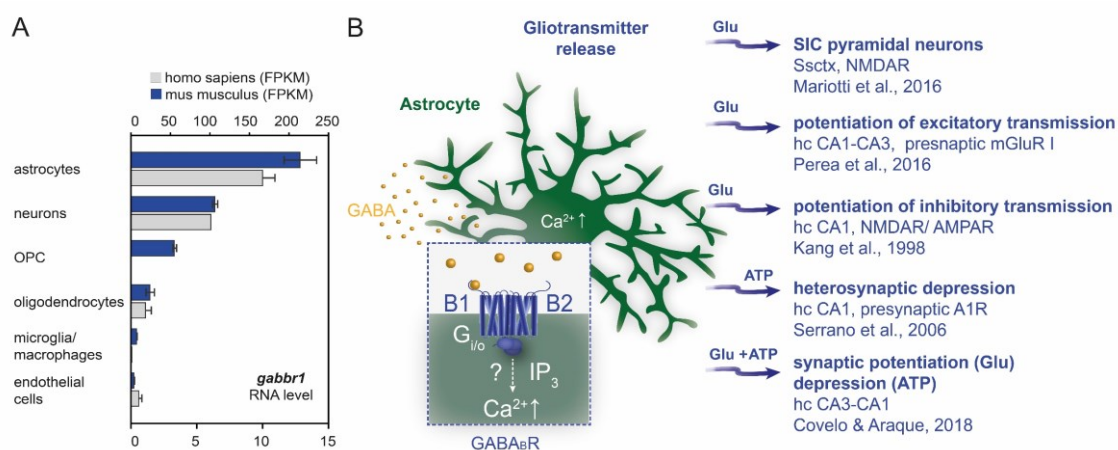


Figure 4 GABAergic astrocytes at the interface of excitation and inhibition

A According to *gabbr1* RNAseq data, the GABA_BR is mainly expressed in astrocytes and neurons in mice and humans. In mice, oligodendrocyte precursor cells (OPCs) and oligodendrocytes express GABA_BRs to a comparatively lesser extent (Zhang et al., 2014). **B** The astroglial GABA_BR is intracellularly coupled to G-proteins. Receptor activation leads to intracellular Ca²⁺ elevations, in an at least partially IP₃ dependent manner. Current research supports the hypothesis of G_{i/o}-coupling and crosstalk with IP₃ pathways downstream of receptor activation. GABA-induced intracellular Ca²⁺ signaling drives glutamate and ATP release, affecting the neural network.

However, it is postulated that these receptors are G_{i/o} protein-coupled, whose activation induce **intracellular Ca²⁺ rises** (Nagai et al., 2019) in an, at least partially, IP₃-dependent manner (Mariotti et al., 2016) resulting in **gliotransmitter release** (Serrano et al., 2006; Perea et al., 2016; Durkee et al., 2019) (Figure 4 B). Possible explanations for this peculiar link between G_{i/o} Proteins and IP₃ might be a collateral stimulation of the PLC pathway (Pierce et al., 2002) or direct action on IP₃ receptors (Zeng et al., 2003). Of note, G_q-coupled receptor activation does not inevitably lead to gliotransmitter release, whereas this causality has been shown for Ca²⁺ uncaging and IP₃ application (Wang et al., 2013). The activating feature of astroglial G_{i/o} proteins is highly distinctive from neurons, since neuronal GABA_BR coupled to G_{i/o} proteins have an inhibitory effect through negative regulation of the adenylate cyclase.

Activation of the astroglial GABA_BR has been linked to a variety of **network modulations** (Figure 4 B) including potentiation (Kang et al., 1998; Perea et al., 2016) as well as depression (Serrano et al., 2006) of synaptic transmission (Covelo and Araque, 2018) and release of synaptogenic molecules enhancing excitatory transmission (Nagai et al., 2019). ATP/ADP release mediates depression of synaptic transmission, while glutamate release potentiates excitatory and inhibitory transmission.

Covelo and colleagues demonstrated that co-release of ATP/ADP and glutamate and associated synaptic plasticity can even occur from one and the same astrocyte (Covelo and Araque, 2018). Importantly, astrocyte-derived **glutamate** promotes **hyperexcitability** and **neuronal synchrony** (see section 4.5.2). Furthermore, GABAergic astroglial signaling has been shown to support hippocampal theta and **gamma oscillations**, that were reduced in astroglial GABA_BR cKO mice (Perea et al., 2016).

Concluding, astroglial GABA_BR signaling at the interface of inhibition and excitation constitutes a hitherto undervalued factor in epileptic network function, which we sought to investigate in the following study.

5. AIMS OF THE STUDY

Previous studies have highlighted the central role of astrocytes in epileptic network function. However, the role of GABAergic signaling to astrocytes, in particular GABA_BR-mediated gliotransmission and its consequences for network excitability in temporal lobe epilepsy (TLE) are not understood.

Therefore, the central aim of this study is to investigate the contribution of astroglial GABA_BR to pathological network function in TLE.

To address this question, we devised the following work packages:

- **Adapt the intracortical kainate injection model of TLE**

The model will be optimized for minimal mechanical damage associated to the injection procedure and genuine baseline recordings will be implemented into the experimental paradigm. Furthermore, cortical surface electrodes (ECoG) will be integrated under the cranial window. This will enable us to conduct longitudinal studies via EEG telemetry or *in vivo* 2P Ca²⁺ imaging/ ECoG and ulterior immunohistochemical analysis.

- **Identify the contribution of astroglial GABA_BR function to seizure activity and histopathological features of TLE**

GABA_BR function will be investigated by means of transgenic mice with astrocyte-specific, inducible GABA_BR deletion (GABA_BR cKO) and expression of the genetically encoded Ca²⁺ sensor GCaMP3. To assess the overall epileptic phenotype, *status epilepticus* will be induced by *intracortical* kainate injection and seizure activity will be continuously evaluated via telemetric EEG recordings with synchronized video monitoring until the early chronic phase.

- **Characterize cortical astroglial Ca²⁺ signals of control and GABA_BR cKO mice in status epilepticus and latent phase**

We will examine the role of cortical GABA_BR-dependent astroglial Ca²⁺ signals during baseline, generalizing seizures (SE) and latent phase, via *in vivo* two-photon Ca²⁺ imaging combined with ECoG recording.

- **Evaluate impact of GABA_BR deletion on histopathological hallmarks of TLE**

Four weeks post kainate, during the early chronic phase, we will assess the extent of hippocampal astro- and microgliosis as well as granule cell dispersion on immune-stained brain slices.

6. MATERIALS AND METHODS

6.2. Materials

6.2.1. Reagents

Standard chemicals were purchased from customary companies including Sigma Aldrich, Eppendorf, Merck, BioRad, Invitrogen, Roche, Carl Roth, Amersham Biosciences, Serva, Thermo Fisher Scientific and BD Falcon.

6.2.2. Consumables and kits

Pipette tips, Sarstedt; glas pipettes, VWR International; Falcon-tubes, Greiner Bio-One; Eppendorf reaction tubes, Eppendorf; Venomix canulas, Braun; 96-well-PCR-reaction-tubes, 4titude; 48-well-culture-plates, Sarstedt; object slides and cover slips, Menzel-Gläser; REExtract-N-Amp™ Tissue PCR Kit, Sigma-Aldrich.

6.2.3. Devices

Table 2 List of devices

Device	Manufacturer
AxioScan.Z1	Zeiss
Centrifuges	Eppendorf
Telemetric EEG recording equipment	Data Sciences International (DSI)
Head holder	Custom-made (G. Stopper, Molecular Physiology)
peqSTAR Thermo Cycler	peqlab Biotechnologie GMBH
Pipettes	Brand
Preparations- and perfusion instruments	F.S.T.
Quantum gel documentation system	peqlab Biotechnologie GMBH
Scales (CPA 8201/CPA 2245)	Sartorius

Shaker DRS-12	neoLab
Robot stereotaxic	Neurostar
Vacuum pump	Integra Biosciences
Vibratom VT1000S	Leica
Water facility Milli-Q	Merck
10 µl Nanofil syringe with 34 GA blunt needle	World Precision Instruments
Biosignal amplifier (g.USBamp)	gTec
Pre-amplifier g.(HEADstage)	gTec
Bead sterilisator	F.S.T.

6.2.4. LCP surface electrodes for ECoG recording

Surface electrodes consisted of triple LCP layers (Dyconex AG, Switzerland) allowing for flexibility, yet maintaining stability, while the electric structure was made of a double gold layer. The gold electrode sites were coated with galvanized gold and at the end of the manufacturing process, electroplated with nanoporous platinum. To improve the mechanical stability and to preclude short circuits during the animal studies, epoxy resin (TC-EP05-24, TOOLCRAFT) was used to cover the connector and pads. Surface electrodes were electroplated and assembled by M. Schweigmann (Trier University of Applied Sciences/ Dpt. of Molecular Physiology, CIPMM, University of Saarland) (Schweigmann, Caudal et al., in press, *Frontiers in Cellular Neuroscience*).

6.2.5. Buffers and aqueous solutions

PBS (Phosphate-buffered saline, 10x; pH 7.4)

NaCl	1 .37	M
KCl	27	mM
Na ₂ HPO ₄	100	mM
KH ₂ PO ₄	18	mM

4 % Formaldehyde in 0.1 M PB (pH 7.4)

Paraformaldehyde (PFA)	4	% (v/v)
NaH ₂ PO ₄	0 .2	M
Na ₂ HPO ₄	0 .2	M
NaOH	10	M

(a few drops to dissolve PFA)

Tris-Acetate-EDTA-buffer (TAE, 50x)

Tris-Base	1	M
Acetic acid (100%)	1mM	
EDTA	1	mM

(Ethylendiamintetraacetate 0.5 M, pH 8)

Materials and Methods

DNA extraction solution (pH 9.5)

KCl	0.25	M
EDTA	0.01	M
Tris-HCl	0.1	M

Neutralisation solution

Bovine serum albumin	3	%
Kathon (Methylchloroisothiazolinone, Methylisothiazolinone)	10	ppm

Cortex buffer (cranial window; pH 7.4)

NaCl	125	mM
KCl	5	mM
Glucose	10	mM
HEPES	10	mM
CaCl ₂	2	mM
MgSO ₄	2	mM

EEG implant cleaning solution in ddH₂O

Tergazyme	1	% (w/v)
-----------	---	---------

Syringe cleaning solution in ddH₂O

Hamilton cleaning solution	25	% (v/v)
----------------------------	----	---------

Immunohistochemistry

Permeabilization-/blocking buffer and buffer for antibodies 5 % horse serum (HS), 0.3 % Triton-X-100 in 1x PBS.

6.2.6. Enzymes

REDTaq™DNA Polymerase (Sigma-Aldrich Co.)

DreamTaq™ Hot Start Green DNA Polymerase (ThermoFischer)

6.2.7. Drugs

Tamoxifen (Caesar & Loretz) in Miglyol 10 mg/ml

Kainate (Tocris) in 0.9 % NaCl 20 mM

Ketaminhydrochlorid (Serumwerk Bernburg AG) 100 mg / ml

Xylazinhydrochlorid (WDT) 20 mg / ml

6.2.8. Antibodies

6.2.8.1. Primary antibodies

Table 3 Primary antibodies for immunohistochemistry

Antigen	Clonality	Host	Dilution	Manufacturer
Cx43	pc	rabbit	1:1000	Sigma
DCX	pc	guinea pig	1:500	Milipore
GFAP	mc	mouse	1:500	Novocastra
GFAP	pc	goat	1:1000	Abcam
GFP	pc	goat	1:1000	Rockland
GFP	pc	chicken	1:1000	Invitrogen
Iba1	pc	rabbit	1:500	Wako
MFGE8	pc	goat	1:1000	R&D Systems
NeuN	mc	mouse	1:500	Milipore

6.2.8.2. Secondary antibodies

Table 4 Secondary antibodies for immunohistochemistry

Host α -target	Conjugated fluorophore	Dilution	Manufacturer
Donkey α -goat Donkey α -chicken	Alexa Fluor® 488	1:1000	Invitrogen
Donkey α -mouse	Alexa Fluor® 546	1:1000	Invitrogen
Donkey α -guinea pig	Alexa Fluor® 633	1:1000	Invitrogen
Donkey α -rabbit	Alexa Fluor® 647	1:1000	Invitrogen
Donkey α -goat	Alexa Fluor® 750	1:1000	Invitrogen
Donkey α -guinea pig	Cy5	1:500	Abcam

6.2.9. Dyes

Table 5 Dyes

Component	Working solution	Manufacturer
4',6-Diamidin-2-phenylindol (DAPI)	0.025 μ g/ml	Sigma, Taufkirchen
Ethidium bromide	0.015 %	Carl Roth, Karlsruhe
Easy ladder	-	Bioline, Neunkirchen

6.2.10. Primers

Table 6 Genotyping primers

Name	Serial number	Sequence	Amplicon
GABA _B forward	24391	5'-TGGGGTGTGTCCTACATGCAGCGGACGG-3'	KI 742 bp
GABA _B reverse	24392	5'-GCTCTTCACCTTTCAACCCAGCCTCAGGCAGGC-3'	WT 526 bp
GCaMP3 KI forward	27632	5'-CACGTGATGACAAACCTTGG-3'	
GCaMP3 KI reverse	27496	5'-GGCATTAAGCAGCGTATCC-3'	KI 245 bp
GCaMP3 WT forward	14025	5'-CTCTGCTGCCTCCTGGCTTCT-3'	WT 327 bp
GCaMP3 WT reverse	14026	5'-CGAGGCGGATCACAAGCAATA-3'	
GLAST forward	11984	5'-GAGGCACTTGGCTAGGCTCTGAGGA-3'	
GLAST reverse	11985	5'-GAGGAGATCCTGACCGATCAGTTGG-3'	KI 400 bp WT 700 bp
CreERT2 reverse	11986	5'-GGTGTACGGTCAGTAAATTGGACAT-3'	

6.2.11. Genetically modified mouse lines

6.2.11.1. Tamoxifen-inducible DNA recombination

We took advantage of the Cre^{ERT2} – loxP system to conditionally delete target genes and express fluorescent reporter proteins, indicating DNA recombination (Feil et al., 2009) (Table 7). The Cre^{ERT2} fusion protein of Cre DNA recombinase and mutant ligand-binding domain of the human estrogen receptor is retained in the cytosol by heat shock proteins (HSP). The Cre^{ERT2} / HSP complex being sensitive to the bioactive tamoxifen metabolite 4-OH-tamoxifen, Cre^{ERT2} can dissociate from HSP upon tamoxifen administration and translocate to the nucleus (Feil et al., 1997). Subsequently, Cre^{ERT2} mediates DNA recombination of target sequences flanked by loxP sites (floxed) (Sternberg and Hamilton, 1981; Hamilton and Abremski, 1984; Jahn et al., 2018). The particular assets of the Cre^{ERT2} – loxP system are cell-type specificity and temporal control of gene recombination. Notably, cell type-specificity is determined by the promotor chosen for Cre^{ERT2} expression (Cre^{ERT2} – driver line).

Table 7 Single transgenic mouse lines

Transgenic mouse line	Brief	MGI ID	Reference
TgH (GLAST-Cre ^{ERT2})	astrocyte-specific Cre ^{ERT2} -driver line	3830051	(Mori et al., 2006)
TgH (GABA _B R1 ^{fl/fl})	GABA _B receptor deletion*	3512743	(Haller et al., 2004)
TgH (Rosa 26-CAG-lsl-GCaMP3)	GCaMP3 reporter expression*	5659933	(Paukert et al., 2014)

CAG: cytomegalovirus immediate early enhancer / chicken beta-actin / rabbit beta-globin hybrid promoter; CreERT2: inducible Cre DNA recombinase fused to mutant ligand-binding domain of the human estrogen receptor; fl: flanked by loxP sites (floxed); GABA_{BR1}: GABA_B receptor subunit 1; GLAST: glutamate aspartate transporter; MGI: Mouse Genome Informatics database; TgH: transgenic mouse line generated via homologous recombination; lsl: floxed stop cassette. *After tamoxifen administration.

6.2.11.2. Astrocyte-specific GABA_B receptor deletion and GCaMP3 reporter expression

In this study, we focussed on astrocyte-specific manipulation of genes of interest and therefore employed the GLAST-Cre^{ERT2} driver line (Mori et al., 2006). The central interest was the conditional GABA_B receptor (GABA_BR) deletion in astrocytes. Hence, the GLAST-Cre^{ERT2} line was crossbred to the GABA_BR1^{fl/fl} line, in which the floxed target gene is the GABA_BR subunit 1 (*gabbr1*), more specifically exons 7 and 8, containing the GABA-binding region (Haller et al., 2004). In addition, the GLAST-Cre^{ERT2} drives expression of the genetically encoded Ca²⁺-indicator GCaMP3 in astrocytes (Table 7, Figure 5 A). The GLAST-Cre^{ERT2} x GABA_BR1^{fl/fl} x GCaMP3 line was employed for *in vivo* 2P-Ca²⁺-imaging combined with ECoG recording, telemetric EEG recording and immunohistochemical analysis. All mice were heterozygous for GLAST-Cre^{ERT2} and homozygous floxed for the GCaMP3 reporter stop cassette. GABA_B cKO animals were homozygous floxed (*gabbr1* fl/fl). Control animals were non-floxed (*gabbr1* wt) or originated from the GLAST-Cre^{ERT2} x GCaMP3 line. All animals were treated with tamoxifen.

6.2.12. Software

Adobe Illustrator, Adobe InDesign, Adobe Photoshop, FIJI, Zen, Neuroscore (DSI), Ponemah 6.51, Noldus MediaRecorder 4.0, MSparkles (Stopper et al., in preparation), MATLAB2019a/b - 2020a/b, Simulink (MATLAB), ScanImage, GraphPad Prism 8, Microsoft Office, NCBI; <http://www.ncbi.nlm.nih.gov/pubmed>, EndNote (Clarivate).

6.2.13. Graphical elements

Individual elements (e.g. receptors and channels) included in Figures 2, 4 and 19 were designed by Jens Grosche (Effigios AG, Leipzig). The graphical abstract, the brain model in Figure 9 A and the syringe icon (e.g. Figure 17 A) were generated with Biorender (<https://biorender.com/>).

6.3. Methods

6.3.1. General

6.3.1.1. Genotyping

Genomic DNA extraction was performed on tail biopsy or ear punch samples by incubation with 62.5 µl of extraction solution for 10 min. Subsequently, the solution was incubated at 95°C for 20 min and finally 50 µl of neutralisation solution was added. For genotyping, DNA samples were incubated with the prepared sample buffer from REDextract-N-Amp PCR KIT (Sigma Aldrich) or DreamTaq™ Hot Start Green DNA Polymerase (ThermoFischer) and different oligonucleotide primers (Table 6). The reactions were run in 96-well PCR plates in peQ ThermoCyclers (PeqLab Biotechnologie GMBH, Erlangen). Gel electrophoresis was run on 1-2 % agarose gels with ethidium bromide (0.015 %), subsequently exposed and documented with the Quantum Gel documentation system (peQlab Biotechnologie GMBH, Erlangen).

6.3.1.2. Tamoxifen treatment

In accordance with previously published data, tamoxifen treatment (TAM) consisted of five consecutive i.p. injections (100 mg/kg), once per day, to achieve maximal recombination level (Jahn et al., 2018). Animals were either treated at 4 or 8 weeks of age, resulting in 8 or 4 week intervals before experiment start, respectively. In the following, animal cohorts will be distinguished according to the time period between TAM treatment and analysis (cKO 4w, cKO 8w, Figure 5 B).

6.3.1.3. Whole body perfusion fixation

Animals were anesthetized with ketamine / xylazine (250 mg / kg and 50 mg / kg bodyweight in 0.9 % NaCl) and dissected by performing a bilateral axillary thoracotomy to expose the heart. A butterfly needle was inserted into the left ventricle and the perfusion with 1x PBS was started by a peristaltic pump. Simultaneously, an incision of the superior vena cava allowed the blood to drain off. After perfusion with 15-20 ml 1x PBS, the animal was perfused with 4 % formaldehyde (FA) in PB. Fixation was considered complete after perfusion of 20-25 ml FA. Subsequently, the brain was dissected and post fixed in 4 % FA overnight (4°C).

6.3.2. Immunohistochemistry

Fixed brains were sliced into coronal sections of 40 µm thickness, in PBS, at a Leica VT1000S vibratome and collected in 48-well culture plates containing 1x PBS. Vibratome sections were incubated for 1 h in blocking buffer (5 % HS, 0.3 % Triton X in 1x PBS) at room temperature. Sections were incubated with primary antibodies, diluted in the blocking solution overnight at 4°C. The next day, sections were washed 3 times (10 min, 1x PBS) and incubated for 2 h at room temperature in the dark, with secondary antibodies and DAPI diluted in blocking buffer. Subsequently, the sections were washed and mounted in Shandon ImmuMount (Thermo Scientific).

6.3.3. Surgeries and downstream *in vivo* procedures

During any surgical intervention, animals were kept on a heating pad and the eyes were covered with Bepanthen eye ointment (Bayer, Germany). Instruments were sterilized in a hot bead sterilizer (FST). Antisepsis was ensured by applying a povidone iodine solution (Betaisodona, Mundipharma GmbH). In general, anaesthesia consisted of a volatile component (isoflurane - 5% for induction and 2% for maintenance - with O₂ (0.6 l/ min) and N₂O (0.4 l/ min)) as well as an analgetic component (buprenorphine (0.1 mg/kg, s.c.)). Analgetic treatment was accompanied by anti-inflammatory drug administration (dexamethasone (0.2 mg/kg, i.p.)), except for kainate injections. Post-surgical care consisted of buprenorphine and dexamethasone administration and addition of tramadol hydrochloride (Grünenthal GmbH) to the drinking water (100 mg/ 200 ml) for three days, including the surgery day.

6.3.3.1. Intracortical kainate injection

Mice were placed in the stereotaxic frame (Robot stereotaxic, Neurostar) and injected with 70 nl of a 20 mM kainate solution (Tocris) in 0.9 % NaCl, above the right dorsal hippocampus (1.9 mm posterior to bregma, 1.5 mm from sagittal suture at a depth of 1.3 mm from the skull surface). Kainate was injected at a rate of 70 nl/ min with a 10 µl Nanofil syringe (34 GA blunt needle, World Precision Instruments, Sarasota, FL, USA).

The syringe was kept in place for 2 min after the injection was completed, to avoid liquid reflux. The skin was closed by simple interrupted sutures (non-absorbable, F.S.T.). Control injections were performed with 0.9 % NaCl (saline). Animals were perfused for immunohistochemical analysis 4 or 28 days post injection.

6.3.3.2. EEG-transmitter implant and recording

Using a stereotaxic frame (Robot stereotaxic, Neurostar, Tübingen, Germany), depth electrodes (extremities (≈ 0.5 cm) of insulation-deprived ETA-F10 transmitter wires) were implanted at 3.4 mm posterior to bregma and bilaterally 1.6 mm from the sagittal suture and fixed to the skull with cyanoacrylate and dental cement. The ETA-F10 transmitter (DSI PhysioTel® ETA-F10, Harvard Biosciences, Inc. Holliston, Massachusetts, USA) itself was placed in a subcutaneous pouch in the flank, allowing for the wires to run subcutaneously to the implantation site. The skin was closed with a simple interrupted suture (absorbable suture thread, EickFil, Eickemeyer) and secured by Michel suture clips (F.S.T.). Cages were placed on individual radio-receiving plates (DSI PhysioTel® RPC-1, Data Sciences International, St. Paul, USA) and recorded EEG signals were transmitted, together with synchronized video recordings (MediaRecorder Software, Noldus Information Technology, Wageningen, Netherlands), to an input exchange matrix (DSI PhysioTel® Matrix 2.0 (MX2), Ponemah software, DSI, Data Sciences International, St. Paul, USA). The animals were monitored at least 30 min before the kainate injection (baseline) and for 24 h (SE) - 14 days post kainate injection (early chronic phase). At the end of the respective recording period, animals were perfused and brains were processed for immunohistochemical analysis (Figure 5 C, E).

6.3.3.3. ECoG electrode implant for combined *in vivo* 2P-LSM

After exposing the skull, a custom-made holder for head restraining was applied and fixed with dental cement (RelyX®, 3M ESPE). Then, a standard craniotomy (3-4 mm in diameter) (Cupido et al., 2014; Kislin et al., 2014) was performed over the somatosensory cortex (3.4 mm posterior to bregma and mediolateral 1.5 mm) and the surface electrode was placed on the dura mater before applying the glass coverslip (Glaswarenfabrik Karl Hecht, #1.5 thickness code). The ground electrode (platinum wire) was placed centred on the cerebellum. Finally, all components were fixed with dental cement. Three days post electrode implant (dpE), the first imaging session (baseline) took place. Within the following 2 days, animals were injected with either kainate or saline and imaged for about 2 h post injection (SE).

Depending on the quality and visibility of the cranial window, animals were imaged on day(s) 4, 8, 9, 10, 13 and/ or 18 post injection. Perfusion for immunohistochemical analysis was performed 28 days post injection (Figure 5 D, E).

6.3.3.4. Awake imaging

Prior to Ca²⁺ imaging sessions, animals were habituated according to adapted protocols without water restriction (Guo et al., 2014; Kislin et al., 2014). During imaging sessions, animals remained head-fixed. Isoflurane anesthesia was used to headfix mice and in between recording sessions. Individual recordings ranged from 5-15 min, depending on the animals' condition.

6.3.4. Microscopy and ECoG recordings

6.3.4.1. *In vivo* two photon laser-scanning microscopy setup

Images were acquired on a custom-made two photon laser-scanning microscope (2P-LSM) setup with a mode-locked Ti:sapphire laser (Vision II, Coherent) using ScanImage software (Pologruto et al., 2003). Additionally, the setup was equipped with XY-galvanometer-based scanning mirrors (Cambridge Technology). The excitation wavelength of the laser was tuned to 890 nm and a 20x / 1.0 water-immersion objective (W Plan-Apochromat, Carl Zeiss) was used. Signals were detected by photomultiplier tubes (PMT) H10770PB-40 (Hamamatsu). Images were acquired with a frame rate of 3.3Hz at a laser power of 30-50 mW (under the objective). Field of views (FOV) consisted of a single focal plane for Ca²⁺-imaging and were chosen 256 μ m x 192 μ m (512 x 384 px), at a depth of 50-100 μ m (from the dura mater).

6.3.4.2. ECoG recording synchronized with *in vivo* 2P-LSM

The ECoG recording system consisted of a 16-channel biosignal amplifier (g.USBamp, gTec) and a custom-made recording software (MATLAB / Simulink, MathWorks, M. Schweigmann). The ECoG signals were acquired with a sampling rate of 1.2 kHz. Raw signals (with exception of the synchronization signals) were filtered with a band pass filter of 0.5-250 Hz and a notch filter (50 Hz). An additional preamplifier (g.HEADstage, gTec) was used to avoid input saturation of the biosignal amplifier. In combined experiments with *in vivo* 2P-LSM, the driving voltage of the scanning mirrors was used to acquire synchronization signals per frame.

6.3.4.3. Automated epifluorescence microscopy on fixed brain slices

Immunostained brain slices were scanned with the automated slide scanner AxioScan.Z1 (Zeiss Jena, Germany). The slide scanner is an epifluorescence microscope equipped with a LED light source (Colibri 7; Zeiss Jena, Germany) as well as Plan-Apochromat 10x / 0.45 and 20x / 0.8 objectives. Images were acquired with appropriate filter sets (Table 8) in 7 μ m thick stacks, applying variance projection settings.

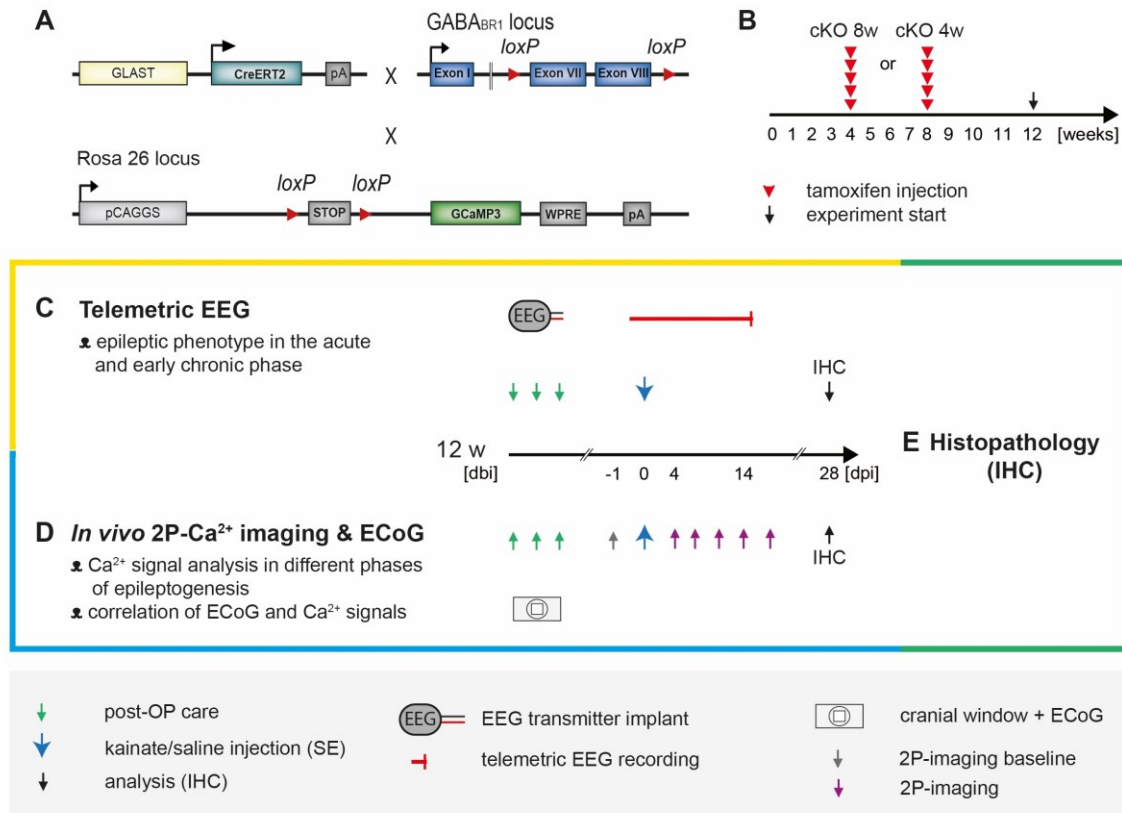


Figure 5 Experimental design

A The tamoxifen-inducible GLAST-CreERT2 x GABABR1^{fl/fl} x GCaMP3 mouse line was employed for deletion of the astroglial GABAB receptor and expression of the Ca²⁺ sensor GCaMP3 in astrocytes. **B** Two different cKO induction protocols were designed to study the effects of GABA_B receptor deletion after a short and a prolonged waiting period between tamoxifen injection and experiment start. **C** Animals were implanted with telemetric EEG transmitters possessing two electrode wires that were implanted intracerebrally. The recording started minimum 30 min before the kainate injection (baseline) and lasted for at least 24 h (SE) and up to 14 days (early chronic phase) post kainate injection. **D** After cranial window surgery and ECoG electrode application, Ca²⁺ imaging sessions took place before kainate injection (baseline), during SE and at various time points post injection. **E** At the end of the respective experiments (kainate injection alone or in combination with telemetric EEG / 2P-imaging and ECoG), animals were generally perfused 28 days post kainate / saline injections for immunohistochemical analysis.

Table 8 AxioScan.Z1 filter sets

Dye	Excitation [nm]	Beam splitter [nm]	Emission [nm]
DAPI	353	405	410 - 440
Alexa Fluor 488	475	495	503 - 537
Alexa Fluor 546/ 555	567	573	580 - 611
Alexa Fluor 633/ 647/ Cy5	630	652	661 - 703
Alexa Fluor 750	735	762	770 - 800

6.3.5. Data analysis

6.3.5.1. Telemetric EEG data

EEG data were analyzed with the Neuroscore software (Version 3.3.1., Data Sciences International). EEG signals were filtered with a 2-200 Hz band pass and 50 Hz band stop (Notch) filter. Absolute spectral powers of the lower γ range (30-50 Hz) were computed by fast Fourier transform (FFT) in 10 s episodes. Baseline recordings were averaged over 5 min and *status epilepticus* (SE) recordings over 10 min. Electrographic recordings were analyzed using a customized detection protocol adapted from (Deshpande et al., 2020) (Table 9). Subsequently, the detected signals were manually screened and verified based on the synchronized video monitoring.

Table 9 Seizure detection parameters in Neuroscore

Absolute threshold [μ V]	10 x standard deviation of the baseline
Maximum spike interval	0.1-2.5 s
Minimum train duration	10 s
Minimum number of spikes	50

Seizures were characterized by high frequency spiking and ceased with a post-ictal depression (flattening of the EEG). Furthermore, seizures were categorized as non-convulsive (nc, stages 1-2) or convulsive (cs, \geq stage 3) according to the following modified Racine scale described by Sharma and colleagues: “*stage 1, absence-like immobility; stage 2, hunching with facial automatism and/or abducted forelimb/s; stage 3, rearing with facial automatism and forelimb clonus; stage 4, repeated rearing with continuous forelimb clonus and falling (loss of righting reflex); and stage 5, generalized tonic–clonic convulsions with lateral recumbence or jumping and wild running followed by generalized convulsions*” (Racine, 1972; Sharma et al., 2018). The total duration of SE was defined from the first recorded seizure to the first seizure-free period lasting at least 1 h. The latent phase duration was considered as the time interval from 36 h post SE until the first spontaneous seizure (= beginning of chronic phase).

6.3.5.2. Analysis of Ca^{2+} imaging and ECoG with MSparkles

Ca^{2+} imaging data and simultaneously acquired ECoG recordings were analyzed with the custom-made MATLAB tool MSparkles version 1.8.19 (Stopper et al., in preparation). Ca^{2+} imaging data were pre-processed and subsequently analyzed with the activity-dependent method (Table 10).

Analyzed Ca^{2+} signal properties (amplitude, duration, integrated fluorescence, ROI area) were averaged per recorded field of view (FOV). ECoG data were processed with an extension of MSparkles' Ca^{2+} analysis module (G.Stopper, unpublished). Pre-processing and analysis parameters are summarized in Table 11.

Table 10 Ca^{2+} signal analysis parameters in MSparkles

Activity-dependent Ca^{2+} signal analysis	
<i>Pre-processing</i>	
Digital gain (offset)	50 brightness level [A.U.]
PURE-LET denoise	
Temporal median filter	Kernel half-size = 2 samples
Stack registration	Reference = frame 1
<i>F₀ configuration</i>	
Smoothing: gauss filter	Kernel half-size = 5 px; $\sigma = 2$
Outlier removal: mean SD	Iterations = 3; $\sigma = 2$
Guidance signal	Order = 6; optimizer = min. error
F ₀ fit	Polynomial order = 5
<i>ROI detection & analysis</i>	
Detrending	$(F - F_0) / F_0$
Segmentation method: correlation	Threshold = 0.6
Range image smoothing	$\sigma = 1$; median filter size = 3
Guided threshold	Detector sensitivity = 95 %
Minimum ROI area	20 px
Signal filtering	Iterations = 3; kernel half-size = 7
Minimum peak prominence	0.15
Signal duration reference	Full width at half maximum (50 %); sub-signals excluded
Maximum signal duration	50 s
Signal classification thresholds (amplitude)	0.3, 0.5, 1, 1.5
<i>Synchronicity analysis</i>	
Synchronicity duration reference	25 %; sub-signals excluded
Synchronicity threshold for analysis	0.5 (=50 % of simultaneously active ROIs)

Table 11 ECoG analysis parameters in MSparkles

ECoG analysis	
<i>Pre-processing</i>	
Notch filter	50 Hz
Band pass filter	2-200 Hz
<i>Spike train detection</i>	
Threshold	200 % of baseline
Maximum spike interval	2.5 s
Minimum train duration	10 s
<i>ECoG and mean Ca²⁺ fluorescence correlation analysis</i>	
Gauss filter (ECoG)	Width = 0.025 s; $\sigma = 10$

Out of eight recording channels, a single channel with the best signal-to-noise-ratio was chosen for analysis. Detected epileptiform events were manually sub-classified in seizures (clear post ictal depression) and spike trains (Figure 6 B). Synchronous Ca²⁺ events involving the simultaneous activation of ≥ 50 % of detected ROIs (Figure 6) were analyzed in terms of general properties (e.g. duration, peak value) and occurrence with respect to the type of epileptiform event.

Ca²⁺ waves originating during strong animal movement or appearing as spreading depression-like waves at the end of epileptiform events were excluded from further analysis. To assess the timing (offset) between the ECoG and Ca²⁺ elevations, the cross-correlation between the average epoch power over all eight ECoG channels (10 s epochs) and synchronicity index was computed. For analysis, only events with correlation coefficients ≥ 0.7 were considered and events with double synchronicity peaks were excluded (Figure 6 C). Positive offset indicates that the EEG epoch power is led by the synchronous Ca²⁺ event and vice versa for negative offset values.

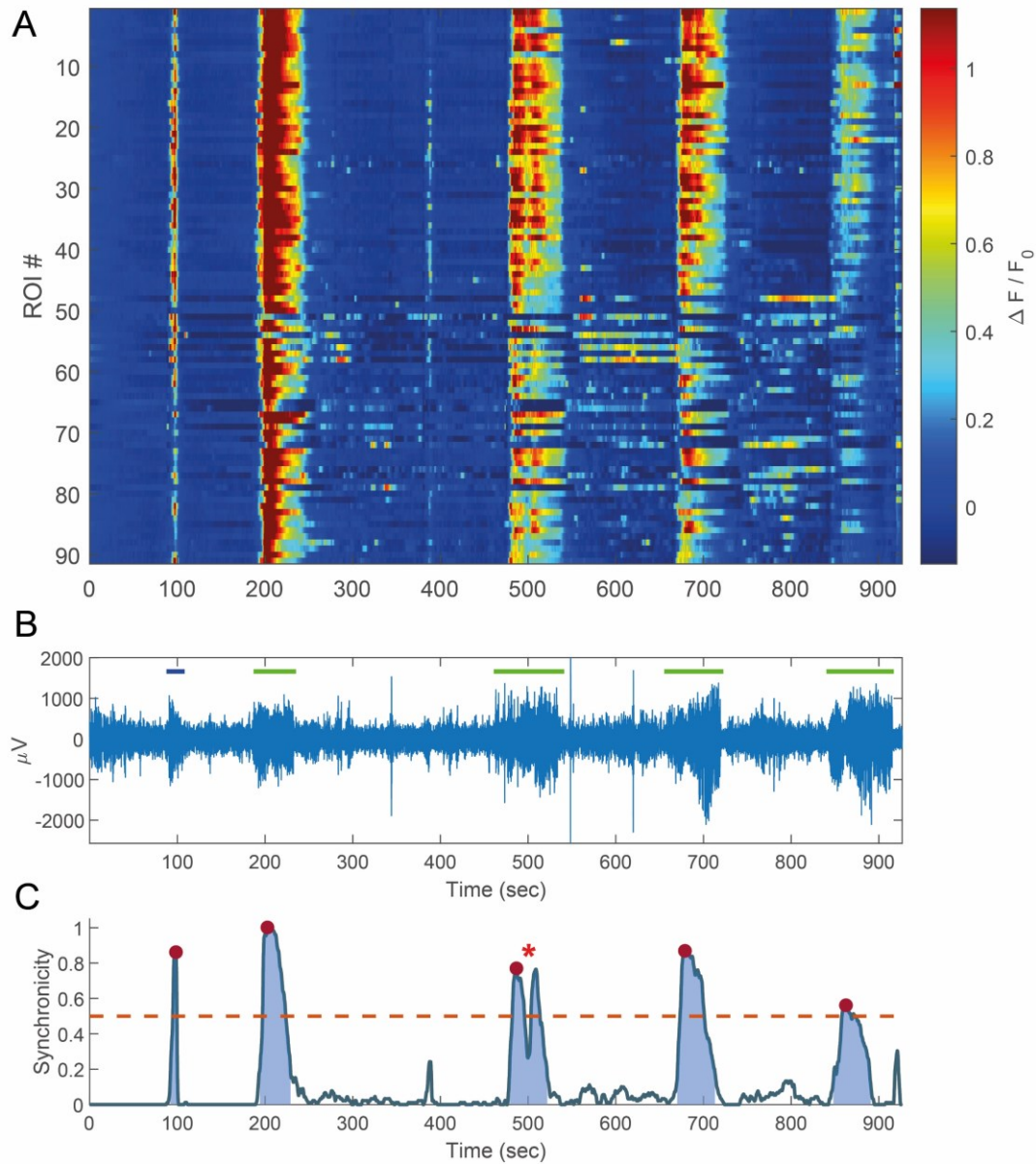


Figure 6 Analysis of epileptiform and synchronous Ca^{2+} events

A Heatmap illustrating synchronous rises in fluorescence ($\Delta F/F_0$). **B** ECoG signal with detected epileptiform events (blue = spike train; green = seizure). **C** Synchronicity index reporting the proportion of simultaneously active ROIs. Red asterisk marks an exclusion criterium for correlation analysis due to double synchronicity peaks.

6.3.5.3. Immunohistochemical data

Immunostainings were analyzed via measurement of fluorescence intensity in cortex and hippocampus of ipsi- and contralateral sides (Figure 7). On average the cortical ROIs measured $3.2 \pm 0.6 \text{ mm}^2$, the hippocampal ROIs measured $2.8 \pm 0.5 \text{ mm}^2$ and hypothalamic areas for normalization measured $0.9 \pm 0.3 \text{ mm}^2$. To assess the extent of granule cell dispersion, the granule cell layer width was measured at four positions (T1-T4) on the upper and lower blades of the dentate gyrus (Deshpande et al., 2020) (Figure 7). The positions were determined by drawing a line from the hilus to the bend of the upper blade (continuous line, Figure 7). At the lateral extremity, another vertical line was drawn (D, Figure 7). T1 / T2 were measured at the lateral extremity of line D and T3 / T4 were measured medially, at halfway from the tip of the hilus. T1-T4 were then averaged per slice.

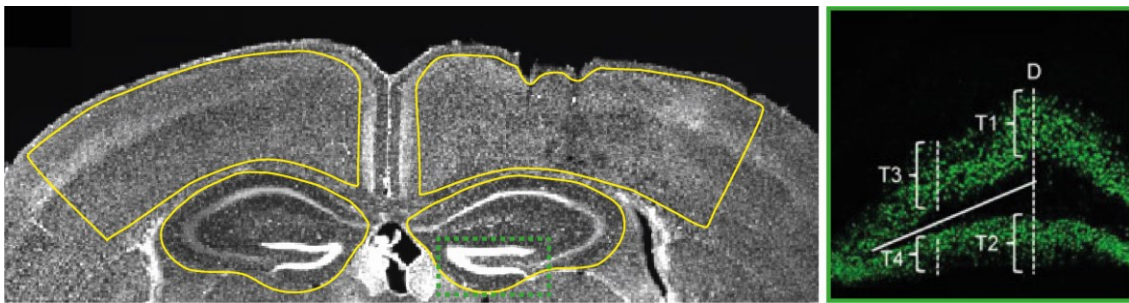


Figure 7 Fluorescence intensity measurement and granule cell dispersion (GCD) assessment

ROIs for fluorescence intensity measurements in cortex and hippocampus (yellow) and measurements of the dentate gyrus granule cell layer width (right panel modified from (Deshpande et al., 2020)).

6.3.5.4. Statistics

Statistical analysis was conducted with GraphPad Prism 8. Datasets were tested for normality and handled according to parametric and non-parametric statistical procedures. Outlier detection was performed with GraphPad Prisms Rout method ($Q = 1 \%$). Data are presented as mean \pm SEM or median with interquartile range (IQR), test details are given in the corresponding figure legends.

6.3.6. Mouse administration and veterinary licenses

Mice administration was performed with PyRAT (Python based Relational Animal Tracking, Scionics Computer Innovation GmbH). Animals were kept and bred in the animal facility of the Center for Integrative Physiology and Molecular Medicine (CIPMM, Homburg) in strict accordance with the European and German guidelines for the welfare of experimental animals. Animal experiments were approved by the Saarland state's "Landesamt für Gesundheit und Verbraucherschutz" in Saarbrücken/ Germany (license number: 71/2013, 36/2016, 08/2021).

7. RESULTS

7.2. Adaptation of the unilateral *intracortical* kainate injection model of temporal lobe epilepsy

7.2.1. Optimized injection procedure

To apply the unilateral *intracortical* kainate injection model of human temporal lobe epilepsy (TLE) (Bedner et al., 2015) for *in vivo* 2P-imaging, we adapted it with the primary objective to further reduce mechanical tissue damage. Essential modifications included the use of a thinner injection needle (34 G vs 28 G) and reduction of injection depth (DV:1.3 mm vs 1.5 mm). In addition, we temporally separated the procedures of EEG transmitter implantation and kainate injection to record a genuine baseline pre kainate administration. The first step in confirming the model validity, was to record telemetric EEG data and perform immunohistochemical analysis after saline injection (Figure 8 A). As expected, saline injection did not induce seizures and only occasionally isolated spikes could be observed (Figure 8 B). We assessed glial cell reaction caused by the cortical lesion in the acute state four days post injection and 28 days post injection, since in the chosen TLE model, histopathological hallmarks manifest three to four weeks post kainate injection (Bedner et al., 2015; Deshpande et al., 2020). We stained for GFAP and Iba1 to visualize the glial scar formed by reactive astrocytes and activated microglia, respectively. Four days post injection, we observed strong glial activation at the injection site that extended beyond the non-acutely lesioned tissue (Figure 8 C). At this time point, microglial reaction is already well advanced, since microglia respond within minutes to hours after CNS injury. The peak of astroglial reactivity however is expected four to seven days later (Burda and Sofroniew, 2014). In the early chronic phase, 28 days post injection, the large inflammatory reaction had subsided and activated astrocytes and microglia were restricted to the lesion core (Figure 8 C). Importantly, no considerable mechanical damage was inflicted on the hippocampus and no prolonged cortical or hippocampal inflammation could be observed outside the lesion core.

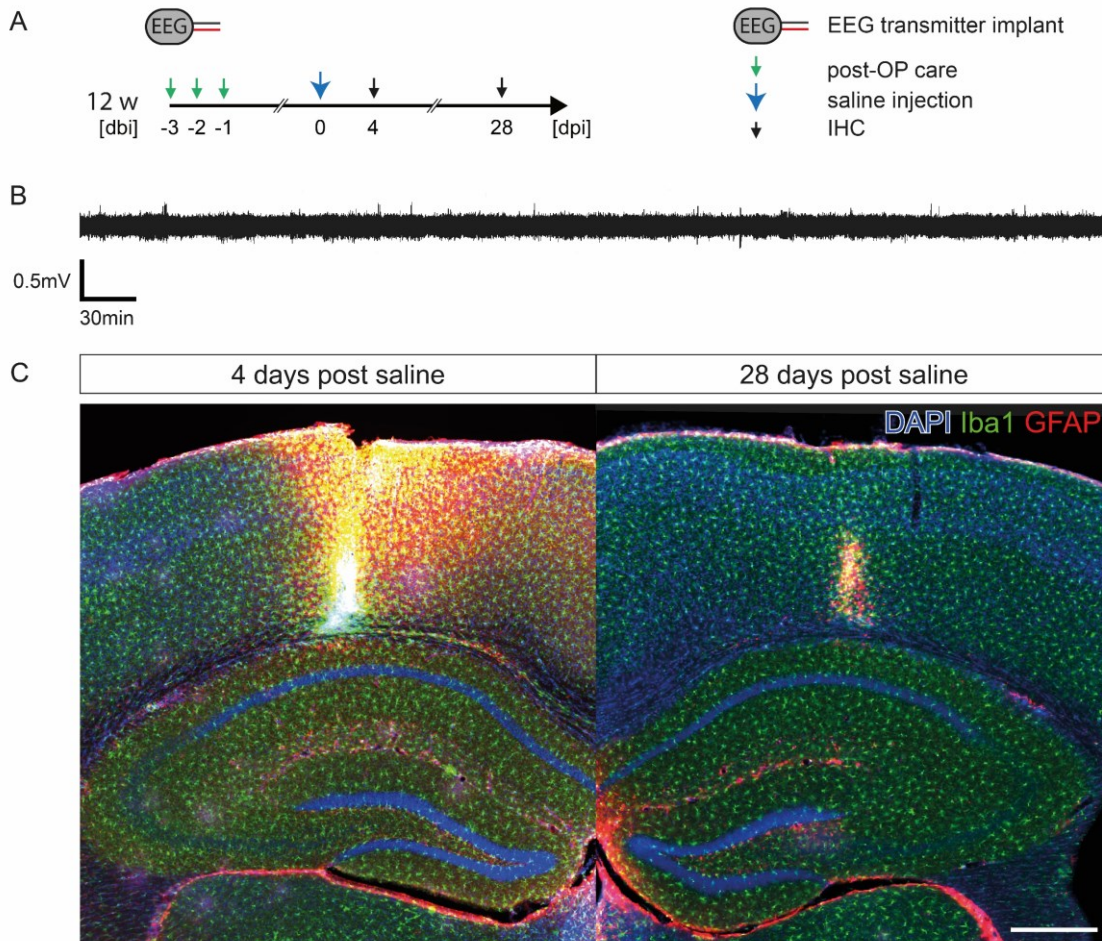


Figure 8 Unilateral intracortical saline injection induces an acute lesion but neither electrographic seizures nor histopathological hallmarks of TLE

A Animals were implanted with EEG transmitters and received a unilateral intracortical saline injection. Immunohistochemical analysis (IHC) was performed 4 or 28 days post injection to assess acute and chronic effects. **B** Saline injection does not induce electrographic seizures; example trace displays the first 12 h post injection. **C** The unilateral intracortical injection provokes an acute cortical lesion, marked by microglial (Iba1) and astroglial (GFAP) activation four days post injection. 28 days post injection, the global inflammatory reaction declined leaving a glial scar restricted to the injection site. The hippocampus was not subjected to mechanical damage and did not exhibit any macroscopic pathological changes. Scale bar = 500 μ m. dbi: days before injection, dpi: days post injection.

7.2.2. Generalizing seizures spread to contralateral cortical areas and evoke stereotypical astroglial Ca²⁺ waves

The intracortical kainate injection model of TLE (Bedner et al., 2015) was further adapted for *in vivo* 2P-imaging synchronized with ECoG recording. In this context, we faced two major concerns. Firstly, we intended to avoid performing the injection inside or in close proximity to the cranial window, since the acute lesion and direct kainate application may additionally modify Ca²⁺ signals. Secondly, we aimed at performing baseline recordings prior to kainate injection in order to obtain individual internal controls. Thus, we exploited the characteristic feature of secondarily generalizing seizures to propagate to other brain areas, including contralateral structures. We temporally and spatially dissociated the cranial window including cortical surface electrode implantation (ECoG, right hemisphere) and kainate injection site (left hemisphere) (Figure 9 A). The eight-channel liquid crystal polymer (LCP) ECoG electrode allowed for simultaneous Ca²⁺ imaging via a central optical window and showed excellent long-term biocompatibility *in vivo* (Figure 9 A, Suppl. figure 7, Schweigmann, Caudal et. al, in press, Frontiers in Cellular Neuroscience). Combined *in vivo* 2P-imaging and ECoG recording in SE revealed the manifestation of large, stereotypical astroglial Ca²⁺ waves during generalized seizures (Figure 9). The described waves occupied the entire field of view (FOV) and could be observed in control and astroglial GABA_BR cKO animals (Figure 9 B).

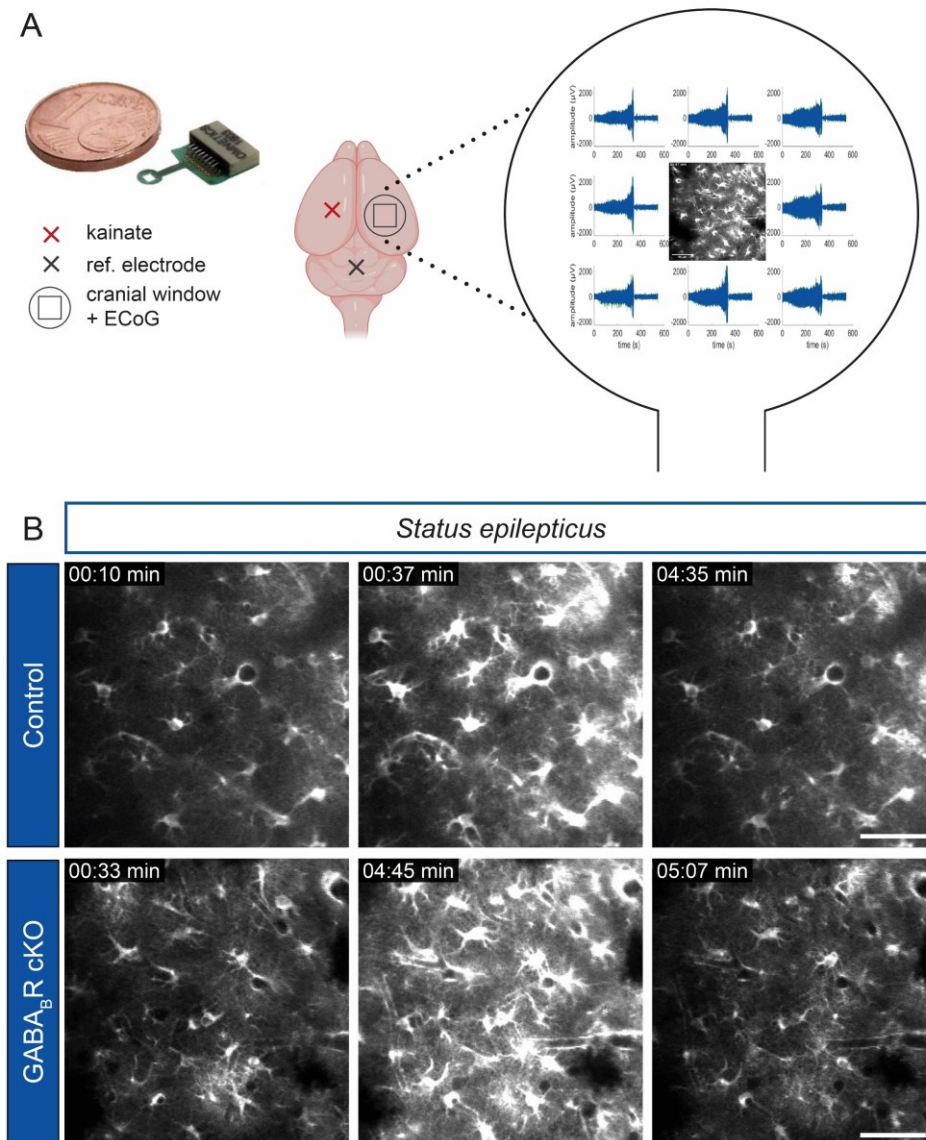


Figure 9 Synchronized ECoG recording and *in vivo* 2P Ca^{2+} imaging revealed the generation of stereotypical astroglial Ca^{2+} waves in the cortex during seizures

A The eight-channel liquid crystal polymer surface micro-electrode was implanted underneath the cranial window, contralateral to the kainate injection site. The central spare square of the LCP electrodes allowed for simultaneous *in vivo* 2P- Ca^{2+} imaging and ECoG recording (blue traces). The eight electrode contacts are arranged in a square manner around the imaging field. In *status epilepticus*, large astroglial Ca^{2+} waves were observed during seizure episodes. **B** These large Ca^{2+} waves encompassed the entire field of view and occurred in controls and GABA_B cKOs. Single frames of *in vivo* 2P-recordings of one field of view (FOV), scale bars = 50 μm .

7.2.3. Cortical astroglial Ca²⁺ signaling is enhanced during kainate-evoked epileptiform activity *in vivo*

The second aspect in the validation of our TLE model for *in vivo* 2P Ca²⁺ imaging was to verify the specificity and reliability of intracortical kainate injection in the modulation of basic Ca²⁺ signal properties in the contralateral hemisphere. In contrast, saline injection gives insight into potential changes of Ca²⁺ signal properties originating from the simple mechanical damage in the contralateral hemisphere. Thus, we considered GABA_BR^{wt} x GLAST-Cre^{ERT2} x GCaMP3 (ctrl 8w) and GABA_BR^{fl/fl} x GLAST-Cre^{ERT2} x GCaMP3 (cKO 8w) mice separately in the analysis of general Ca²⁺ signal properties in baseline, *status epilepticus* (SE) and four days post (4 dpi) kainate (KA) or saline (sal) injection (Figure 10 A).

In SE, Ca²⁺ signal amplitude was increased two-fold compared to baseline (SE ctrl KA = 1.2 $\Delta F/F_0$ vs base ctrl KA = 0.6 $\Delta F/F_0$; p = 0.0005; medians) and 1.7-fold compared to SE after saline injection in controls (SE ctrl KA = 1.2 $\Delta F/F_0$ vs SE ctrl sal = 0.7 $\Delta F/F_0$; p = 0.049; medians) (Figure 10 B). GABA_BR cKOs showed similar increases of Ca²⁺ signal amplitude of 1.4 times compared to baseline (SE cKO KA = 0.7 $\Delta F/F_0$ vs base cKO KA = 0.5 $\Delta F/F_0$; p = 0.007; medians) and SE post saline (SE cKO KA = 0.7 $\Delta F/F_0$ vs SE cKO sal = 0.5 $\Delta F/F_0$; p = 0.03; medians) (Figure 10 C). Moreover, kainate injection prolonged Ca²⁺ signal duration in both groups during SE. In comparison to baseline, kainate-treated control animals exhibited a prolongation of 5.6 s (SE ctrl KA = 12.6 s vs base ctrl KA = 7.0 s; p = 0.001; medians) (Figure 10 D). Meanwhile, direct comparison of kainate- and saline-induced SE showed a non-significant prolongation in controls (SE ctrl KA = 12.6 s vs SE ctrl sal = 7.8 s; p = 0.08; medians) (Figure 10 D). Likewise, kainate-treated cKOs displayed prolongation of Ca²⁺ signals by 5.0 s relative to baseline (SE cKO KA = 12.7 s vs base cKO KA = 7.7 s; p < 0.0001; medians) and 6.1 s relative to saline injection (SE cKO KA = 12.7 s vs SE cKO sal = 6.6 s; p < 0.0001; medians) (Figure 10 E). In line with signal amplitudes and durations, integrated fluorescence was elevated in both controls and cKO during SE. Controls exhibited a 2.6-fold rise in integrated fluorescence compared to baseline (SE ctrl KA = 32.0 $\Delta F/F_0*s$ vs base ctrl KA = 12.2 $\Delta F/F_0*s$; p = 0.0003; medians) and SE post saline (SE ctrl KA = 32.0 $\Delta F/F_0*s$ vs SE ctrl sal = 12.4 $\Delta F/F_0*s$; p = 0.03; medians) (Figure 10 F). In the same order of magnitude, cKOs showed 2.4 and 2.7-fold integrated fluorescence elevations in SE compared to baseline (SE cKO KA = 23.8 $\Delta F/F_0*s$ vs base cKO KA = 9.9 $\Delta F/F_0*s$; p < 0.0001; medians) and saline injection (SE cKO KA = 23.8 $\Delta F/F_0*s$ vs SE cKO sal = 8.6 $\Delta F/F_0*s$; p < 0.0001; medians), respectively (Figure 10 G).

Results

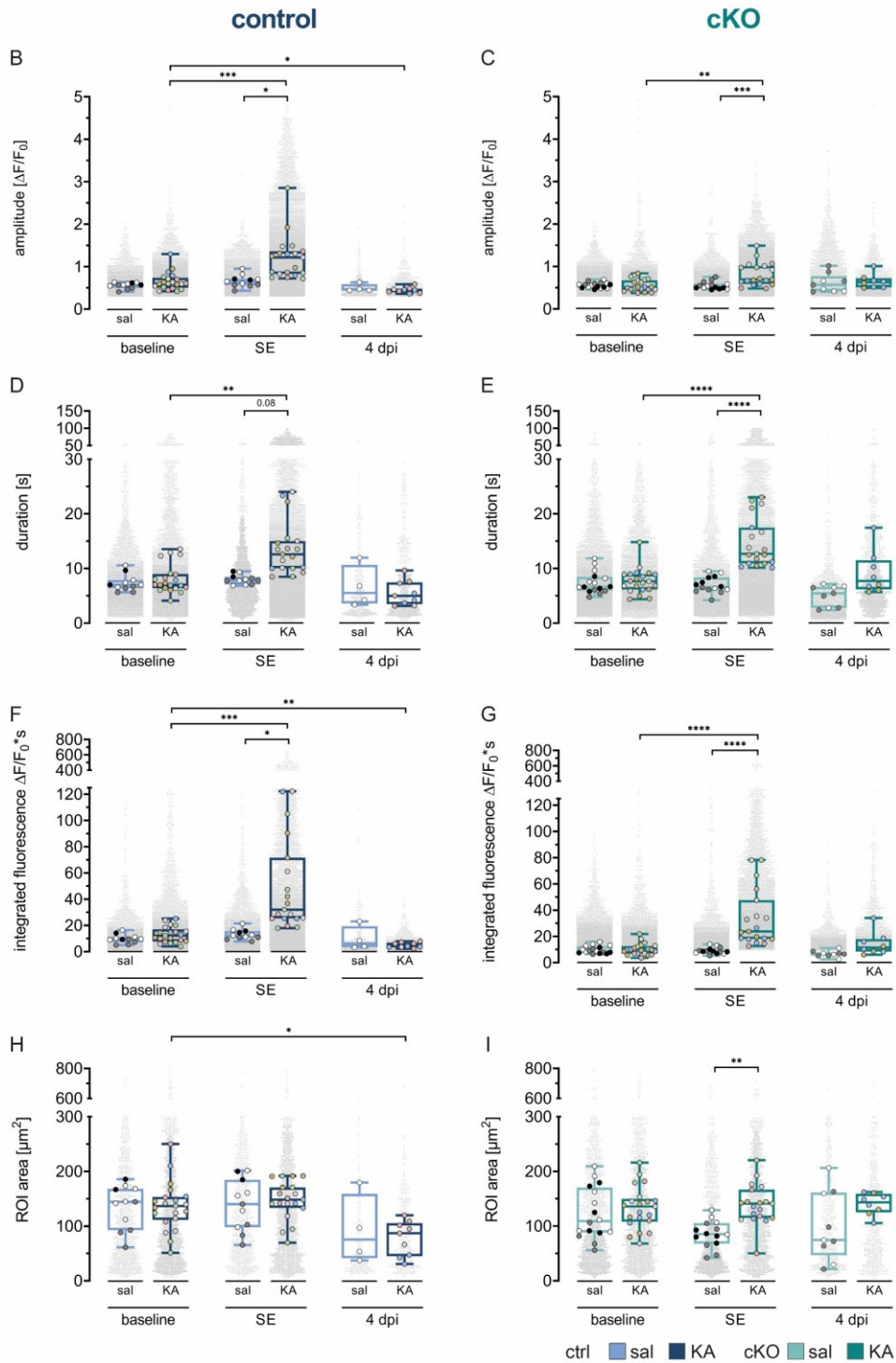
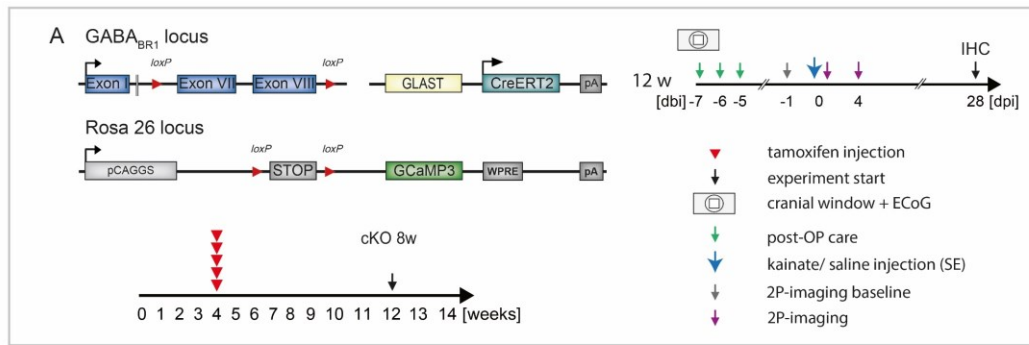


Figure 10 Kainate but not saline injection acutely enhanced general Ca²⁺ signal characteristics

A GABA_BR cKO and GCaMP3 expression in astrocytes was induced eight weeks prior to the experiment start. *In vivo* 2P Ca²⁺ imaging was performed during baseline, status epilepticus (acute) and four days post saline or kainate injection (4 dpi, latent phase). **B** Ca²⁺ signal amplitude was increased post kainate injection compared to baseline and saline injection in control. Four days post kainate injection (4 dpi), signal amplitudes fell below baseline levels. **C** In cKO, Ca²⁺ signal amplitude was enhanced in kainate-induced SE with respect to baseline and saline injection. **D-E** Ca²⁺ signals are prolonged post kainate injection in control and cKO. **F** Integrated fluorescence was increased in controls during kainate-induced SE and reduced four days post kainate. **G** Kainate raised integrated fluorescence levels during SE in cKOs. **H** In controls, ROI area was unaffected by kainate-induced SE but reduced four days post kainate injection (4 dpi). **I** ROI area was transiently increased during kainate-induced SE in cKOs.

Stats: large data points represent averages of field of views (n), colour-coded per animal (N). Baseline ctrl saline n = 11 FOV, N = 3 animals; baseline ctrl kainate n = 21 FOV, N = 5 animals; Baseline cKO saline n = 16 FOV, N = 3 animals; baseline cKO kainate n = 21 FOV, N = 5 animals; SE ctrl saline n = 12 FOV, N = 3 animals; SE ctrl kainate n = 19 FOV, N = 5 animals; SE cKO saline n = 14 FOV, N = 3 animals; SE cKO kainate n = 19 FOV, N = 5 animals; 4 dpi ctrl saline n = 4 FOV, N = 1 animals; 4 dpi ctrl kainate n = 9 FOV, N = 3 animals; 4 dpi cKO saline n = 9 FOV, N = 2 animals; 4 dpi cKO kainate n = 8 FOV, N = 2 animals. Kruskal-Wallis test followed by Dunn's post hoc test. Grey data points in the background display single Ca²⁺ signals.

ROI area was unaffected by kainate injection in controls, while an expansion from 85 µm post saline to 141 µm post kainate (medians, p = 0.004) was observed in cKO (Figure 10 H, I).

Four days post kainate injection (4 dpi, latent phase), GABA_BR cKO Ca²⁺ signal dimensions return to baseline levels (Figure 10 C, E, G, I) while control animals present reduced signal amplitude (4 dpi ctrl KA = 0.45 ΔF/F₀ vs base ctrl KA = 0.6 ΔF/F₀; p = 0.02; medians) (Figure 10 B), integrated fluorescence (4 dpi ctrl KA = 4.1 ΔF/F₀*s vs base ctrl KA = 12.2 ΔF/F₀*s; p = 0.007; medians) (Figure 10 F) and ROI area (4 dpi ctrl KA = 87 µm vs base ctrl KA = 137 µm; p = 0.03; medians) (Figure 10 H).

Recapitulating, kainate specifically induced robust increases of Ca²⁺ signal amplitude, signal duration and integrated fluorescence in SE, across groups. Modulation of ROI area was less notorious in SE. In the latent phase, cKO Ca²⁺ signal dimensions return to baseline levels while controls experience lasting reductions. Saline injection had no effects on contralateral Ca²⁺ signal amplitude, signal duration, integrated fluorescence or ROI area at any investigated time point, in any group (Figure 10 B - I).

Thus, *in vivo* 2P Ca²⁺ imaging contralateral to the kainate injection site (Figure 9) is unaffected by the injection procedure in terms of general Ca²⁺ signal dimensions and constitutes a valid model to study astroglial Ca²⁺ signaling in epileptic network function.

7.3. Astroglial GABA_BR loss induces anti-epileptic phenotype

The selected TLE model recapitulates the chronology of events seen in the human condition, namely the initiation by a precipitating event (acute phase) followed by an electrographically silent phase (latent phase) and finally the spontaneous recurrence of seizures (chronic phase) (Bedner et al., 2015). To investigate the global role of astroglial GABA_BR cKO in TLE, we implanted telemetric EEG transmitters in GABA_BR^{fl/fl} x GLAST-Cre^{ERT2} x GCaMP3 mice and monitored seizure activity together with synchronized video recording from 30 min pre kainate injection (baseline) until 14 days post kainate (early chronic phase). GABA_BR cKO was induced at two different time points to investigate whether the longevity of pre-existing GABA_BRs after excision of floxed DNA sequences would affect the outcome. The first cohort, cKO 4w, has a four week waiting period between cKO induction and experiment start, while the second cohort cKO 8w is induced earlier and therefore has a prolonged receptor deletion period of eight weeks (Figure 11 A).

Experimental *status epilepticus* (SE) elicited by kainate injection, corresponding to the acute phase, is characterized by high seizure frequency (Figure 11 B). In our paradigm, SE lasted in median for 2.83 h (IQR = 1.86) in control animals. The cKO 4w group exhibited a similar median SE duration of 2.91 h (IQR = 0.63), while the cKO 8w group displayed a slight, yet not significant, reduction to 1.96 h of median SE duration (IQR = 2.58) (Figure 11 C). Similarly, the average duration of individual seizures in SE did not vary significantly among control and GABA_BR cKO animals. In median, seizures had a duration of 47.5 – 54.6 s (ctrl: median = 53, IQR = 20.1; cKO 4w: median = 54.6, IQR = 19.1; cKO 8w: median = 47.5, IQR = 50.3) (Figure 11 B, D). The total number of seizures during SE was unchanged in GABA_BR cKO 4w but significantly reduced by 70 % in the cKO 8w group (ctrl: median = 24, IQR = 18; cKO 4w: median = 21, IQR = 13; cKO 8w: median = 7, IQR = 16; $p = 0.02$) (Figure 11 B, E). Further sub-classification of seizures into non-convulsive (nc) and convulsive (cs) (see section 6.3.5.2) uncovered that control animals tend to have more non-convulsive than convulsive seizures, while this trend is gradually reversed after GABA_BR cKO induction (Figure 11 F). Moreover, this classification revealed that the astroglial GABA_BR cKO specifically reduces the number of non-convulsive seizures from 11 (ctrl) to 2 (cKO 8w) in median, after a prolonged waiting period post cKO induction (ctrl_{nc}: IQR = 8.5; cKO 8w_{nc}: IQR = 8; $p = 0.03$) (Figure 11 F).

In addition, we calculated the total time spent in ictal activity by summing up the individual seizure durations. Despite similar average seizure durations in all groups (Figure 11 D), GABA_BR cKO 8w animals spent significantly less time in ictal activity compared to controls (Figure 11 G), due to the reduced seizure number in general (Figure 11 E). While controls spent 22.5 min in ictal activity during SE, cKO 8w animals experienced a 3.6-fold reduction, corresponding to 6.2 min total time in ictal activity in median (Figure 11 G).

The severity of SE is commonly assessed by quantifying (lower) γ -band power (30-50 Hz), since it has been associated with hypersynchronous network activity, seizure onset and seizure propagation in the temporal lobe (Sato et al.; Lévesque et al., 2009; Deshpande et al., 2020). Firstly, we quantified the relative increase of γ -band power during SE over baseline. In general, γ -band power was increased at least 2.7 times over baseline level during SE (Figure 11 H, I). Notably, control animals displayed a higher increase in γ -band power than GABA_BR cKO animals (medians, 3.6 x vs. 2.7-2.8 x, $p = 0.03$). To further clarify the origin of this reduction, we quantified absolute γ -band powers separately in baseline (Figure 11 J) and SE (Figure 11 K). During baseline conditions, GABA_BR cKO 8w animals had significantly reduced γ -band power compared to controls and cKO 4w (median 1.8-fold reduction, $p = 0.0001$) (Figure 11 H, J). In SE, cKO 4w show a slight, non-significant 1.3-fold median decrease in γ -band power, while cKO 8w show a significant, 2.5-fold median reduction compared to controls and a median reduction by 50 % compared to cKO 4w (Figure 11 H, K). Consequently, the lowest γ -band powers in baseline and SE were observed in GABA_BR cKO 8w, after a prolonged receptor deletion period. The intermediate cKO 4w time point did only slightly reduce γ -band power during SE, but not in baseline conditions.

As previously mentioned, the acute phase is followed by a latent phase characterized by the absence of electrographic seizures until the spontaneous recurrence of a seizure, marking the beginning of the chronic phase. Control and cKO 8w animals had similar latent phases of 6.3 and 6.5 days in median, while cKO 4w animals had a longer latency of 8 days in median (ctrl: IQR = 2.3; cKO 4w: IQR = 5.5; cKO 8w: IQR = 8.5; $p = 0.02$) (Figure 11 L).

Results

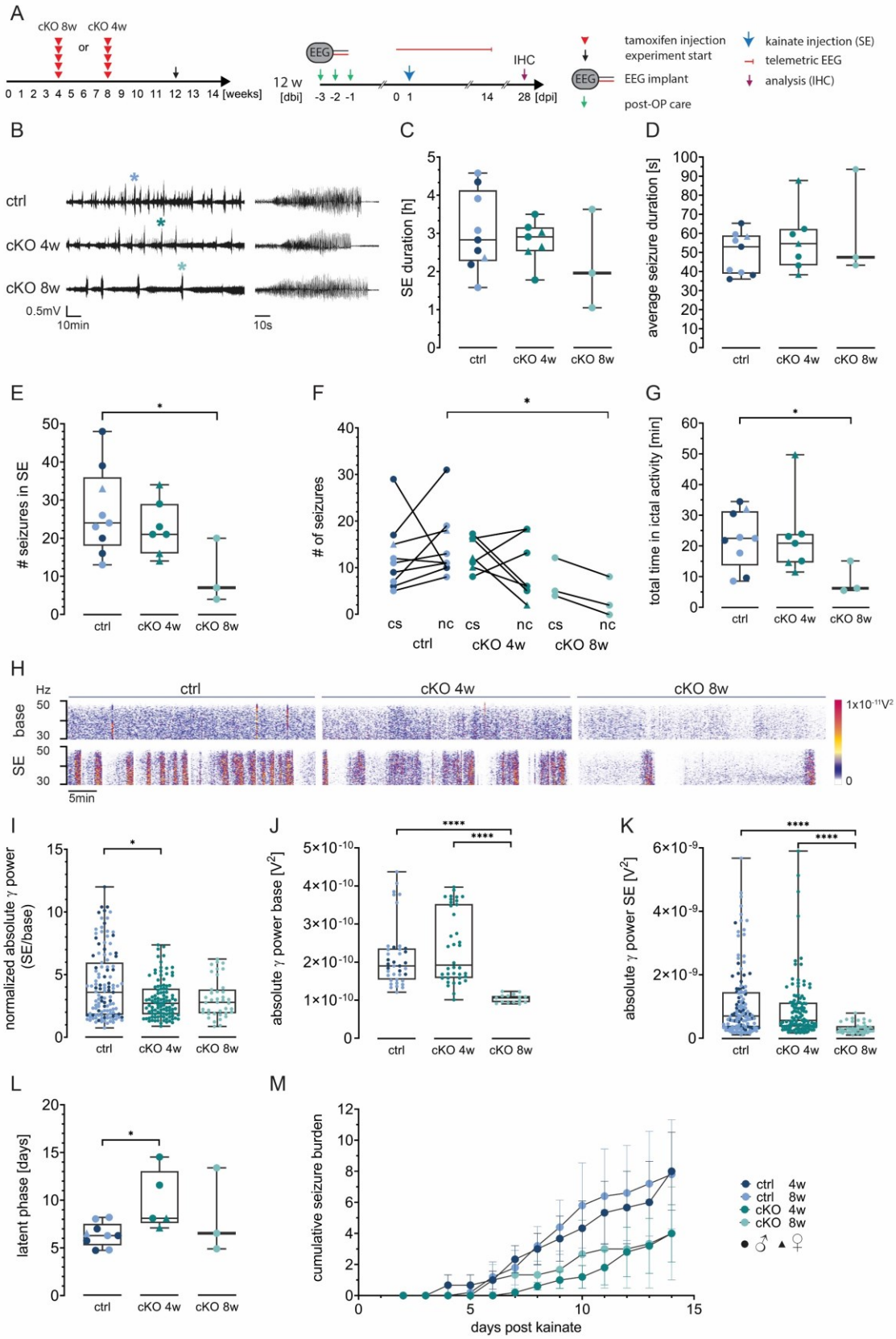


Figure 11 Astroglial GABA_BR loss reduces seizure burden and γ band power

A Two different protocols to study the GABA_BR cKO effect after a short (cKO 4w) or long (cKO 8w) period post tamoxifen injection. Telemetric EEG recording was performed from 30 min pre (baseline) until 14 days post kainate injection. Brains were further processed for immunohistochemical analysis 28 days post kainate. **B** Representative EEG traces during *status epilepticus* (SE). Individual seizures highlighted by stars are magnified in the right panel. **C** SE duration was not significantly different between control and astroglial GABA_BR cKO animals, irrespective of cKO induction time point. **D** Average seizure duration was comparable between all cohorts. **E** The median number of seizures during SE was reduced by 70% in cKO 8w compared to control animals. **F** Behaviour-based classification of seizures into convulsive (cs) and non-convulsive (nc) revealed specific reduction of nc seizures in the GABA_BR cKO 8w group. **G** The prolonged cKO induction period (cKO 8w) reduced the total time spent in ictal activity during SE to 30% relative to controls and cKO 4w animals. **H** Power spectra of the lower γ range (30-50 Hz) during baseline (base) and SE illustrate the increase of lower γ power in SE as well as the reduction of baseline lower γ power in astroglial GABA_BR cKOs. **I** Normalized lower γ power (SE/base) reflects an up to 3.6-fold increase of lower γ power in SE over baseline levels in control animals but was reduced in GABA_BR cKOs. Spectral powers were calculated via fast Fourier transform (FFT) in 10s episodes, averaged over 10min during SE and normalized to the baseline average. **J** Prolonged GABA_BR cKOs (8w) had significantly reduced baseline absolute lower γ power compared to cKO 4w and controls. Spectral powers were calculated via FFT in 10 s episodes and averaged over 5 min. **K** In SE, absolute lower γ power was significantly reduced in GABA_BR cKOs with cKO 8w induction compared to controls and cKO 4w. Spectral powers were calculated by FFT in 10 s episodes and averaged over 10 min. **L** The latent period lasted for 6.3 days in median (ctrl and cKO 8w), but up to 8 days in cKO 4w animals. **M** The cumulative seizure burden post SE up to the early chronic phase suggests sustained anti-epileptic effect of astroglial GABA_BR cKO. Data are displayed as mean \pm SEM. Stats: Data points indicate individual animals. Control N = 9, cKO 4w N = 7, cKO 8w N = 3. Kruskal-Wallis test followed by uncorrected Dunn's test. * p < 0.05, **** p > 0.0001.

Disease progression and severity is represented by the number of spontaneous seizures during the chronic phase (Deshpande et al., 2020). We quantified the cumulative seizure burden, by summing up individual seizures, until day 14 post kainate injection. In this early chronic phase, both GABA_BR cKO cohorts show a similar reduction in chronic cumulative seizure number compared to controls (Figure 11 M). Until two weeks after kainate injection, control animals had 8 seizures while GABA_BR cKOs had 4 seizures on cumulated average. Due to the high inter-individual variability inherent to *in vivo* disease models, no statistical differences were detected. However, the already apparent differences are likely to become more obvious later in disease progression.

Summarizing, the astroglial GABA_BR deletion potently reduced the acute seizure burden in SE, which was accompanied by reduced power in the lower γ -band in baseline conditions as well as in SE. These effects were dependent on a longer receptor deletion period (cKO 8w). Our data further suggest a reduction in early chronic seizure burden in GABA_BR cKO, irrespective of cKO induction protocol.

7.4. The role of GABA_BR-dependent astroglial Ca²⁺ signaling in generalized epileptic network function

Based on the previous finding of reduced seizure burden after astroglial GABA_BR deletion, we hypothesized a role for GABA_BR-signaling in the maintenance and promotion of secondarily generalizing seizures. More specifically, we focused astroglial Ca²⁺ signaling in the cortex during generalized epileptiform activity, since it was previously shown to promote the spread of epileptiform activity within the hippocampus (Heuser et al., 2018). To gain a comprehensive insight into the modulation of cortical astroglial Ca²⁺ signaling in TLE, we explored general Ca²⁺ signal properties in baseline, *status epilepticus* and latent phase (4 days post kainate) by combining *in vivo* 2P Ca²⁺ imaging and electrocorticography (ECoG). These experiments were conducted in control and GABA_BR mutant mice with GCaMP3 expression, 8 weeks post tamoxifen administration (cKO 8w).

7.4.1. Basic Ca²⁺ signal properties are not affected by astroglial GABA_BR deletion prior to kainate or saline injection

To investigate the role of astroglial GABA_BRs in physiological conditions, we compared basic Ca²⁺ signal properties before kainate or saline injection (baseline) of control and GABA_BR cKO 8w mice (Figure 12 A). Ca²⁺ signals were analyzed using the custom-made MATLAB tool MSparkles (Stopper et al., in preparation). Specifically, regions of interest (ROI) were automatically generated via the activity-dependent analysis mode (see section 6.3.5.2). To evaluate the recorded Ca²⁺ signals, we focused on basic properties such as peak amplitude ($\Delta F/F_0$), signal duration (s), integrated fluorescence (integral of fluorescence amplitude during the lifetime of the signal, $\Delta F/F_0*s$) and ROI area (μm^2).

Ca²⁺ signal amplitudes were similar between all groups, ranging from 0.51 – 0.60 $\Delta F/F_0$ in median (Figure 12 B). Similarly, Ca²⁺ signals had median durations of 6.6 – 7.6 s and did not significantly differ between groups (Figure 12 C). Along the same lines, no significant difference in integrated fluorescence was detected among the different cohorts (9.6-12.2 $\Delta F/F_0*s$ in median) (Figure 12 D). Control and GABA_BR cKOs also exhibited comparable ROI areas extending from 109 – 144 μm^2 in median (Figure 12 E).

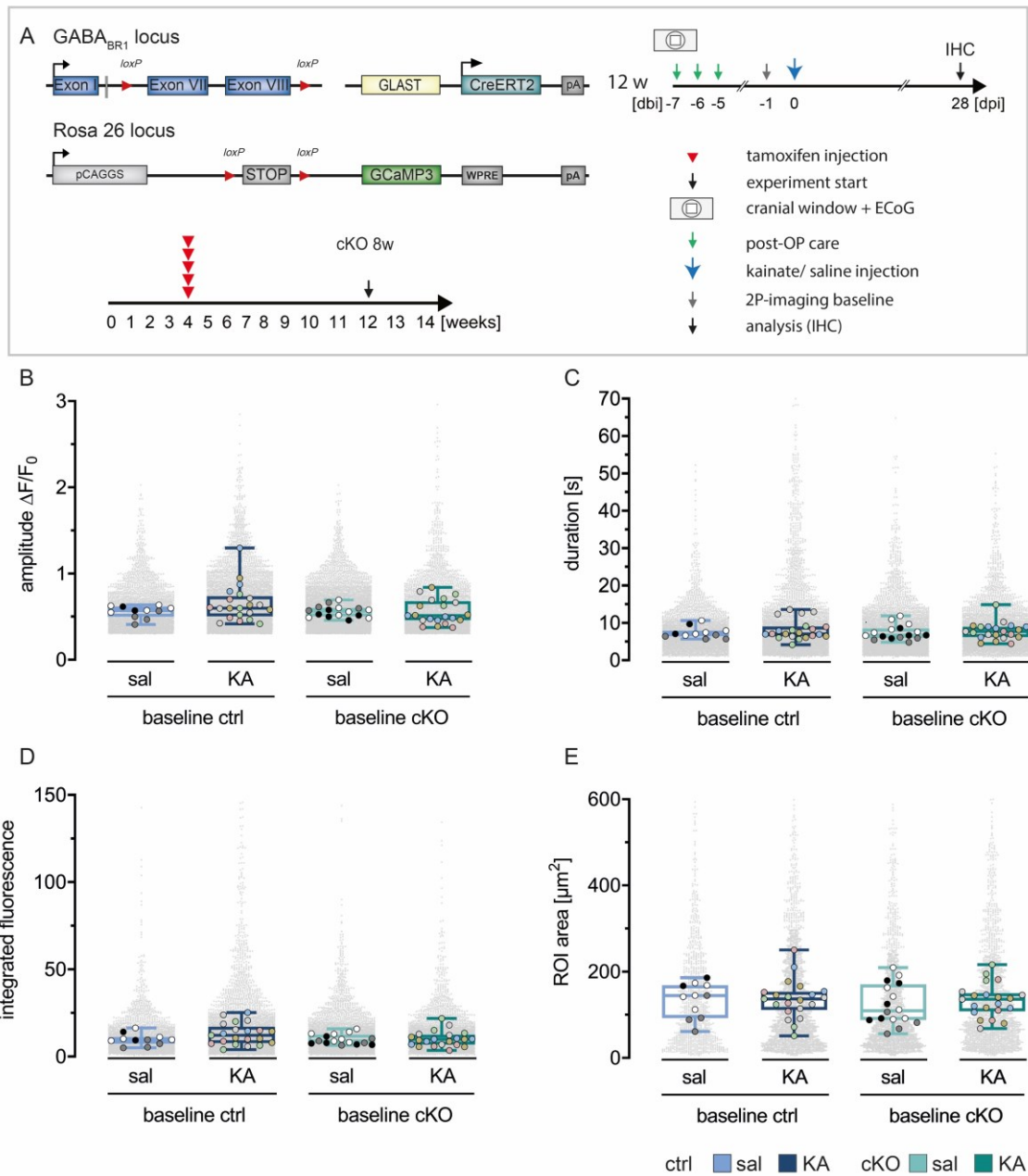


Figure 12 General Ca²⁺ signal properties do not differ between control and GABA_BR cKO during baseline

A GABA_BR cKO and GCaMP3 expression in astrocytes was induced eight weeks prior to the experiment start. *In vivo* 2P Ca²⁺ imaging was performed before saline or kainate injection to establish baseline conditions. **B** Baseline Ca²⁺ signal amplitude was comparable between control and cKO. **C** In median, baseline Ca²⁺ signals had a duration of 6.6 – 7.6 s across cohorts. **D** Integrated fluorescence levels were similar in all groups during baseline imaging. **E** ROI area ranged from 109 – 144 μm^2 and did not significantly differ between controls and cKOs. Stats: large data points represent averages of field of views (n), colour-coded per animal (N). Baseline ctrl saline n = 11 FOV, N = 3 animals; baseline ctrl kainate n = 21 FOV, N = 5 animals; Baseline cKO saline n = 16 FOV, N = 3 animals; baseline cKO kainate n = 21 FOV, N = 5 animals. Kruskal-Wallis test followed by Dunn’s post hoc test. Grey data points in the background display single Ca²⁺ signals.

When comparing control and GABA_BR cKO baseline recordings of the two different tamoxifen protocols (4w vs 8w), no differences in Ca²⁺ signal amplitude, duration or ROI area were detected (Suppl. figure 1). Only the integrated fluorescence was increased in controls from 5.9 ΔF/F₀*s in cKO 4w to 12.2 ΔF/F₀*s in cKO 8w. GABA_BR cKOs displayed a non-significant increase in integrated fluorescence between 4w and 8w protocols (5.7 ΔF/F₀*s in 4w versus 10.0 ΔF/F₀*s in 8w) (Suppl. figure 1 D). Summarizing, the deletion of the astroglial GABA_BR did not change basic Ca²⁺ signal properties in physiological conditions, compared to controls. In comparison, 4w control and cKO groups showed an increase in integrated fluorescence of comparable magnitude versus 8w groups, potentially reflecting the prolonged GCaMP3 expression due to an earlier tamoxifen injection time point. Of note, baseline values of cohorts that later received saline or kainate injection did not differ within control or cKO groups, establishing equal starting conditions.

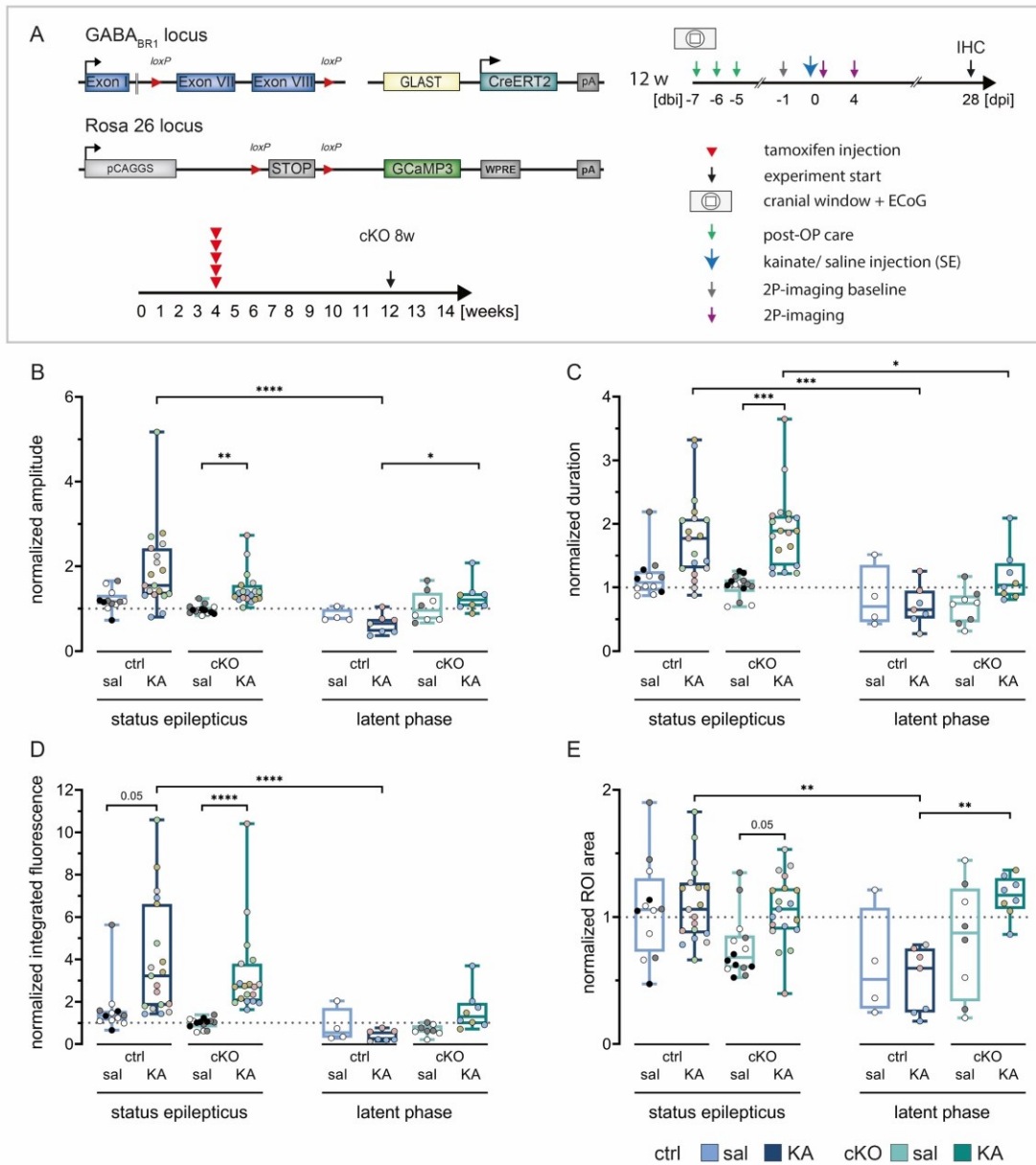
7.4.2. Astroglial Ca²⁺ signal properties are amplified in GABA_BR cKOs during *status epilepticus* and depressed in controls during the latent period

To elucidate the impact of astroglial GABA_BR on Ca²⁺ signaling during *status epilepticus* and latent phase, we profited from our experimental design and normalized the investigated Ca²⁺ dimensions to the individual baselines. Hence, we compared relative changes of Ca²⁺ signal amplitude, signal duration, integrated fluorescence and ROI area between GABA_BR^{wt} x GLAST-Cre^{ERT2} x GCaMP3 and GABA_BR^{fl/fl} x GLAST-Cre^{ERT2} x GCaMP3 animals, eight weeks post tamoxifen injection (cKO 8w) (Figure 13 A).

Figure 13 Ca²⁺ signal dimensions are acutely enhanced in GABA_BR cKOs and reduced in controls during the latent phase

A Astroglial GABA_BR cKO and GCaMP3 expression was induced eight weeks prior to experiment start. *In vivo* 2P Ca²⁺ imaging was performed during baseline, status epilepticus (acute) and latent phase (four days post saline or kainate injection). **B** Normalized Ca²⁺ signal amplitude was significantly increased in kainate-induced SE compared to saline in cKOs. In the latent phase, kainate-treated controls had reduced Ca²⁺ signal amplitudes compared to SE as well as compared to kainate-treated cKO in the latent phase. **C** Kainate-injected cKOs displayed acutely prolonged Ca²⁺ signal durations in SE compared to saline, which returned to baseline levels in the latent phase. Controls displayed a non-significant prolongation of Ca²⁺ signal duration in kainate vs saline-induced SE, but a significantly shorter duration in the latent phase compared to SE. **D** Integrated fluorescence was increased in controls and cKOs in kainate-induced SE, compared to saline. During the latent phase, controls showed a decrease in integrated fluorescence with respect to SE. **E** Normalized ROI area remained unchanged in SE but was reduced in controls during the latent period, compared to SE control and cKOs in the latent period. Stats: large data points represent averages of field of views normalized to their respective baselines (n), colour-coded per animal (N). SE ctrl saline n = 12 FOV, N = 3 animals; SE ctrl kainate n = 19 FOV, N = 5 animals; SE cKO saline n = 14 FOV, N = 3 animals; SE cKO kainate n = 19 FOV, N = 5 animals; 4 dpi ctrl saline n = 4 FOV, N = 1 animals; 4 dpi ctrl kainate n = 7 FOV, N = 3 animals; 4 dpi cKO saline n = 8 FOV, N = 2 animals; 4 dpi cKO kainate n = 8 FOV, N = 2 animals. Kruskal-Wallis test followed by Dunn's post hoc test.

Results



During *status epilepticus* (SE), normalized Ca^{2+} signal amplitude reached comparable levels post kainate in control and GABA_BR cKOs (1.6 and 1.4 in median) (Figure 13 B). However, when compared to saline injection, the relative increase in amplitude was more consistent in cKO than control animals ($p = 0.002$) (Figure 13 B). Likewise, Ca^{2+} signal duration was extended 1.8 and 1.9 times over baseline in control and cKO, respectively, while this prolongation was significant in cKOs but not controls, in comparison to saline injection ($p = 0.0004$) (Figure 13 C). Integrated fluorescence was amplified 3.2-fold in control and 2.7-fold over baseline in cKO, constituting major rises compared to saline (control $p = 0.055$, cKO $p < 0.0001$) (Figure 13 D).

In contrast to the previously mentioned Ca^{2+} signal properties, ROI area was only raised in cKOs during SE (0.7 vs 1.1 in median, $p = 0.05$), as previously described (Figure 13 E; Figure 10 H, I). Moreover, no differences in the above mentioned Ca^{2+} signal properties were encountered among controls and $\text{GABA}_{\text{B}}\text{R}$ cKOs irrespective of tamoxifen induction protocols during SE (4w vs 8w) (Suppl. figure 2).

In the latent phase, Ca^{2+} signal dimensions tended to decrease and approach baseline levels (normalized value ≈ 1), supported by the absence of significant differences to saline injections. Control Ca^{2+} signal amplitude was significantly diminished versus SE (median of 0.7 vs 1.6, $p < 0.0001$) and cKO in the latent phase (median of 0.7 vs 1.2, $p = 0.03$) (Figure 13 B). Ca^{2+} signal duration was significantly reduced in cKO compared to SE (median of 1.0 vs 1.9, $p = 0.04$), but did not differ among groups within the latent phase (Figure 13 C). In control animals, integrated fluorescence fell below baseline levels in the latent phase versus SE (median of 0.2 vs 3.2, $p < 0.0001$), however no direct differences among groups surfaced at this time point (Figure 13 D). Finally, normalized ROI area was exclusively affected in control animals during the latent phase, displaying a reduction by 40 % compared to control in SE (median of 0.6 vs 1.0, $p = 0.003$) and a 50 % reduction compared to cKO in the latent period (median of 0.6 vs 1.2, $p = 0.003$) (Figure 13 E).

Overall, in the acute phase (SE) no direct differences in normalized Ca^{2+} signal amplitude, signal duration, integrated fluorescence or ROI area were detected between control and $\text{GABA}_{\text{B}}\text{R}$ cKO mice. However, the described increases in amplitude, duration and integrated fluorescence versus saline injection were more robust in cKO. During the latent phase, Ca^{2+} signal dimensions showed a general downward trend, leading to recuperation of baseline levels in cKO. Meanwhile, kainate-treated controls fell below baseline levels, thereby exposing significant differences between control and cKO.

7.4.3. Ca²⁺ signal architecture is differentially modulated in control and GABA_BR cKO during the latent phase

Hypothesizing that Ca²⁺ signal architecture might be founded on the liaison of two basic signal characteristics, we investigated the correlation between signal amplitude and duration in baseline, *status epilepticus* (SE) and latent period (4 days post injection) of kainate-injected mice (Figure 14 A, B).

In baseline conditions, neither control nor astroglial GABA_BR cKO mice displayed a positive or negative correlation between Ca²⁺ signal amplitude and duration (Figure 14 B, C). Subsequent kainate administration induced overall positive correlations in control as well as cKO during SE, implying increasing signal amplitude with increasing signal duration (Figure 14 B, C). This positive correlation between Ca²⁺ signal amplitude and duration remained transient. In the latent phase, the positive correlation is reverted in cKOs, returning to baseline levels, while controls tend towards an overall negative correlation (Figure 14 B, C). Thus, in control animals, longer lasting signals exhibit lower amplitudes.

In general, this temporal course parallels the previous Ca²⁺ imaging results. Control and cKO Ca²⁺ signals were similarly modulated in the acute phase, followed by a rebound of cKOs towards baseline conditions. In contrast, controls experienced a lasting reduction in Ca²⁺ signal dimensions (Figure 13, Figure 14).

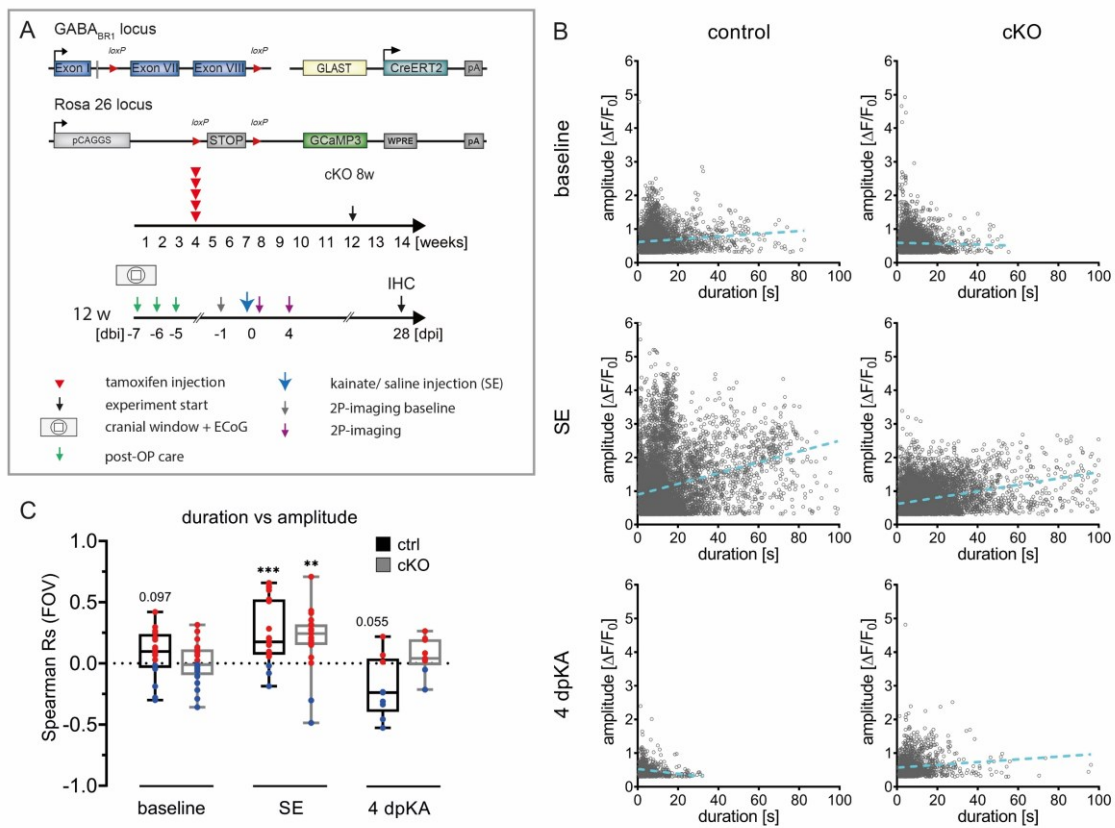


Figure 14 Ca²⁺ signal architecture is altered during epileptogenesis

A GABA_BR cKO and GCaMP3 expression in astrocytes was induced eight weeks prior to the experiment start. *In vivo* 2P Ca²⁺ imaging was performed during baseline, kainate-induced status epilepticus (acute) and four days post kainate injection (latent phase). **B** Correlation of Ca²⁺ signal amplitude and duration were modulated in control and cKO across different phases of epileptogenesis (individual Ca²⁺ signals shown). **C** In baseline conditions, Ca²⁺ signal amplitude and duration did not correlate in control or cKOs. Kainate-induced SE generated positive correlations between Ca²⁺ signal amplitude and duration in both groups. During the latent phase (4 days post kainate), cKOs lose the kainate-induced correlation while controls pivot towards a negative correlation between Ca²⁺ signal amplitude and duration. Stats: One-sample Wilcoxon test of spearman correlations (R) per field of view (FOV); baseline n = 20 FOVs, SE n = 19 FOVs, 4dpKA n = 9 FOVs.

7.4.4. Stereotypical Ca^{2+} waves during epileptiform activity are delayed in GABA_B cKO

After investigation of general Ca^{2+} properties, we focussed on the large stereotypical astroglial Ca^{2+} waves, emerging during seizure activity in the cortex (Figure 9). More specifically, we characterized epileptiform events and Ca^{2+} waves, investigated how consistently these events coincided and how the offset between synchronous astroglial Ca^{2+} rises and ECoG power varied in controls and GABA_B cKOs. To this end, *in vivo* 2P Ca^{2+} imaging with synchronized ECoG was performed in $\text{GABA}_B^{\text{wt}} \times \text{GLAST-Cre}^{\text{ERT2}} \times \text{GCaMP3}$ and $\text{GABA}_B^{\text{fl/fl}} \times \text{GLAST-Cre}^{\text{ERT2}} \times \text{GCaMP3}$ mice, eight weeks post tamoxifen application (cKO 8w) in baseline and kainate-induced SE (Figure 15 A). By analogy with seizure classification in telemetric EEG data (Figure 11), we distinguished between seizures (Figure 15 C, D; green bars on ECoG trace) and spike trains (Figure 15 C; blue bar on ECoG trace), based on the presence or absence of post ictal depression, respectively. Detection and quantification of stereotypical astroglial Ca^{2+} waves was achieved via computation of the synchronicity index, describing the proportion of simultaneously active ROIs inside the field of view (FOV). In the following, we considered Ca^{2+} sync events displaying a synchronicity threshold ≥ 0.5 , meaning at least 50 % of detected ROIs were simultaneously active (Figure 15 C, D; orange dotted line).

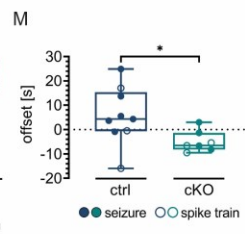
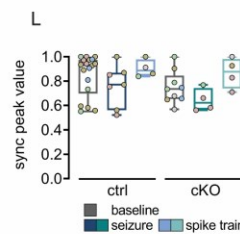
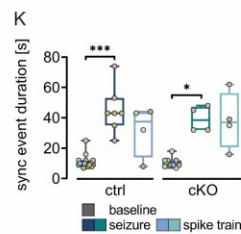
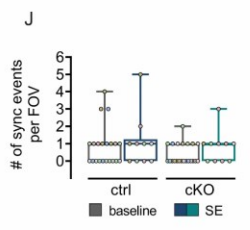
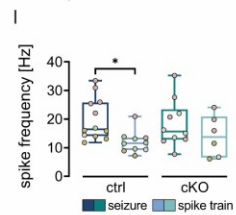
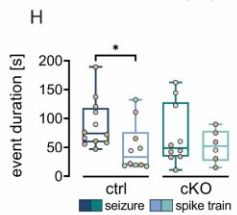
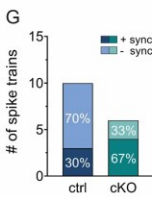
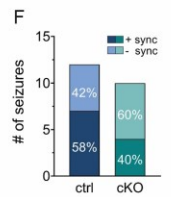
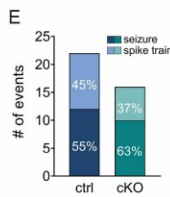
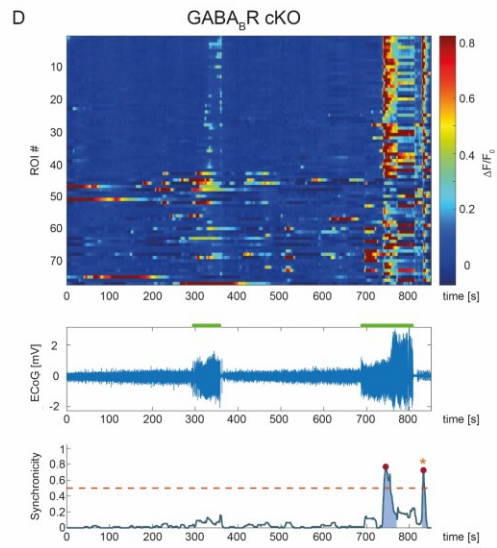
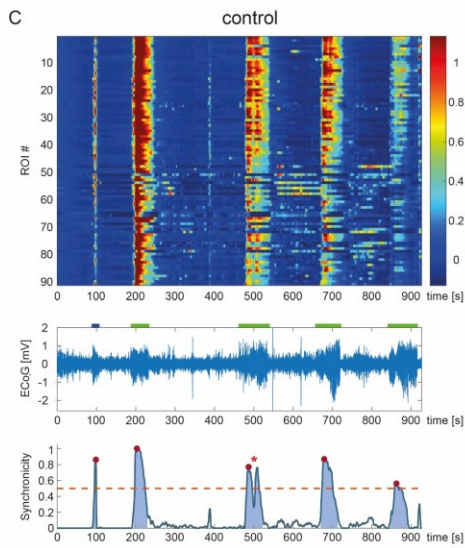
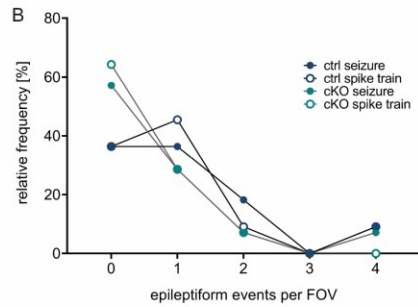
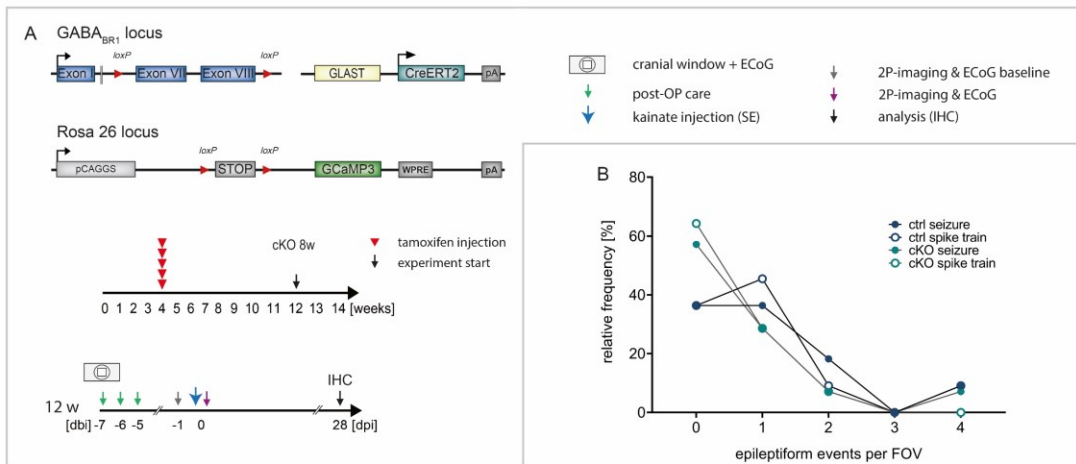
Overall, not every recorded FOV comprised an epileptiform event. In fact, the probability of recording at least one seizure or one spike train per FOV equaled 64 % in controls and between 36 % (spike train) and 43 % (seizure) in cKOs (Figure 15 B). When considering the total number of epileptiform events, controls had an almost equal amount of seizures (55 %) and spike trains (45 %), whereas in cKO about two-thirds of events were seizures (63 %) and one-third were spike trains (37 %) (Figure 15 E). Analysing the coincidence of epileptiform events and synchronous Ca^{2+} events (sync), we found that in controls, seizures are more often accompanied by sync events (58 % of seizures) than in cKOs (40 % of seizures) (Figure 15 C, D, F). Conversely, 67 % of cKO spike trains coincided with Ca^{2+} sync events, which amounted to only 30 % of spike trains in control (Figure 15 G).

Next, we characterized the two types of epileptiform events in terms of duration and spiking frequency. In control animals, seizures could be distinguished from spike trains based on a 40 s longer event duration (seizure = 74 s vs spike train = 33 s; $p = 0.04$; medians) (Figure 15 H, I) and a 40 % higher spiking frequency (seizure = 16.5 Hz vs spike train = 11.6 Hz; $p = 0.01$; medians) (Figure 15 H, I). Contrarily, these parameters were not distinctive in cKOs. Seizures and spike trains had comparable durations (seizure = 48.9 s vs spike train = 52.3 s; medians) and spiking frequencies (seizure = 15.6 Hz vs spike train = 13.8 Hz; medians) (Figure 15 H, I). In addition, no difference in epileptiform event duration or spiking frequency was found between controls and GABA_BR cKOs (Figure 15 H, I).

Figure 15 Stereotypical Ca²⁺ waves associated with epileptiform activity in the cortex are delayed in GABA_BR cKOs

A Astroglial GABA_BR cKO mice with GCaMP3 expression in astrocytes were implanted with ECoG electrodes underneath a cranial window eight weeks post tamoxifen administration. Subsequently, we performed *in vivo* 2P-Ca²⁺ imaging with synchronized ECoG recording in baseline and SE conditions. **B** Histogram of number of epileptiform events per field of view (FOV). In general, GABA_BR cKO animals tended to display more FOVs with zero epileptiform events and equal or less FOVs with one to four epileptiform events. **C** Representative heatmap of fluorescence amplitude ($\Delta F/F_0$) synchronized with ECoG (blue trace) and detected synchronicity peaks (> 0.5 sync index) in control animals. Green bars indicate seizures, blue bar indicates spike train and orange asterisk indicates excluded events. **D** Representative heatmap of fluorescence amplitude ($\Delta F/F_0$) synchronized with ECoG (blue trace) and detected synchronicity peaks (> 0.5) in GABA_BR cKO animals. Green bars indicate seizures, blue bar indicates spike train and orange asterisk indicates excluded events. **E** Controls experienced almost equal numbers of seizures and spike trains, while in GABA_BR cKOs two-thirds of epileptiform events were seizures and one-third were spike trains. **F** In controls, 60 % of seizures were accompanied by a synchronous Ca²⁺ event, whereas cKO seizures coincided with sync events in 40 % of the cases. **G** Spike trains were associated with synchronous Ca²⁺ events in one-third of control cases but two-third of cKO events. **H-I** Seizures can be distinguished from spike trains due to longer event duration (H) and higher spiking frequency (I) in control but not in cKO animals. **J** Synchronous Ca²⁺ events involving at least 50% of ROIs occur in baseline and SE. **K** Seizure-associated synchronous event duration was increased four times in SE compared to baseline in control and cKO. **L** Synchronicity peak values of detected events were comparable among groups in baseline and SE. **M** Offset between epileptiform event and synchronous Ca²⁺ event calculated via cross-correlation of average EEG epoch power and synchronicity index of Ca²⁺ events. In controls, synchronous Ca²⁺ rises lead EEG epoch power by 4.3 s in median, while cKO synchronous Ca²⁺ rises trail EEG epoch power by 6.6 s in median. Stats: individual data points represent single events, colour code indicates events from the same animal. (H-L) Kruskal-Wallis test followed by Dunn's post hoc test. (M) Mann-Whitney test. * $p < 0.05$, ** $p < 0.01$, *** $p < 0.001$, **** $p < 0.0001$.

Results



Subsequently, we studied the occurrence and properties of synchronous Ca^{2+} events. In both controls and cKOs, simultaneous Ca^{2+} activity of at least 50 % of ROIs could not only be detected during SE, but also in baseline conditions. In SE, we observed one sync event per FOV in median in controls and cKOs (Figure 15 J). Baseline recordings revealed a median of one sync event per FOV in controls but a median of zero in cKO (Figure 15 J). However, baseline and SE sync events differed significantly in their duration. In control and cKO sync events associated to seizures lasted 4.2 -4.3 times longer than in baseline (ctrl base = 10 s vs ctrl seizure = 43 s, $p = 0.0005$; cKO base = 9 s vs cKO seizure = 38.5 s, $p = 0.04$; medians) (Figure 15 K). Nevertheless, GABA_BR deletion did not affect the sync event duration (Figure 15 K). Furthermore, the detected synchronicity peak values were conserved among baseline and SE as well as control and cKO, ranging from 0.62 to 0.93 in median (Figure 15 L).

Finally, we calculated the cross-correlation between average ECoG power and synchronicity index to obtain the offset between epileptiform events and stereotypical, astroglial Ca^{2+} waves. A positive offset indicates that the Ca^{2+} sync event leads ECoG power, whereas a negative offset implies that the Ca^{2+} sync event trails ECoG power (see section 6.3.5.2). Median offset values revealed a significantly different timing of ECoG power and synchronicity index in control versus GABA_BR cKO. In controls, the Ca^{2+} sync events led by 4.3 s in median while the opposite was true in cKO, where Ca^{2+} sync events trailed ECoG power by 6.6 s in median ($p = 0.02$) (Figure 15 M).

In summary, cortical epileptiform activity was associated with stereotypical, synchronous Ca^{2+} events which preceded elevation of ECoG power in controls. In GABA_BR cKO, synchronous Ca^{2+} events were delayed and trailed ECoG power elevations. In addition, synchronous Ca^{2+} events in controls were more often associated with seizures, while we observed a stronger association of synchronous Ca^{2+} events with spike trains in cKOs. Taken together, this suggests a promoting effect of stereotypical astroglial Ca^{2+} waves on epileptiform activity, that was reduced by delayed synchronous Ca^{2+} events after GABA_BR deletion.

7.4.5. Development of regular epileptiform activity is disturbed in GABA_BR cKO

After establishing the crucial importance of stereotypical astroglial Ca²⁺ wave timing, we sought to investigate how epileptiform event properties (spiking frequency, duration) and Ca²⁺ sync properties (sync peak value, duration) correlate during *status epilepticus* (SE). Thus, synchronized *in vivo* 2P Ca²⁺ imaging and ECoG data of control and GABA_BR cKO animals with GCaMP3 expression, eight weeks post tamoxifen injection (cKO 8w) were tested for Pearson's correlation (Figure 16 A-C).

In control animals, properties of epileptiform events and synchronous Ca²⁺ events were tightly linked. Duration of epileptiform event positively correlated with spiking frequency ($r = 0.84$, $p = 0.004$) (Figure 16 B/1) and duration of synchronous Ca²⁺ events ($r = 0.87$, $p = 0.003$) (Figure 16 B/3) but negatively correlated with synchronicity peak value ($r = -0.67$, $p = 0.050$) (Figure 16 B/2). Complementarily, spiking frequency showed a positive correlation with the duration of synchronous Ca²⁺ events ($r = 0.68$, $p = 0.046$) (Figure 16 B/5) and a trend for negative correlation with synchronicity peak value ($r = -0.61$, $p = 0.08$) (Figure 16 B/4). Hence, during SE in controls, longer epileptiform events exhibit higher spiking frequencies and are associated with longer lasting synchronous Ca²⁺ events of reduced synchronicity peak values.

After astroglial GABA_BR deletion however, properties of epileptiform events and Ca²⁺ sync events displayed a complete lack of correlation (Figure 16 B, C). No association of epileptiform event duration with spiking frequency ($r = 0.05$, $p = 0.91$) (Figure 16 C/1), synchronicity peak value ($r = -0.12$, $p = 0.8$) (Figure 16 C/2) or duration of synchronous Ca²⁺ events ($r = 0.02$, $p = 0.96$) (Figure 16 C/3) was observed in cKOs. Likewise, spiking frequency did not correlate with duration of synchronous Ca²⁺ events ($r = -0.41$, $p = 0.36$) (Figure 16 C/5). The only parallel to control animals was a trend for negative correlation of spiking frequency and synchronicity peak value ($r = -0.72$, $p = 0.069$) (Figure 16 C/4).

Concluding, astroglial GABA_BR cKO lead to formation of atypical epileptiform activity during SE, infringing on the fundamental interdependence of epileptiform event duration, spiking frequency and synchronous Ca²⁺ event duration, as well as associated synchronicity peak value. These findings further support a promoting role of Ca²⁺ wave for epileptiform activity.

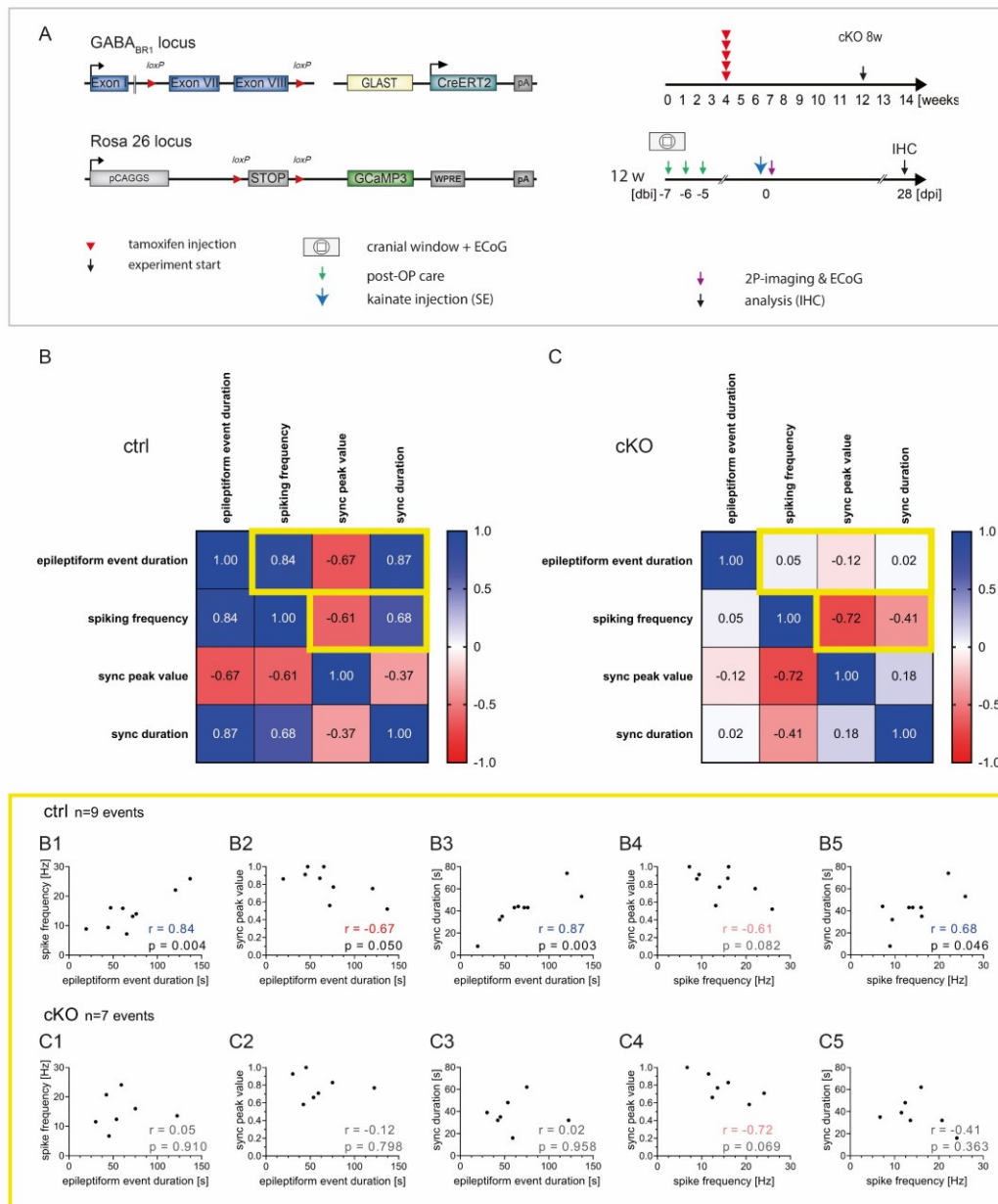


Figure 16 GABA_{BR} cKOs develop atypical epileptiform activity

A Astroglial GABA_{BR} cKO mice with GCaMP3 expression in astrocytes were implanted with ECoG electrodes underneath a cranial window eight weeks post tamoxifen administration. Subsequently, we performed *in vivo* 2P-Ca²⁺ imaging with synchronized ECoG recording in baseline and SE conditions. **B-C** Overview of Pearson correlation coefficients (r) in control (B) and cKO (C). Blue colour indicates positive correlation and red colour negative correlation. In controls, epileptiform event duration positively correlated with spiking frequency (B1) and synchronous event duration (B3). In contrast, epileptiform event duration negatively correlated with synchronicity peak value (B2). Spiking frequency showed a trend for negative correlation with synchronicity peak value (B4) while it was positively correlated with synchronous event duration (B5). In cKOs, none of the observed parameters showed a significant correlation with each other (C1-5). The only similarity with controls was the trend for negative correlation between spiking frequency synchronicity peak value (B4, C4). Stats: Pearson's correlation coefficient (r).

7.5. GABA_BR loss attenuates histopathological hallmarks of TLE

Lastly, we examined how the anti-epileptic effect of astroglial GABA_BR deletion translates to histopathological outcomes of TLE. In animal models of TLE, histopathological hallmarks such as hippocampal sclerosis and associated granule cell dispersion develop in the chronic phase, three to four weeks post kainate injection. Therefore, we conducted longitudinal histopathological analysis on brains from the different experimental procedures (simple injection, telemetric EEG recording and in vivo 2P imaging), four weeks post kainate injection (Figure 17 A, Figure 18 A).

7.5.1. Chronic hippocampal astro- and microgliosis is diminished in GABA_BR cKO mice

Assessment of hippocampal sclerosis was executed via fluorescence intensity measurements (FI) of GFAP, as a classic marker for reactive astrocytes, and complemented by Iba1 staining to visualize foci of microglia reactivity (Figure 17 B, C). For quantification purposes, all values were normalized to the hypothalamic area (ht) of the respective stainings on the same slices (Figure 17 D, E).

Confirming previous results, simple saline injection did not generate characteristic histopathological features of TLE and chronic reactivity of astrocytes and microglia was confined to the glial scar at the injection site between cortex and marginal dorsal CA1 (Figure 8, Figure 17 B, D, E, Suppl. figure 3). In contrast, kainate injection elicited prominent clusters of reactive astrocytes (GFAP) and microglia (Iba1) in hippocampal CA1, CA3 and dentate gyrus (Figure 17 B, C).

Saline injection did not induce changes in ipsilateral fluorescence intensity of GFAP (saline ipsi = 0.99 vs saline contra = 1.2; medians; $p = 0.60$) (Figure 17 D) or Iba1 (saline ipsi = 0.94 vs saline contra = 0.90; medians; $p = 0.95$) (Figure 17 E). In general, ipsilateral sides were always more affected by kainate injection than contralateral sides (Figure 17 B, C). GFAP fluorescence intensity however, showed a significant 13 % ipsilateral increase compared to contra exclusively in cKO 4w (ipsi = 2.3 vs contra = 2.0; medians; $p = 0.02$) (Figure 17 D). Meanwhile, Iba1 reactivity was 1.4 times higher in ipsilateral versus contralateral sides of control (ipsi = 2.2 vs contra = 1.6; medians; $p = 0.004$) and cKO 4w (ipsi = 1.8 vs contra = 1.3; medians; $p = 0.0002$), but not cKO 8w (ipsi = 1.3 vs contra = 1.2; medians; $p = 0.2$) (Figure 17 E).

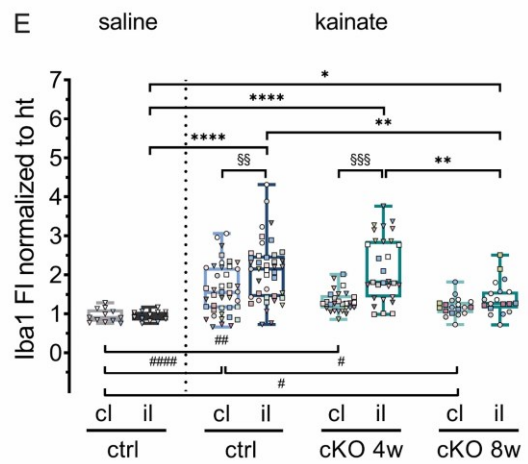
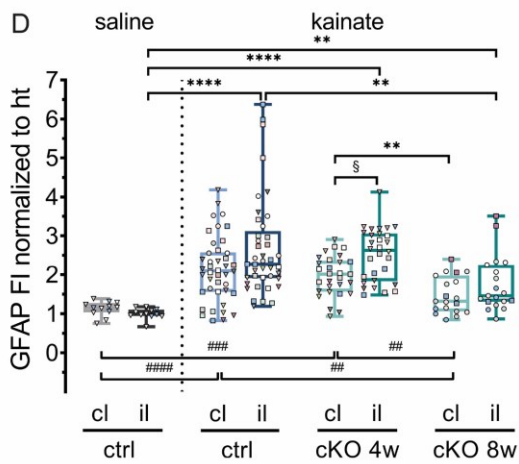
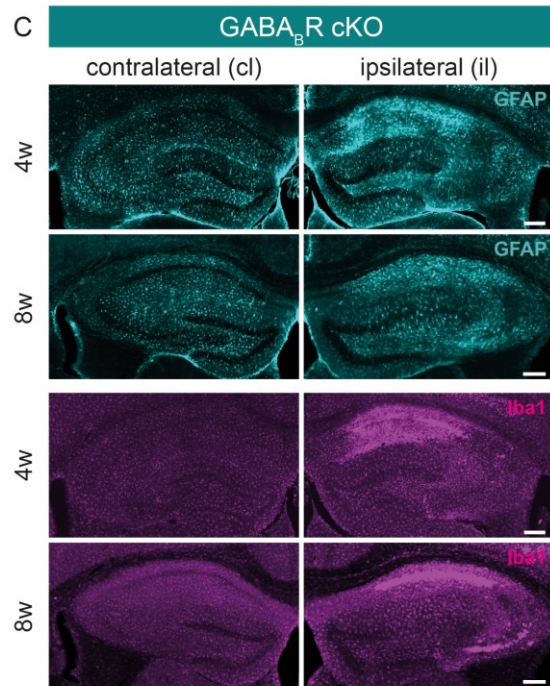
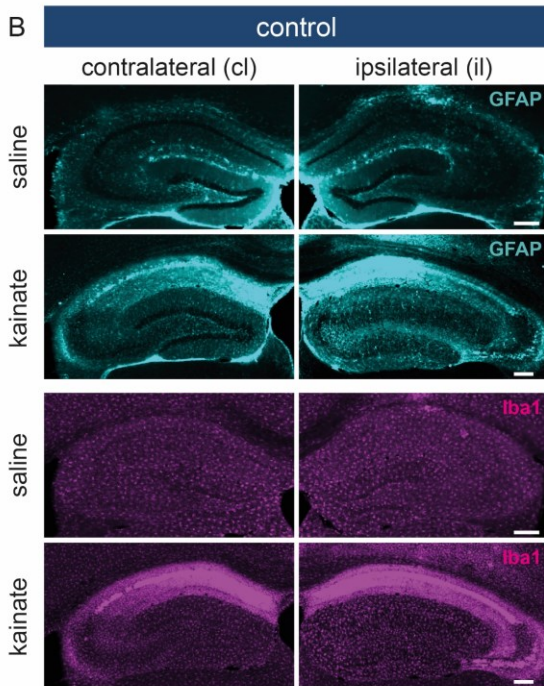
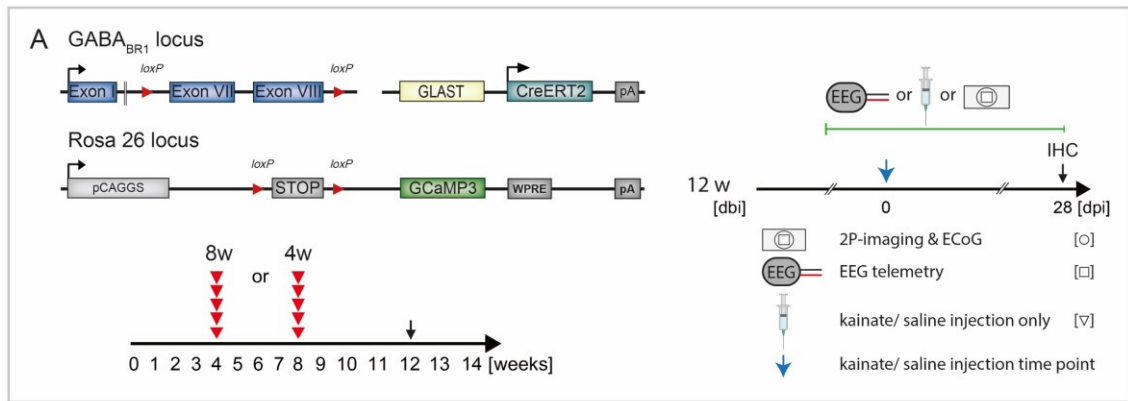
Comparing ipsilateral reactivity of astrocytes and microglia among groups, all kainate-treated groups displayed significantly enhanced GFAP and Iba1 fluorescence intensity, compared to saline, in hippocampus (Figure 17 D, E) as well as cortex (Suppl. figure 3). Among kainate-injected animals, controls showed a 1.5 - fold increased GFAP fluorescence compared to cKO 8w (control ipsi = 2.3 vs cKO 8w ipsi = 1.5; medians; $p = 0.002$) (Figure 17 D). Iba1 reactivity exposed a similar pattern of decreasing fluorescence intensity from ipsilateral sides of controls to cKO 8w (control ipsi = 2.2 vs cKO 8w ipsi = 1.3; medians; $p = 0.002$) and also from cKO 4w to cKO 8w (cKO 4w ipsi = 1.8 vs cKO 8w ipsi = 1.3; medians; $p = 0.002$) (Figure 17 E).

Summarizing, the adapted unilateral *intracortical* kainate injection model of TLE could be validated for histopathological investigation of astroglial and microglial reactivity in the chronic phase. In addition, prolonged astroglial GABA_BR cKO (cKO 8w) attenuated the manifestation of hippocampal sclerosis in form of reactive, GFAP⁺ astrocytes and concomitant microglial activation in ipsi - and contralateral sides.

Figure 17 Chronic activation of hippocampal astrocytes and microglia is attenuated in GABA_BR cKO

A Astroglial GABA_BR cKOs and controls of two different tamoxifen protocols (4w and 8w) were processed for immunohistochemical analysis (IHC) four weeks post kainate or saline injection (chronic phase). For this analysis, kainate or saline-injected animals of the different parallel experimental schedules (EEG telemetry [□], injection only [∇] and 2P-imaging with ECoG [○]), as well as controls of both tamoxifen protocols were pooled. **B-C** Representative coronal hippocampal slices stained for reactive astrocytes (GFAP) and microglia (Iba1). While saline injections induced a reduced, punctual activation of astrocytes and microglia at the dorsal extremity of CA1, kainate induced an extended glial activation encompassing CA1 as well as occasionally dentate gyrus and CA3, in all cohorts. In general, activation was more pronounced to the ipsilateral side, however control animals displayed also prominent contralateral glial activation post kainate injection (B, bottom panels). Scale bars = 250 μm. **D** Kainate injection induced significant ipsilateral increases in hippocampal GFAP fluorescence intensity (FI) in all cohorts, compared to saline. While controls and cKO 4w display a similar level of ipsilateral GFAP FI, astroglial activation was reduced in cKO 8w compared to control and cKO 4w. Kainate induced enhanced contralateral GFAP immunoreactivity compared to saline with strongest effect in control and weakest in cKO 8w. **E** Ipsilateral hippocampal Iba1 FI was significantly increased in all cohorts four weeks post kainate, compared to saline. Similar to GFAP, Iba1 reactivity was reduced in cKO 8w compared to controls and cKO 4w. Compared to saline, kainate induced heightened contralateral Iba1 immunoreactivity across groups but again, cKO 8w were the least affected.

Stats: individual data points correspond to brain slices (n) and slices from the same animal (N) are colour coded. Saline ctrl N = 4, n = 12; ctrl N = 14, n = 42; cKO 4w N = 10, n = 29; cKO 8w N = 7, n = 19. Family-wise comparisons with Kruskal-Wallis test (* ipsilateral sides, # contralateral sides, § ipsi- vs contralateral) followed by uncorrected Dunn's post hoc test. * $p < 0.05$, ** $p < 0.01$, *** $p < 0.001$, **** $p < 0.0001$.



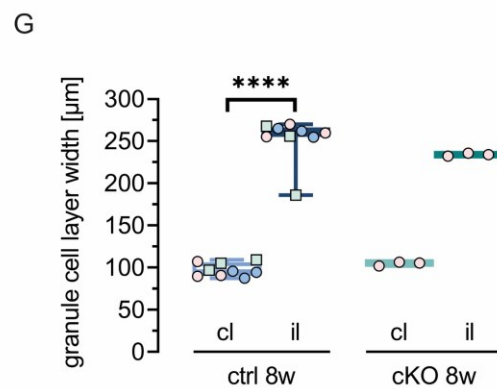
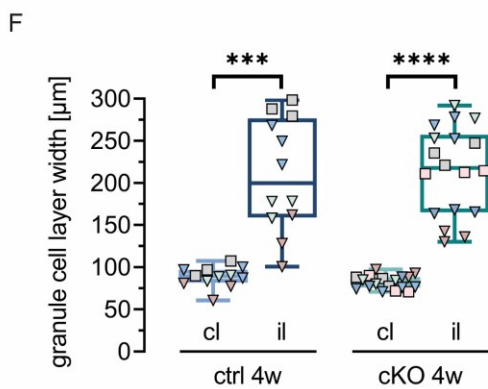
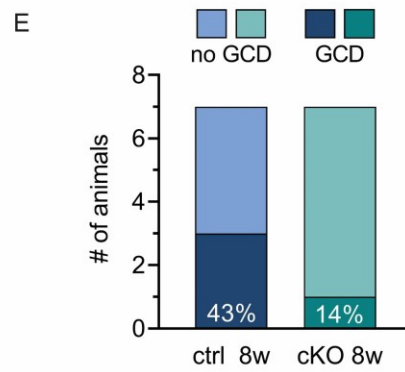
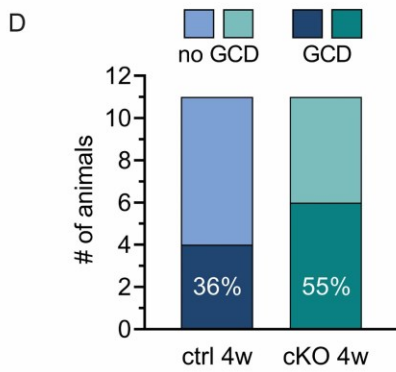
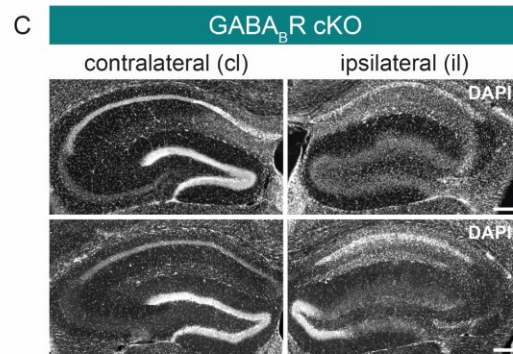
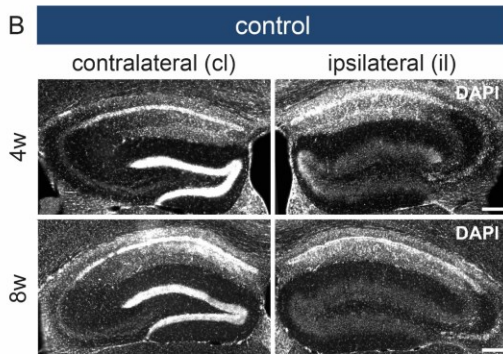
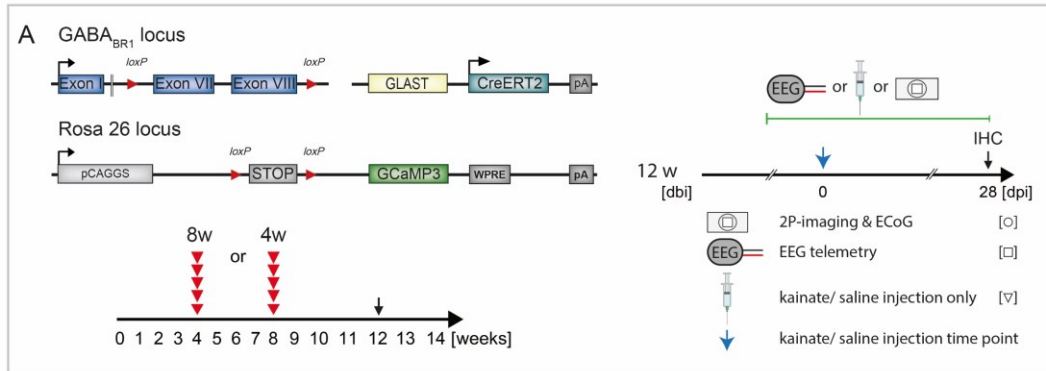
7.5.2. Granule cell dispersion incidence is reduced in GABA_BR cKO

In the context of hippocampal sclerosis, granule cell dispersion (GCD) constitutes a notorious histopathological feature of TLE. This phenomenon describes the dentate gyrus' granule cell layer widening, due to aberrant migration of mature granule cells. To evaluate the impact of astroglial GABA_BR deletion on GCD, we quantified the incidence and extent of granule cell layer broadening. Characteristically, only ipsilateral sides were affected by GCD, in all groups (Figure 18 B, C). Importantly, saline never induced GCD. Independent of tamoxifen administration schedule (4 w vs 8 w, Figure 18 A), control animals displayed comparable frequencies of GCD ranging from 36 % (4w) to 43 % (8w) (Figure 18 D, E). In contrast, GABA_BR cKO 4w animals exhibited a ~20 % increased incidence, compared to control (control 4w = 36 % vs cKO 4w = 55 %) (Figure 18 D). A prolonged receptor deletion (cKO 8w) however, drastically reduced GCD occurrence by ~30 % in comparison to controls (control 8w = 43 % vs cKO 8w = 14 %) and by ~40 % compared to cKO 4w (cKO 4w = 55 % vs cKO 8w = 14 %) (Figure 18 D, E). Concerning the extent of GCD, no GABA_BR-dependent effect could be observed (Figure 18 F, G). Across groups, ipsilateral granule cell layer width was at least doubled, compared to contralateral. Controls experienced a 2.2 – fold expansion four weeks post tamoxifen (ctrl 4w: ipsi= 199.9 µm vs contra = 89.3 µm; medians; p = 0.0003) and a 2.7 -fold widening eight weeks post tamoxifen (ctrl 8w: ipsi= 259.6 µm vs contra = 95.5 µm; medians; p < 0.0001). GABA_BR cKOs exhibited a 2.6 – times enlarged ipsilateral granule cell layer four weeks post cKO induction (cKO 4w: ipsi= 217.8 µm vs contra = 82.3 µm; medians; p < 0.0001) and 2.2 – times broader ipsilateral granule cell layer eight weeks post cKO induction (cKO 8w: ipsi= 233.9 µm vs contra = 105.4 µm; medians). Concluding, prolonged astroglial GABA_BR cKO reduced the incidence but not the severity of GCD.

Figure 18 Astroglial GABA_BR cKO reduces occurrence but not severity of granule cell dispersion

A Astroglial GABA_BR cKOs and controls (4w and 8w) were processed for immunohistochemical analysis (IHC) four weeks post kainate injection (chronic phase). For this analysis, kainate-injected animals of the different parallel experimental schedules (EEG telemetry [□], injection only [∇] and 2P-imaging with ECoG [o]) were pooled. **B-C** Representative coronal hippocampal slices stained with DAPI revealed the typical ipsilateral widening of the granule cell layer (granule cell dispersion, GCD) in control as well as cKOs of both tamoxifen protocols Scale bars = 250 µm. **D** In 4w control and cKO animals, the GCD incidence ranges between 36 – 55 %, matching the expected results based on literature and patient data. **E** In both 4w control and cKO, the ipsilateral granule cell layer was more than doubled in width compared to contralateral. **F** In accordance with the 4w groups, 8w controls had a 43% incidence of GCD, while the 8w cKOs' GCD incidence was reduced to 14 %. **G** Ipsilateral widening of the granule cell layer was comparable in 8w control and cKO. Stats: individual data points correspond to brain slices (n) and slices from the same animal (N) are colour-coded. Ctrl 4w N = 4, n = 12; ctrl 8w N = 3, n = 9; cKO 4w N = 6, n = 18; cKO 8w N = 1, n = 3. Kruskal-Wallis test followed by uncorrected Dunn's post hoc test. * p < 0.05, ** p < 0.01, *** p < 0.001, **** p < 0.0001.

Results



8. DISCUSSION

Linked to their Ca²⁺ signaling competence and subsequent gliotransmitter release, astrocytes modulate neuronal excitability in health and disease. The particular astroglial feature of Ca²⁺-dependent glutamate release upon GABAergic stimulation of metabotropic GABA_B receptors adds further complexity to neuron-glia interactions and places astrocytes at the interface of excitation and inhibition (Caudal et al., 2020). Investigation of astroglial GABA_BR contribution to epileptic network function by means of telemetric EEG recording, *in vivo* two-photon Ca²⁺ imaging synchronized with ECoG recording and immunohistochemical analysis yielded the following key results:

- Astroglial GABA_BR loss reduces γ -band power and acute seizure burden.
- Stereotypical cortical astroglial Ca²⁺ waves coinciding with epileptiform activity during *status epilepticus* are delayed in the absence of astroglial GABA_BRs.
- Depression of astroglial cortical Ca²⁺ signaling during the latent phase is prevented in astroglial GABA_BR deficient mice.
- GABA_BR deletion in astrocytes attenuates hippocampal astro- and microgliosis and reduces the incidence of granule cell dispersion in the chronic phase.
- Adaptation of the *intracortical* kainate injection model for TLE offers genuine baseline recordings, leads to milder seizure activity and is compatible for *in vivo* 2P Ca²⁺ imaging.

8.1. Anti-epileptic effect of astroglial GABA_BR deletion during progression of TLE

8.1.1. GABA_BR mutant mice display reduced γ -power but unchanged global astroglial Ca²⁺ dynamics during baseline

In cortex and hippocampus, astrocytes are functionally associated with GABAergic interneurons which crucially shape network synchronization and underly the generation of γ -oscillations (Lee et al., 2014; Mederos and Perea, 2019; Mederos et al., 2021). By performing telemetric EEG recordings before kainate administration (baseline), we detected reduced lower γ -power (30-50 Hz) in astroglial GABA_BR cKO mice. These results are in line with previous *in vivo* reports after astroglial GABA_BR ablation, demonstrating cognitive impairments linked to decision-making and working memory (Perea et al., 2016; Mederos et al., 2021). Thus, GABA_BR-dependent astroglial modulation of neural circuits is critical for physiological network function and depends on the appropriate interplay of excitation and inhibition (Buzsáki and Wang, 2012). Moreover, GABAergic stimulation of astrocytes elicits GABA_BR-dependent Ca²⁺ transients in various brain regions such as somatosensory cortex, hippocampus and striatum (Mariotti et al., 2016; Covelo and Araque, 2018; Nagai et al., 2019). We did not detect differences in cortical Ca²⁺ signal amplitude, duration, integrated fluorescence or ROI area between control and mutant mice in baseline conditions. This might be primarily due to our epilepsy-directed focus on Ca²⁺ signals at the network level, comprising the gliapil in general but omitting microdomains of fine (perisynaptic) astroglial processes, where GABA_BR are localized (Charles et al., 2003; Mariotti et al., 2018; Lia et al., 2021). In addition, three-dimensional 2P imaging might give more insight into astroglial GABA_BR-dependent Ca²⁺ signaling (Bindocci et al., 2017). Moreover, astroglial Ca²⁺ dynamics are governed by a multitude of receptors and transporters, other than GABA_BRs (Shigetomi et al., 2016). Notably, GABA-evoked astroglial Ca²⁺ oscillations can be elicited via GAT-3 dependent Na⁺ rises and subsequent activity of Na⁺/Ca²⁺ exchangers (Boddum et al., 2016; Matos et al., 2018). Furthermore, the recruitment of astrocytes and associated Ca²⁺-dependent gliotransmission has been shown to vary with interneuronal subtypes (Mariotti et al., 2018; Matos et al., 2018) and/ or intensity of interneuron activity (Covelo and Araque, 2018). Thus, heterogeneity of functional astrocyte-interneuron interactions may lead to varying thresholds for astroglial Ca²⁺ responses across brain regions and activity states (Losi et al., 2014; Mederos and Perea, 2019).

8.1.2. Loss of astroglial GABA_BRs reduces acute seizure burden and delays stereotypical astroglial Ca²⁺ waves during *status epilepticus*

Our experiments demonstrated that astroglial GABA_BR deletion reduced the number of seizures during SE by ~ 70 %, which was also reflected in a reduced lower γ -power during that period. Oscillations in the γ -range do not only contribute to fine tuning of neural networks in physiological conditions but actually constitute a measure for the severity of SE (Deshpande et al., 2020). Moreover, we found that the number of non-convulsive seizures was targeted by the general reduction, rather than convulsive seizures, suggesting a heightened threshold for seizure development. Interestingly, control animals displayed a positive correlation between epileptiform event duration and spiking frequency. This correlation was absent in GABA_BR mutant mice, hinting at aberrant epileptiform activity.

GABA_BR-mediated signaling involves activation of G_{i/o}-proteins and crosstalk with G_q-pathways leading to intracellular Ca²⁺ rises and subsequent gliotransmitter release (Mariotti et al., 2016; Nagai et al., 2019). As an essential underlying mechanism for the reduced SE severity in GABA_BR-deficient mice, we propose reduced astroglial glutamate release following sustained GABAergic stimulation and therefore abolished potentiation of excitatory transmission (Perea et al., 2016; Covelo and Araque, 2018; Durkee et al., 2019) (Figure 19). In support of this model, a reduction in γ -power has been associated to a reduced vesicular astroglial glutamate release after astrocyte-specific expression of tetanus toxin *in vivo* (Lee et al., 2014). Astroglial glutamate release is mediated by several pathways. For instance, synaptobrevin 2, participating in the SNARE-protein complex, is associated to glutamate release from astrocytes (Schwarz et al., 2017). Unpublished observations of our group suggest a downregulation of synaptobrevin 2 (VAMP2) in GABA_BR cKO astrocytes on RNA level, in physiological conditions (Stopper, 2018) (Figure 19). Besides the vesicular release of astroglial glutamate, G_{i/o}- β/γ subunits can stimulate glutamate release through the two-pore domain potassium channel TREK-1 and intracellular Ca²⁺ rises mediate opening of glutamate permeable anion channel Best1 (Woo et al., 2012). In addition, glutamate release can be mediated via reverse operation of glutamate transporters in pathological settings (Anderson and Swanson, 2000).

Network excitability further depends on astroglial K⁺ buffering capacities, especially under enhanced neuronal activity (Butt and Kalsi, 2006). GABA_BR cKOs displayed upregulation of the inwardly-rectifying K⁺ channel Kir 2.1 on astrocytes in physiological conditions (unpublished RNA-sequencing data, (Stopper, 2018)). Therefore, K⁺ uptake might be more efficient in mutant mice and thereby increase seizure threshold (Figure 19).

However, K⁺ buffering is also dependent on astroglial gap junction coupling which has yet to be evaluated in GABA_BR-deficient astrocytes. Furthermore, network excitability may also be affected by astrocyte-derived neurotrophic factors, such as BDNF. Increased BDNF protein levels in hippocampal astrocytes were found after astroglial GABA_BR deletion *in vivo* (Liu et al., 2020). While intracerebral BDNF injections trigger seizures, BDNF overexpression has controversial effects on epileptogenesis in mice and rats. Nevertheless, chronic BDNF delivery via engineered human cells in rat hippocampi reduced spontaneous seizure burden by 80 % and attenuated histopathological alterations in a pilocarpine model of TLE (Scharfman et al., 2002; Bovolenta et al., 2010; Heinrich et al., 2011; Falcicchia et al., 2018).

GABA_BR function is additionally determined by a panoply of interaction partners discovered in neurons. Through these interactions, GABA_BR complexes form a so-called signalosome, resulting in pronounced diversity of downstream effects (Fritzius and Bettler, 2020). For example, they can directly interact with glutamate receptors (NMDAR, AMPAR, mGluR1/4) and mediate sensitization of mGluR1 (Hirono et al., 2001; Couve et al., 2004; Tabata et al., 2004; Kantamneni, 2015). Similar amplification of metabotropic glutamatergic receptor function could be linked to astroglial GABA_BR-dependent Ca²⁺ signaling. However, the magnitude of physiological impact requires further investigation (Meier et al., 2008). Nevertheless, crosstalk of astroglial mGluRs and GABA_BRs might gain influence in epilepsy due to upregulation of mGluRs in astrocytes and the capacity to release glutamate in response to glutamatergic stimulation (Umpierre et al., 2019; Caudal et al., 2020).

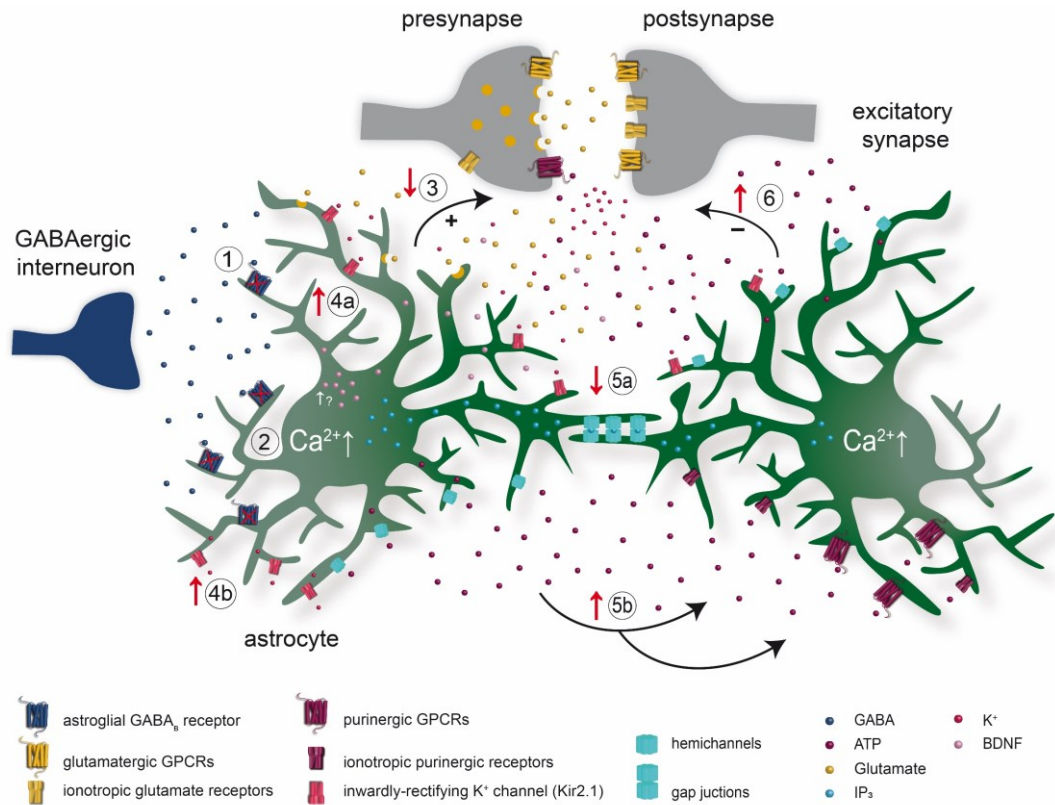


Figure 19 Putative mechanisms contributing to anti-epileptic effects of astroglial GABA_BR deletion

In GABA_BR-deficient astrocytes (1), Ca²⁺- dependent (2) glutamatergic gliotransmission is likely reduced (3). Furthermore, downregulated expression of synaptobrevin 2 (SNARE protein on glutamatergic vesicles) may contribute to reduced glutamate release and subsequent potentiation of excitatory transmission (3). Network excitability might be reduced in GABA_BR cKO due to upregulation of Kir2.1 and improved K⁺ buffering (uptake 4a, release 4b), as well as the chronically increased release of brain-derived neurotrophic factor (BDNF). The delay in stereotypical Ca²⁺ waves could be linked to a dominance of paracrine, ATP-dependent propagation of Ca²⁺ signals (5b) rather than intercellular IP₃ diffusion through gap-junctions (5a). The paracrine signaling mode includes ATP release through hemichannels and volume-regulated anion channels. Increased extracellular ATP/ADP levels can in turn reduce excitatory transmission via presynaptic A1 receptors (6).

In neuropathological models, acute phases are generally characterized by astroglial Ca^{2+} signal hyperactivity (Kuchibhotla et al., 2009; Jiang et al., 2016; Shigetomi et al., 2019), as we observed in control and mutant mice during SE. Cortical Ca^{2+} signal amplitude, duration and integrated fluorescence were acutely enhanced and kainate application induced a positive correlation between signal amplitude and duration. Moreover, we identified large stereotypical Ca^{2+} waves in cortical astrocytes during generalizing epileptiform activity. Stereotypy was reflected by the conserved duration (~ 40 s) and maximally attained synchronicity index across groups, independent of the associated type of epileptiform event (seizure or spike-train). These waves were distinct from spreading depression-like events in terms of reduced apparent propagation velocity and lack of directionality (Ayata and Lauritzen, 2015). Stereotypical Ca^{2+} signals during epileptiform activity have been previously observed in hippocampal neurons and astrocytes *in vivo* (Heuser et al., 2018; Zhang et al., 2019). Globally, astroglial Ca^{2+} signals are suspected to promote and sustain epileptiform activity, supported by reduced astroglial Ca^{2+} signaling after anti-epileptic drug application *in vivo* (Tian et al., 2005b). In brain slices, Ca^{2+} oscillations in astrocytes were shown to promote focal epileptiform activity (Gómez-Gonzalo et al., 2010). *In vivo*, synchronous astroglial Ca^{2+} elevations preceded neuronal activation in a Zebrafish PTZ model and in a mouse model of kainate-induced seizures (Heuser et al., 2018; Diaz Verdugo et al., 2019). Strikingly, kainate-induced epileptiform activity was drastically reduced when intracellular Ca^{2+} elevations in astrocytes were blocked by deletion of the IP_3 receptor type 2 (Heuser et al., 2018).

In line with these discoveries, we found that stereotypical astroglial Ca^{2+} waves led ECoG power rises by ~ 4 s in the cortex of control animals during epileptiform activity. Moreover, the duration of Ca^{2+} waves displayed a positive correlation with epileptiform event duration and spiking frequency in control animals. In contrast, GABA_BR mutant mice with reduced seizure burden had lost these interdependences and displayed delayed Ca^{2+} waves, trailing ECoG power by ~ 6 s. Thus, we concluded that stereotypical Ca^{2+} waves promote epileptiform activity in the cortex. Mechanistically, the delay of Ca^{2+} waves in GABA_BR cKOs can be explained by different modes of astroglial Ca^{2+} signal propagation (Figure 19). Principally, astroglial Ca^{2+} signals can propagate via IP_3 diffusion through gap junctions or in a paracrine fashion via vesicular ATP release or release through hemichannels and volume-regulated anion channels (Scemes and Giaume, 2006; Fujii et al., 2017).

Since ATP release mechanisms and receptor-mediated regeneration of the intracellular Ca^{2+} transient requires more time, we suspect that the delay of Ca^{2+} waves in GABA_BR-deficient mice is due to a shift towards the ATP-pathway (Leybaert and Sanderson, 2012). In support of this hypothesis, RNA expression of connexin 43 was downregulated in GABA_BR cKO astrocytes in physiological conditions (unpublished data, (Stopper, 2018)). However, the functional correlate of this downregulation has yet to be determined via astrocyte coupling assays, since the formation of functional gap junctions does not only depend on connexin protein levels but also on their subcellular localization and phosphorylation status (Deshpande et al., 2017).

Increased extracellular ATP/ADP availability can in turn induce depression of excitatory transmission via presynaptic A1 receptors (Serrano et al., 2006). This could complement the reduction of excitatory transmission due to reduced glutamate release by astrocytes and compensate for reduced GABA_BR-dependent ATP release in mutant mice (Covelo and Araque, 2018) (Figure 19).

Concluding, our results demonstrate a critical role for astroglial GABA_BR-signaling in seizure generation and timing of stereotypical Ca^{2+} waves with respect to ECoG power elevations during generalized epileptiform events. Therefore, we hypothesize that astroglial GABA_BR-signaling endorses epileptiform activity and facilitates its propagation during *status epilepticus* by sustaining stereotypical Ca^{2+} dynamics and potentiating excitatory neurotransmission, for example via glutamate release. However, it remains to be determined which mechanisms dominate at which step of seizure generation (epileptic focus, hippocampus) and/ or secondary spreading (hippocampus and cortex).

8.1.3. Astroglial GABA_BR deletion confers resilience against Ca^{2+} signal depression during the latent phase

The latent phase, starting after SE and ending with the first spontaneously recurrent seizure, is presumed to be a crucial time window for epileptogenesis. During this phase, a plethora of molecular and anatomical changes lead to modulation of network excitability, predisposing the brain to abnormal electrical activity (Goldberg and Coulter, 2013; Pitkänen et al., 2015). In this context, astrocyte (dys-) functions have been highlighted as key players in terms of gliotransmission, extracellular ion homeostasis and energy metabolism (Verhoog et al., 2020).

After acute pathological insults in general, astroglial Ca^{2+} dynamics are highly heterogenous (Shigetomi et al., 2019). Four days post kainate injection, we observed a depression in cortical Ca^{2+} signal amplitude, duration, integrated fluorescence and ROI area in control animals.

A similar reduction in Ca^{2+} signal activity was found in rat hippocampal slice preparations in a pilocarpine model, two weeks post SE. This condition was accompanied by atrophy of distal astroglial processes, correlating with a decreased size of Ca^{2+} events (Plata et al., 2018). In contrast, $\text{GABA}_{\text{B}}\text{R}$ cKO Ca^{2+} dynamics demonstrated resilience against the general depression observed in controls. We attributed this resilience of $\text{GABA}_{\text{B}}\text{R}$ cKOs to their reduced seizure burden during SE, leading to diminished excitotoxic cell death and reactivity of astrocytes (Ding et al., 2007). Moreover, we saw a prolongation of the latent phase four weeks after receptor deletion, which remains to be confirmed eight weeks post receptor deletion.

Furthermore, network alterations which enhance excitatory transmission can occur in the latent phase. Astroglial $\text{GABA}_{\text{B}}\text{R}$ -dependent upregulation of the synaptogenic cue thrombospondin-1 has been linked to increased excitatory synapse formation and enhanced cortico-striatal synaptic transmission (Nagai et al., 2019). Temporally, this mechanism could be initiated during SE and affect epileptogenesis during the latent and chronic phase, since excitatory synapse formation requires at least a couple of hours (Friedman et al., 2000).

Summarizing, $\text{GABA}_{\text{B}}\text{R}$ cKO animals were less impacted during the latent phase, reflected by the resilience of Ca^{2+} dynamics. We presume that this effect is predominantly due to the reduced seizure burden in SE.

8.1.4. Chronic histopathological features of TLE are attenuated in $\text{GABA}_{\text{B}}\text{R}$ deficient mice

In the early chronic phase, four weeks post kainate injection, we quantified the extent of hippocampal astro- and microgliosis and assessed the incidence as well as severity of granule cell dispersion (GCD). Prolonged astroglial $\text{GABA}_{\text{B}}\text{R}$ deletion (cKO 8w) had a consistent attenuating effect on astro- and microgliosis, compared to shorter $\text{GABA}_{\text{B}}\text{R}$ deletion (cKO 4w) and controls. While mild, initial astrogliosis can be beneficial in restoring homeostasis, prolonged and exacerbated astrogliosis is generally regarded as detrimental for CNS repair (Sofroniew, 2014; Verhoog et al., 2020). The establishment of correlations between seizure burden and different aspects of hippocampal sclerosis (mainly gliosis and neuronal cell loss) has been inconsistent.

However, in the intrahippocampal kainate mouse model of TLE, the magnitude of early neuronal cell loss and structural changes in the hippocampus had a predictive value for hippocampal sclerosis and chronic seizure burden (Janz et al., 2017). Thus, it is conceivable that the reduced seizure burden in GABA_BR cKO animals had an attenuating effect on the development of histopathological hallmarks.

In line with this, astroglial GABA_BR ablation also reduced GCD incidence but did not impact its severity. GCD is characterized by the migration of mature neurons of the dentate gyrus granule cell layer along radial-glia like scaffolds in response to reelin deficiency (Heinrich et al., 2006). Therefore, besides reduced seizure burden, the protective effect of GABA_BR cKO could originate from a crosstalk between GABA_BRs and reelin signaling observed in neurons (Hamad et al., 2021). To confirm the unchanged extent of granule cell layer widening, measurements must be repeated on stainings with the granule cell marker Prox 1, yielding a more accurate representation (see section 8.2.).

Besides the reduction of acute seizure burden in SE after prolonged receptor deletion, we observed a similar trend of reduced cumulative seizure burden in the early chronic phase (until day 14 post kainate) independent of receptor deletion protocols. Nonetheless, attenuation of histopathological hallmarks four weeks post kainate was more pronounced after prolonged receptor deletion. At this stage, this suggests a higher impact of SE severity over early chronic seizure burden on the histopathological outcomes. The reduced cumulative seizure burden after short receptor deletion might be due to the progressive degradation of pre-existing GABA_BRs during these two weeks (see section 8.3.1). Moreover, epilepsy is a highly progressive disorder and epileptogenesis therefore continues throughout the chronic phase, reflected by increasing seizure frequency for example (Pitkänen et al., 2015). Thus, the anti-epileptic effect of astroglial GABA_BR cKO might be more pronounced at later time points.

In conclusion, these observations suggest a pivotal role of astroglial GABA_BR-signaling in the progression of epileptogenesis. GABA_BR deletion had a protective effect starting with reduced seizure burden in SE and extending to the chronic phase with attenuated histopathological hallmarks.

8.1.5. Potential roles of inflammation and microglia-astrocyte cooperation in TLE

The pathophysiology of epilepsy is linked to inflammatory processes governed by microglia, astrocytes and their interaction (Aronica and Gorter, 2007; Vezzani et al., 2011; Devinsky et al., 2013; Sano et al., 2021). The immediate reaction consists in the release of pro-inflammatory cytokines such as interleukin 1 β (IL-1 β), interleukin 6 (IL-6), tumor necrosis factor alpha (TNF α), complement component subunit 1q (C1q) as well as ATP (De Simoni et al., 2000; Vezzani et al., 2008; Liddelow et al., 2017). Importantly, treatment with anti-inflammatory drugs reduces seizure activity (Vezzani et al., 2000; Li et al., 2012a) and prevents astrocyte uncoupling (Müller, 2018). Another crucial link in the inflammatory reaction related to epilepsy is the cooperation of microglia and astrocytes (Devinsky et al., 2013).

More specifically, astrocytes and microglia collaborate on the release of TNF α (Bezzi et al., 2001). Notably, TNF α was shown to drastically enhance astroglial P2Y1 receptor-dependent glutamate release (Santello et al., 2011) and interference with the TNF α -gated P2Y1 receptor-dependent glutamate release from astrocytes has been proven a promising strategy to counteract aberrant synaptic activity in epilepsy (Nikolic et al., 2018). Considering the numerous interaction partners of the GABA_BR “signalosome”, similar interactions involving cytokines and/ or glutamate release are plausible contributing factors to the anti-epileptic effect of astroglial GABA_BR deletion.

8.2. The adapted intracortical kainate model of TLE displays reduced acute seizure burden and provides genuine baseline recordings

This study was based on a modified version of the *intracortical* kainate injection model for human mesial temporal lobe epilepsy with hippocampal sclerosis (hMTLE-HS) developed by Bedner and colleagues (Bedner et al., 2015; Deshpande et al., 2020; Henning et al., 2021). We chose this model because of its extensive homology with the human condition, recapitulating the key phases (*status epilepticus* (SE), latent phase and chronically spontaneously recurrent seizures) as well as histopathological hallmarks of TLE. However, the *intracortical* administration route, inevitably leads to an acute lesion, due to the injection procedure. We aimed to use this model, among other techniques, for *in vivo* 2P Ca^{2+} imaging, knowing that astroglial Ca^{2+} signals are sensitive to brain insults (Burda and Sofroniew, 2014; Shigetomi et al., 2019). Therefore, we adapted the model in terms of injection procedure and uncoupling of injection site and imaging area to further minimize mechanical damage and kainate toxicity.

As described before in the intrahippocampal kainate injection model, we could confirm that saline injection does not produce seizures and does not lead to the development of histopathological hallmarks of TLE (Heinrich et al., 2006; Twele et al., 2017). Most importantly, saline injection did not significantly alter contralateral cortical astroglial Ca^{2+} signals during the acute (SE) or latent phase. In addition to the spatial segregation of injection site and imaging field, our adaptations included the temporal separation of EEG transmitter or ECoG electrode implantation and kainate injection. Thus, we were able to record genuine baselines in EEG/ECoG and Ca^{2+} imaging, which are generally rarely performed due to surgical procedures associated with intracerebral kainate administration.

In this study, astroglial Ca^{2+} activity was recorded before intracortical injections, during SE and four days post injection, corresponding to the latent phase. Furthermore, few animals could be repeatedly imaged up to 18 days post kainate or saline injection (chronic phase) (Suppl. figure 4, Suppl. figure 5, Suppl. figure 6). Chronic *in vivo* 2P imaging is a well-established and widely used technique to study CNS function, over several weeks and sometimes up to four months (Holtmaat et al., 2009; Cupido et al., 2014; Lee et al., 2018; Augustinaite and Kuhn, 2020). However, the actual success rates for such stable windows are rarely reported. When combined with contralateral intracortical injections, we experienced success rates of $\approx 50\text{-}70\%$ for cranial window stability until at least four days post injection and gradually declining visibility after one week post injection.

Some groups suggest waiting periods of several weeks post surgery before the first imaging session (Lee et al., 2018). Despite excellent long-term biocompatibility (Suppl. figure 7), this was not applicable in our study since the contact of ECoG electrodes and brain surface is ideal during the first three to four weeks post implantation for the majority of preparations. To specifically study the chronic phase, two alternative approaches could be used. Avoiding intracerebral injections by using systemic kainate administration could improve cranial window stability, however this model has an increased mortality rate and presents extra-temporal lesions (Lévesque et al., 2016). Alternatively, the cranial window with ECoG electrode implantation could be performed several weeks post kainate injection.

In comparison with the model developed by Bedner and colleagues, our control animals had comparable, SE durations (3.1 ± 0.3 h vs. 4.4 ± 2.4 h, mean \pm SEM; (Bedner et al., 2015), average individual seizure durations (50 ± 4 s vs. 62 ± 20 s, mean \pm SEM; (Bedner et al., 2015)), latent phase duration (6.4 ± 0.4 days vs. 5 ± 2.9 days, mean \pm SEM; (Bedner et al., 2015) cumulative early chronic seizure burden (8 seizures at day 14 vs. 10-12 seizures at day 15, mean; (Deshpande et al., 2020)) and mortality rates (5-7%).

When considering the number of seizures during the total SE duration, we detected 27 ± 4 seizures (mean \pm SEM), whereas Bedner and colleagues reported 3.5-fold higher numbers of 95 ± 36 seizures (mean \pm SEM). In subsequent publications, the number of seizures was assessed during the first hour of SE. Here, 53 ± 25.4 seizures/h (mean \pm SEM) (Deshpande et al., 2020) and a median of 12 seizures/h (Henning et al., 2021) were detected, revealing the variability associated with *in vivo* disease models. Moreover, our control animals spent in median 23 min in ictal activity during total SE, whereas Deshpande and colleagues reported ≈ 36 min during the first hour of SE.

Common histopathological findings in animal models of TLE and surgically resected human tissue are grouped under the umbrella term “hippocampal sclerosis” (Thom, 2014). We focussed on the extent of astro- and microgliosis, quantified via GFAP and Iba1 immunostaining, respectively, as well as incidence and severity of granule cell dispersion to evaluate the contribution of astroglial GABA_BRs to the development of histopathological hallmarks in TLE. In our hands, control animals developed marked ipsilateral astro- and microgliosis, four weeks post kainate injection, mainly extending between CA1 and CA3 as described previously in the intracortical as well as intrahippocampal model (Bedner et al., 2015).

In general, several groups reported the absence of major contralateral morphological alterations, even though contralateral hippocampi were shown to exhibit seizure activity in intracortical as well as intrahippocampal mouse models (Marx et al., 2013; Bedner et al., 2015) and an intrahippocampal guinea pig model of non-convulsive SE (Noè et al., 2019). Thus, it is argued that epileptiform activity per se might transiently induce glial activation, documented for example by a great overlap in gene expression between ipsi- and contralateral hippocampi 24 days does not induce long-term neuronal loss or gliosis (Marx et al., 2013; Bedner et al., 2015; Noè et al., 2019). In contrast, our control animals exhibited GFAP and Iba1 immunoreactive clusters in the contralateral dorsal hippocampus, declining in intensity along the septo-temporal axis, four weeks post kainate. This discrepancy can be partially resolved by taking into consideration the employed model. The absence of contralateral gliosis was explicitly addressed in the intrahippocampal guinea pig model, three days as well as two months post kainate (Noè et al., 2019). However, this model induces non-convulsive SE, thereby being less severe than the generalizing convulsive seizures observed in our study. In addition, neuroimaging studies and post-mortem analyses have found bilateral hippocampal damage in humans (Cendes et al., 2014). The fact that we did not observe marked contralateral activation in GABA_BR cKO animals, which exhibited a generally reduced seizure number during SE, led us to hypothesize that the contralateral gliosis is linked to the propagation of seizure activity. In contrast to the intracortical and intrahippocampal models, we employed a thinner injection needle and reduced injection depth (DV = 1.3 mm vs. DV = 1.7 mm and DV = 1.8-2.0 mm, respectively (Heinrich et al., 2006; Marx et al., 2013; Bedner et al., 2015)). Therefore, reduced injection depth could preserve communication via the hippocampal commissural pathway to a greater extent and support more sustained contralateral seizure propagation (Wang et al., 2014).

Furthermore, we assessed granule cell dispersion (GCD) by quantifying the incidence of this phenomenon and measuring the granule cell layer width in the dentate gyrus. In agreement with published data, GCD exclusively developed ipsilaterally (Heinrich et al., 2006; Bedner et al., 2015). We constated ipsilateral granule cell layer widths of 200-250 μm compared to 110-220 μm reported at the same time point (four weeks post kainate) (Deshpande et al., 2020; Henning et al., 2021). It is possible that we introduced a general overestimation of granule cell layer width by measuring with DAPI staining instead of the granule cell marker Prox1, as seen in the discrepancy of contralateral granule cell layer width (90-100 μm vs. 75-80 μm (Deshpande et al., 2020)).

However, GCD is a highly variable condition. It does not only present an elevated inter-individual but also an intra-individual anatomical variability along the rostro-caudal axis. Moreover, we obtained GCD incidences of 36-43 %, which is comparable to the incidence in epilepsy patients (Thom et al., 2005; Blümcke et al., 2009). Higher incidences observed by others might be due to a certain progressive character of GCD at later time points of the chronic phase, reflected by a ~ 2-fold ipsilateral expansion relative to contra at three months post kainate, which was increased to ~ 4-fold nine months post kainate (Bedner et al., 2015). Another likely explanation is the reduced seizure number in our model. Similarly, the comparatively lower seizure number was accompanied by a higher variability in GCD in the study by Henning and colleagues (Henning et al., 2021).

In summary, the adapted *intracortical* kainate injection model of TLE is a powerful and reliable tool to study different cell populations and their signaling with *in vivo* 2P-imaging most adequately during baseline, *status epilepticus* and latent phase. In comparison to the model from Bedner and colleagues, the adapted *intracortical* TLE model is generally milder, especially in terms of acute seizure burden and time spent in ictal activity. Nonetheless, it reliably recapitulates similar latency periods as well as early chronic seizure burden and typical histopathological findings.

8.3. Technical aspects of employing genetically modified mice

Transgenic mouse lines allowing for cell-type specific, optionally inducible, manipulation of neural cells, in terms of target gene deletion and/ or expression of fluorescent reporters, are valuable tools to study neuron-glia interactions (Hirrlinger et al., 2005; Nimmerjahn et al., 2005; Pascual et al., 2005; Hirrlinger et al., 2006; Livet et al., 2007; Saab et al., 2012; Jahn et al., 2015; Saab et al., 2016). However, as for any model system, one must carefully consider advantages and inconveniences with respect to the experimental paradigm.

8.3.1. Emergence of anti-epileptic effect requires prolonged receptor deletion period

In the present study, the protective effect of astroglial GABA_BR cKO was dependent on a prolonged receptor deletion period of eight weeks between tamoxifen administration and experiment start. After only four weeks post tamoxifen, tendencies of reduced acute seizure burden and astro- as well as microgliosis in the chronic phase surfaced, but became obvious only after eight weeks. Since cortical astroglial GABA_BR RNA expression could be reduced by 70 % three weeks post tamoxifen treatment (Stopper, 2018), these data suggest successful DNA recombination and milder phenotypes may be attributed to a particular membrane stability of remaining astroglial GABA_BRs. In support of this hypothesis, neuronal GABA_BRs displayed reduced basal endocytosis and have been shown to be largely resistant to classic agonist-induced internalization and degradation in hippocampal and cortical cultures (Fairfax et al., 2004). Next to post-translational modifications, GABA_BR plasma membrane stability in neurons was linked to the interaction of the GABA_BR2 subunit's carboxyl-terminal domain with PDZ (PSD-95/Dlg/ZO-1 homology) scaffold proteins (Balasubramanian et al., 2007). Another aspect is the recycling of internalized GABA_BRs to the cell membrane, which could contribute to the apparent resistance to agonist-induced internalization. In fact, the GABA_BR agonist baclofen was shown to enhance receptor recycling in cortical neurons *in vitro* (Grampp et al., 2008).

On the other hand, a prolonged waiting period between tamoxifen administration and experiment start increases the potential for development of compensatory mechanisms (El-Brolosy and Stainier, 2017). Nevertheless, the gradual development of the anti-epileptic phenotype with increasing receptor deletion period in line with known GABA_BR function, e.g. glutamate release enhancing excitatory neuronal transmission, points towards a dominance of effects directly associated to GABA_BR-signaling.

8.3.2. Glutamate transporter activity and radial glia recombination in the GLAST-Cre^{ERT2} driver line

Astrocyte-specificity of GABA_BR deletion and GCaMP3 reporter expression was achieved by selecting the GLAST-Cre^{ERT2} driver line, in which the tamoxifen-sensitive Cre DNA recombinase is targeted to the glutamate-aspartate transporter (GLAST/ EAAT1) locus (Mori et al., 2006). This mouse line is excellent for cortical 2P Ca²⁺ imaging and immunohistological studies in the hippocampus, due to superior recombination efficiencies in the forebrain, compared to the GFAP-Cre^{ERT2} line for example (Hirrlinger et al., 2006; Jahn et al., 2015).

However, two potential inconveniences must be considered. First, use of heterozygous GLAST-Cre^{ERT2} animals could imply a dysfunctional astroglial glutamate uptake. This is a sensitive issue in the context of epilepsy, since this condition is associated with enhanced extracellular glutamate levels and deletion of GLAST can induce hyperexcitability and seizures (During and Spencer, 1993; Cavus et al., 2005; Jen et al., 2005). Despite reduced GLAST mRNA levels, however, no alterations in transporter currents were detected in a previous study (Saab et al., 2012).

The second inconvenience concerns recombination in radial glia cells, especially in the neurogenic niche of the hippocampal dentate gyrus (Mori et al., 2006; DeCarolis et al., 2013). Thus, we verified the possibility that mature neurons differentiated from radial glia were affected by GABA_BR deletion and contributed to the anti-epileptic phenotype. Quantification of recombined neurons in the GABA_BR^{wt}/GABA_BR^{f/f} x GLAST-Cre^{ERT2} x GCaMP3 line, eight weeks post tamoxifen treatment, revealed negligible numbers of recombined NeuN⁺ neurons in the dorsal cortex, hippocampal CA1 and dentate gyrus (Suppl. figure 8). Hence, we attribute the anti-epileptic properties to astroglial GABA_BR deletion.

8.3.3. GCaMP3 is adequate to study astroglial Ca²⁺ dynamics on a global scale

Finally, the use of the genetically encoded Ca²⁺ sensor GCaMP3 allows for non-invasive, chronically stable Ca²⁺ imaging across large field of views. Despite slower kinetics and reduced Ca²⁺ affinity compared to GCaMP6f or GCaMP7, we chose GCaMP3 for its higher baseline fluorescence and greater adequacy to study network-level astrocyte Ca²⁺ dynamics as opposed to Ca²⁺ microdomain dynamics (Podor et al., 2015; Ye et al., 2017). It is further worth mentioning that side effects of Ca²⁺ buffering due to chronic GCaMP sensor expression have been reported, especially in neurons. Altered neuronal physiology was reflected by distortion of Ca²⁺ signals, nuclear GCaMP accumulation, apoptosis, modified gene expression, and rare observation of interictal spike-like events (Tian et al., 2009; Steinmetz et al., 2017; Yang et al., 2018). In baseline conditions, we observed an increased integrated fluorescence especially in controls eight weeks post tamoxifen, compared to four weeks (Suppl. figure 1). Ca²⁺ signal amplitude, duration and ROI area however remained unaffected by prolonged GCaMP3 expression eight weeks post tamoxifen, in baseline as well as SE (Suppl. figure 1, Suppl. figure 2). Other than this, we did not observe overt impacts of GCaMP3 expression on astrocytes in the context of this study. To assure overall technical coherence among experiments and exclude a bias due to transgene expression, control as well as mutant mice were all heterozygous for GLAST-Cre^{ERT2}, homozygous for GCaMP3 and received tamoxifen.

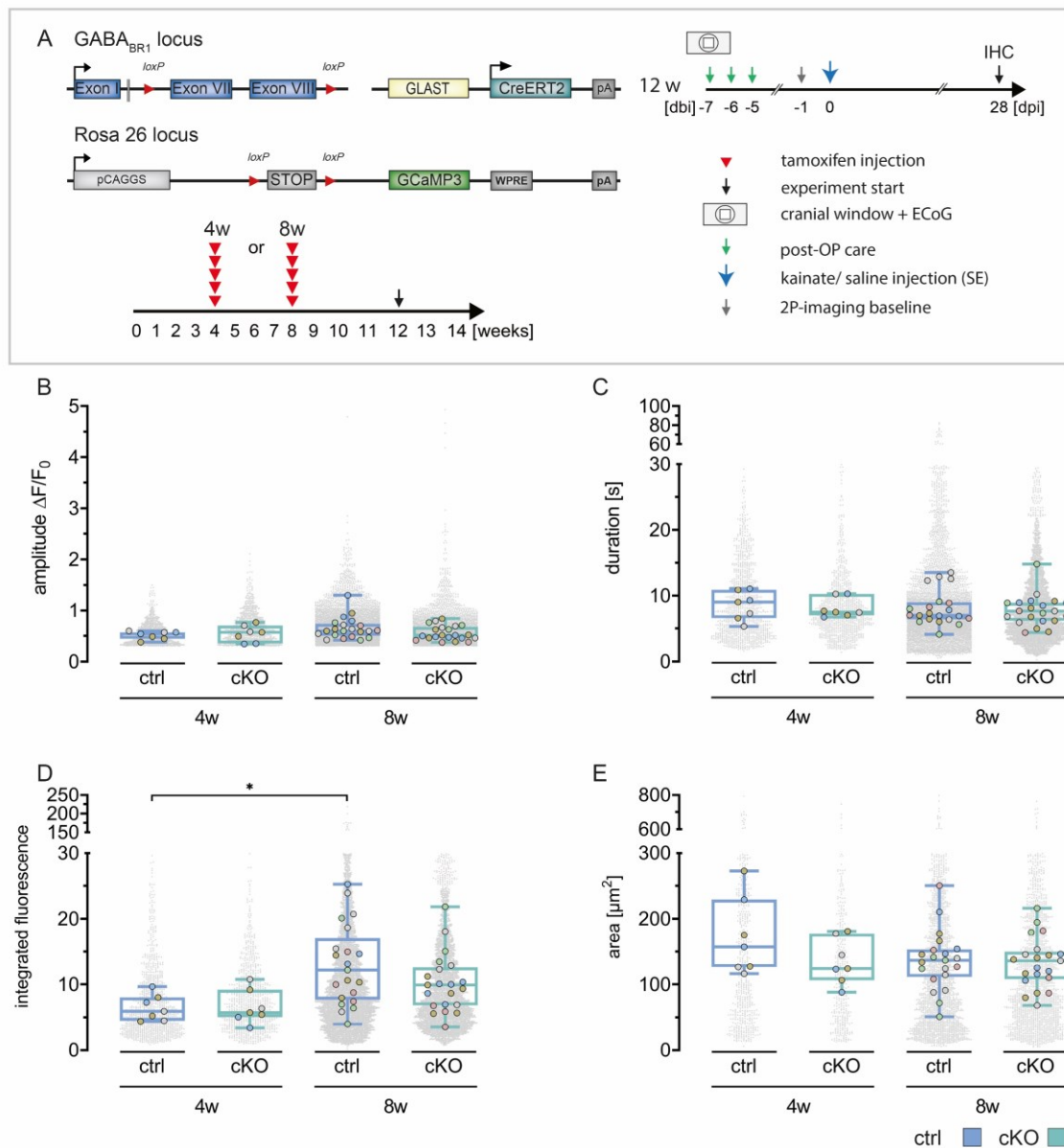
9. CONCLUSION AND OUTLOOK

In the present study, we identified an anti-epileptic effect of astroglial GABA_BR deletion in a mouse model of temporal lobe epilepsy (TLE). Mutant mice displayed a reduced number of seizures during *status epilepticus* (SE), associated with delayed stereotypical Ca²⁺ waves. In the latent phase, astroglial Ca²⁺ signals in GABA_BR deficient mice were resistant to the depression discovered in controls. GABA_BR deletion further led to attenuated histopathological hallmarks during the early chronic phase.

The molecular mechanisms underlying the anti-epileptic properties of astroglial GABA_BR ablation remain to be evaluated. First, analysis of additional time points during the latency period and later chronic phase (≥ 3 months), complemented by a time course of GABA_BR protein levels on sorted astrocytes, will contribute to the hypothesis refinement. A key experiment will be to determine whether astroglial vesicular glutamate release is reduced in GABA_BR-deficient mice, via *in vitro* assays using a genetically encoded glutamate sensor (Schwarz et al., 2017). To verify enhanced paracrine Ca²⁺-wave propagation, extracellular ATP levels during SE can be assessed with a genetically encoded, membrane-targeted ATP sensor *in vivo* (Conley et al., 2017). In addition, functional astroglial gap junction coupling status could be determined using a biocytin based assay. Moreover, whether upregulation of Kir 2.1 indeed enhances K⁺-buffering capacities of astrocytes could be evaluated in extracellular K⁺-clearance measurements with K⁺-sensitive microelectrodes. To evaluate the contribution of inflammatory processes, cytokine levels at different stages of our TLE model will be assessed via enzyme-linked immunosorbent assay (ELISA) (protein level) or quantitative real-time PCR (RNA expression).

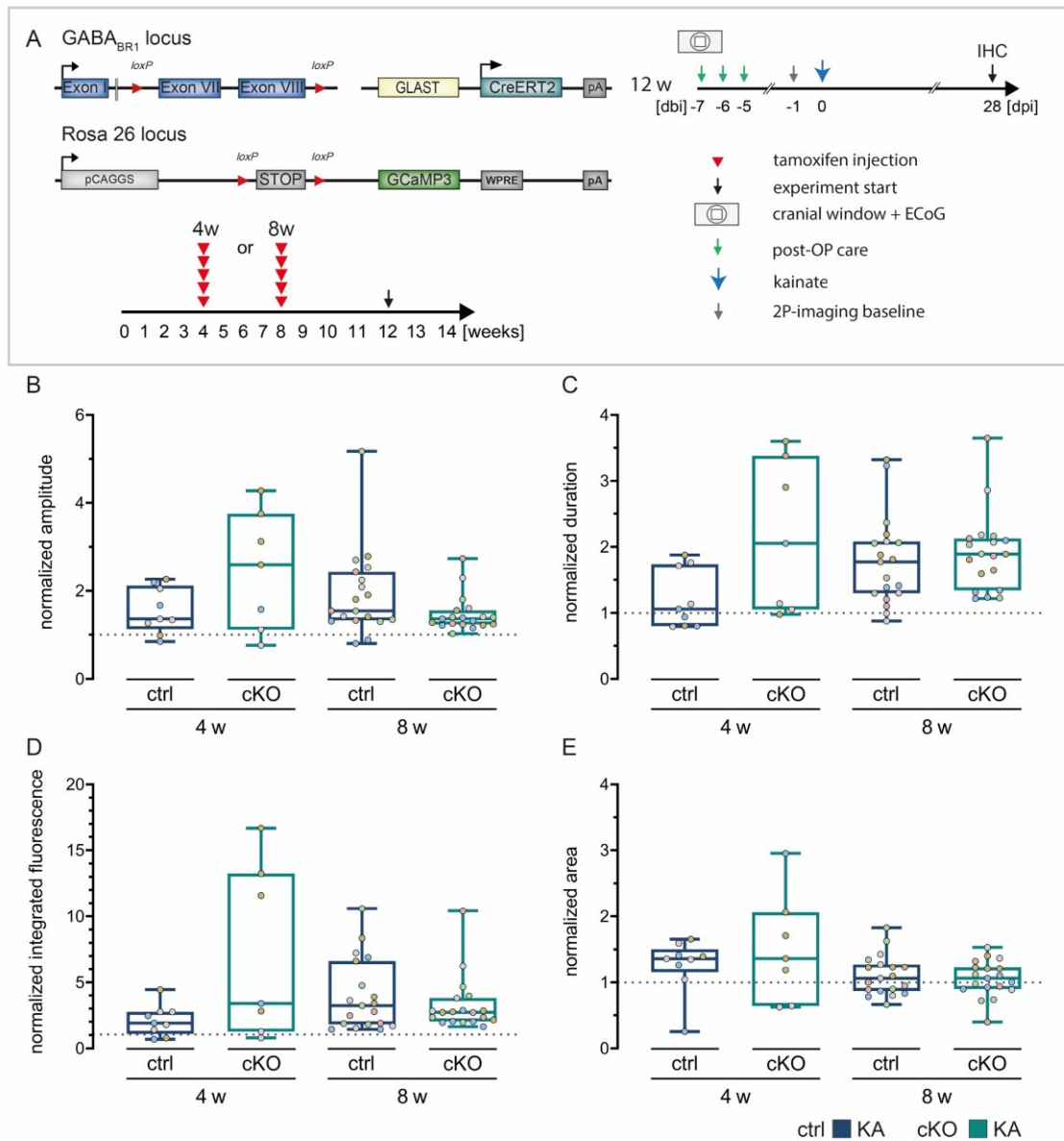
In a larger perspective, our adapted *intracortical* kainate model for TLE can be employed to study any (glio-) transmission system linked to or independent of Ca²⁺ signaling, in different cell populations of the CNS. Highly relevant targets in epilepsy would be purinergic signaling in general as well as interaction of neurons, microglia and astrocytes.

10. APPENDIX: SUPPLEMENTARY FIGURES



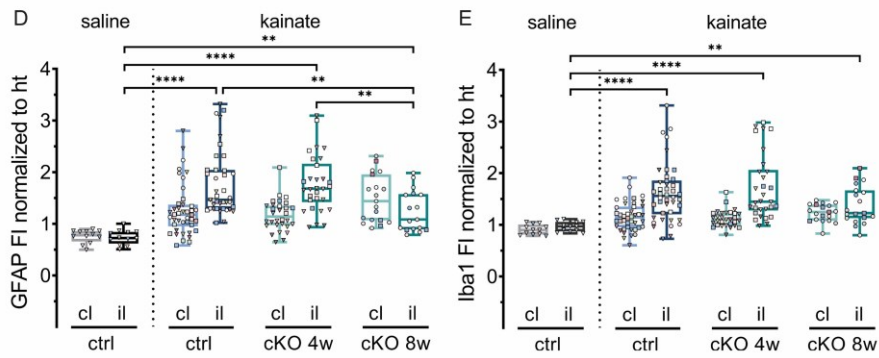
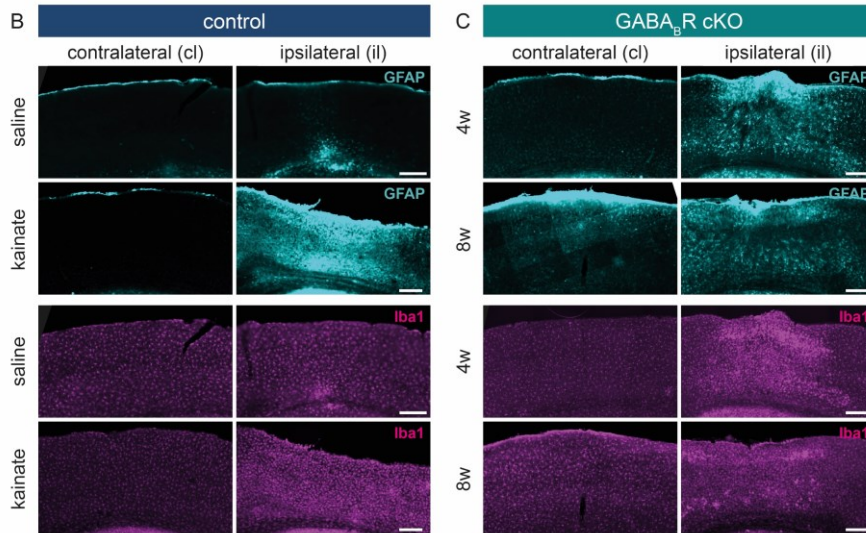
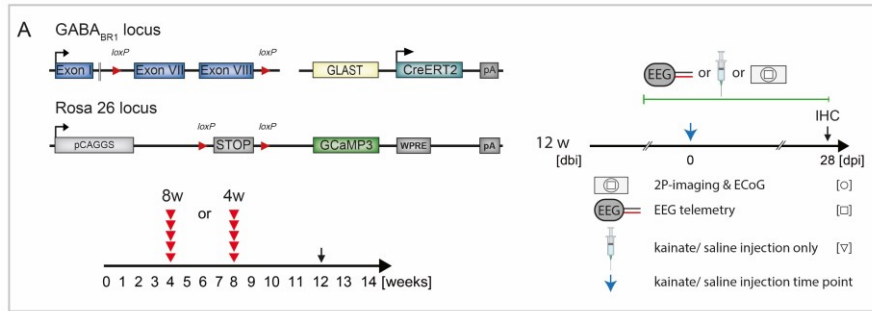
Suppl. figure 1 Controls and GABA_B cKOs display similar Ca²⁺ dynamics in baseline conditions.

A GABA_BR cKO and GCaMP3 expression in astrocytes was induced four or eight weeks before the experiment start. *In vivo* 2P Ca²⁺ imaging was performed in baseline conditions. **B** Baseline Ca²⁺ signal amplitude was comparable between control and cKO. **C** Baseline Ca²⁺ signals had a median duration of 7.1 – 9.1 s across groups. **D** Integrated fluorescence levels were increased in controls of the 8w protocol, compared to 4w. **E** ROI area ranged from 124 – 157 μm^2 and did not significantly differ between controls and cKOs. Stats: large data points represent field of views (n), colour-coded per animal (N). Ctrl 4w n = 7 FOV, N = 3 animals; cKO 4w n = 7 FOV, N = 3 animals; ctrl 8w n = 21 FOV, N = 5 animals; cKO 8w n = 21 FOV, N = 5 animals. Kruskal-Wallis test followed by Dunn's post hoc test. Grey data points in the background display single Ca²⁺ signals.



Suppl. figure 2 Basic Ca^{2+} signal properties during SE do not differ between controls and $GABA_{BR}$ cKOs, irrespective of tamoxifen protocol.

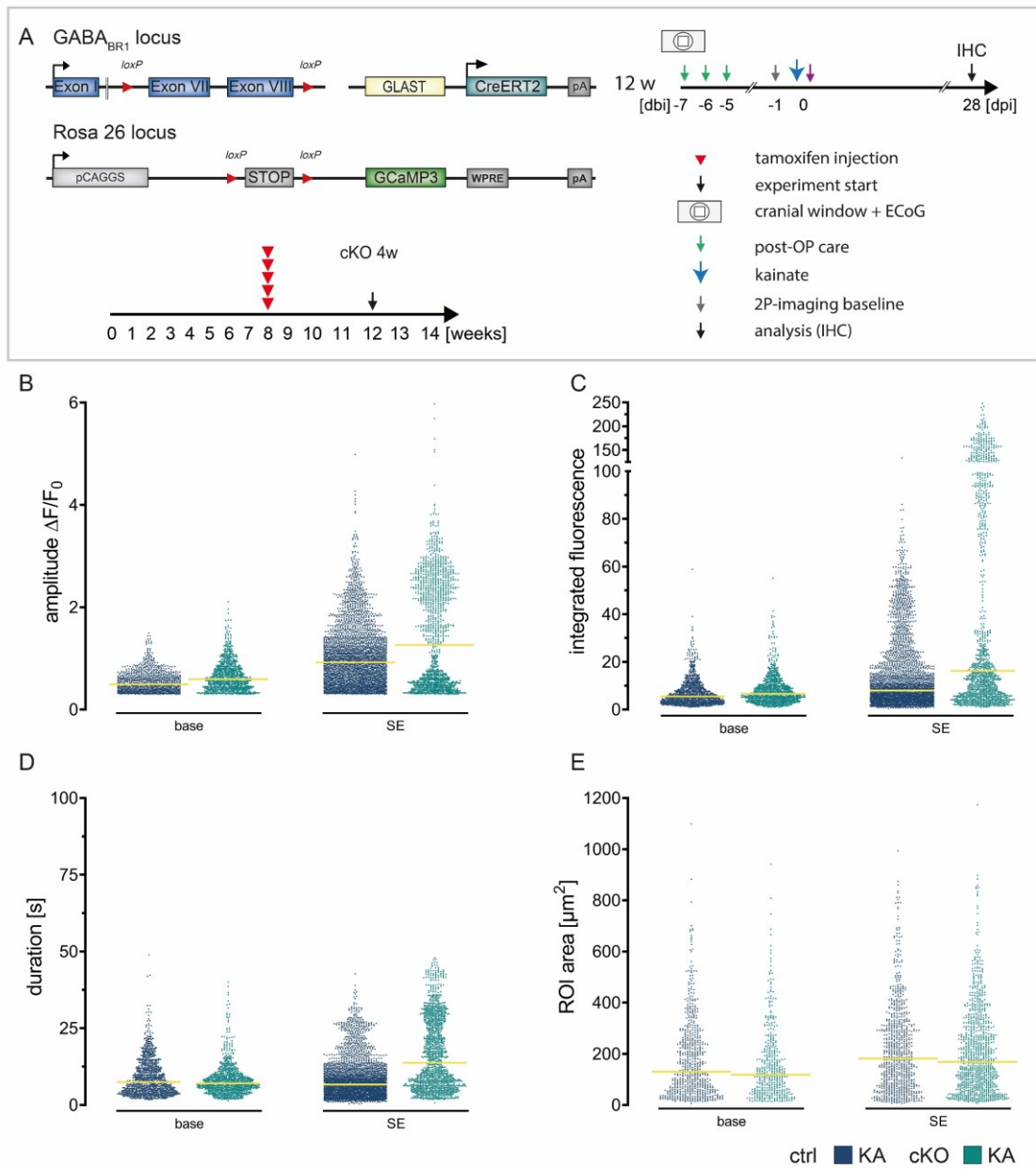
A $GABA_{BR}$ cKO and GCaMP3 expression in astrocytes was induced four or eight weeks prior to experiment start. *In vivo* 2P Ca^{2+} imaging was performed in baseline conditions and SE. Data are presented as normalized values of SE over baseline. **B** Normalized Ca^{2+} signal amplitude was comparable between controls and cKOs of both tamoxifen protocols. **C** Ca^{2+} signals during SE lasted 1.1 – 2.1 times longer in median, relative to baseline. **D** Integrated fluorescence levels were increased by 1.9 – 3.4 times in median, during SE versus baseline. **E** ROI area was enlarged 1.1 -1.4 times in SE. Stats: large data points represent field of views (n), colour-coded per animal (N). Ctrl 4w n = 9 FOV, N = 3 animals; cKO 4w n = 7 FOV, N = 3 animals; ctrl 8w n = 19 FOV, N = 5 animals; cKO 8w n = 19 FOV, N = 5 animals. Kruskal-Wallis test followed by Dunn's post hoc test.



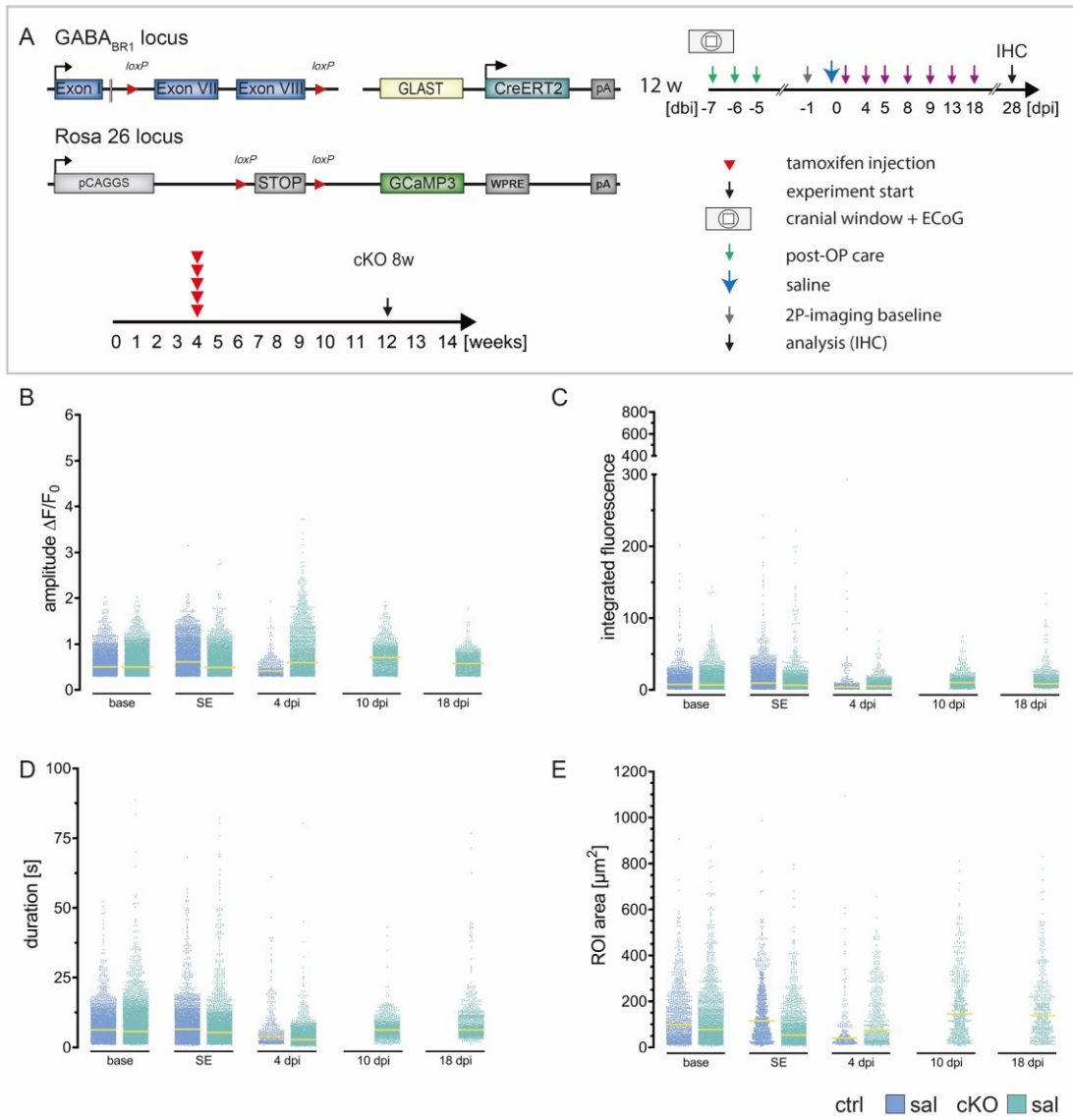
Suppl. figure 3 Chronic ipsilateral activation of cortical astrocytes is reduced in GABA_BR cKO.

A Astroglial GABA_BR cKOs and controls of two different tamoxifen protocols (4w and 8w) were processed for immunohistochemical analysis (IHC) four weeks post kainate or saline injection (chronic phase). For this analysis, kainate or saline-injected animals of the different parallel experimental schedules (EEG telemetry [□], injection only [∇] and 2P-imaging with ECoG [○]), as well as controls of both tamoxifen protocols were pooled. **B-C** Representative coronal slices stained for reactive astrocytes (GFAP) and microglia (Iba1). While saline injections induced a reduced, punctual activation of astrocytes and microglia at the injection site, kainate induced an extended ipsilateral glial activation in all cohorts. Occasionally, contralateral cortical activation of astrocytes and microglia could be observed in animals that had received a cranial window (see cKO 8w). Scale bars = 250 μm. **D** Kainate injection induced significant ipsilateral increases in GFAP fluorescence intensity (FI) in all cohorts, compared to saline. While controls and cKO 4w display a similar level of ipsilateral GFAP FI, astroglial activation was reduced in cKO 8w compared to control and cKO 4w. **E** Iba1 FI was significantly increased in all cohorts four weeks post kainate, compared to saline. No difference was detected in ipsilateral Iba1 reactivity among control and cKO cohorts.

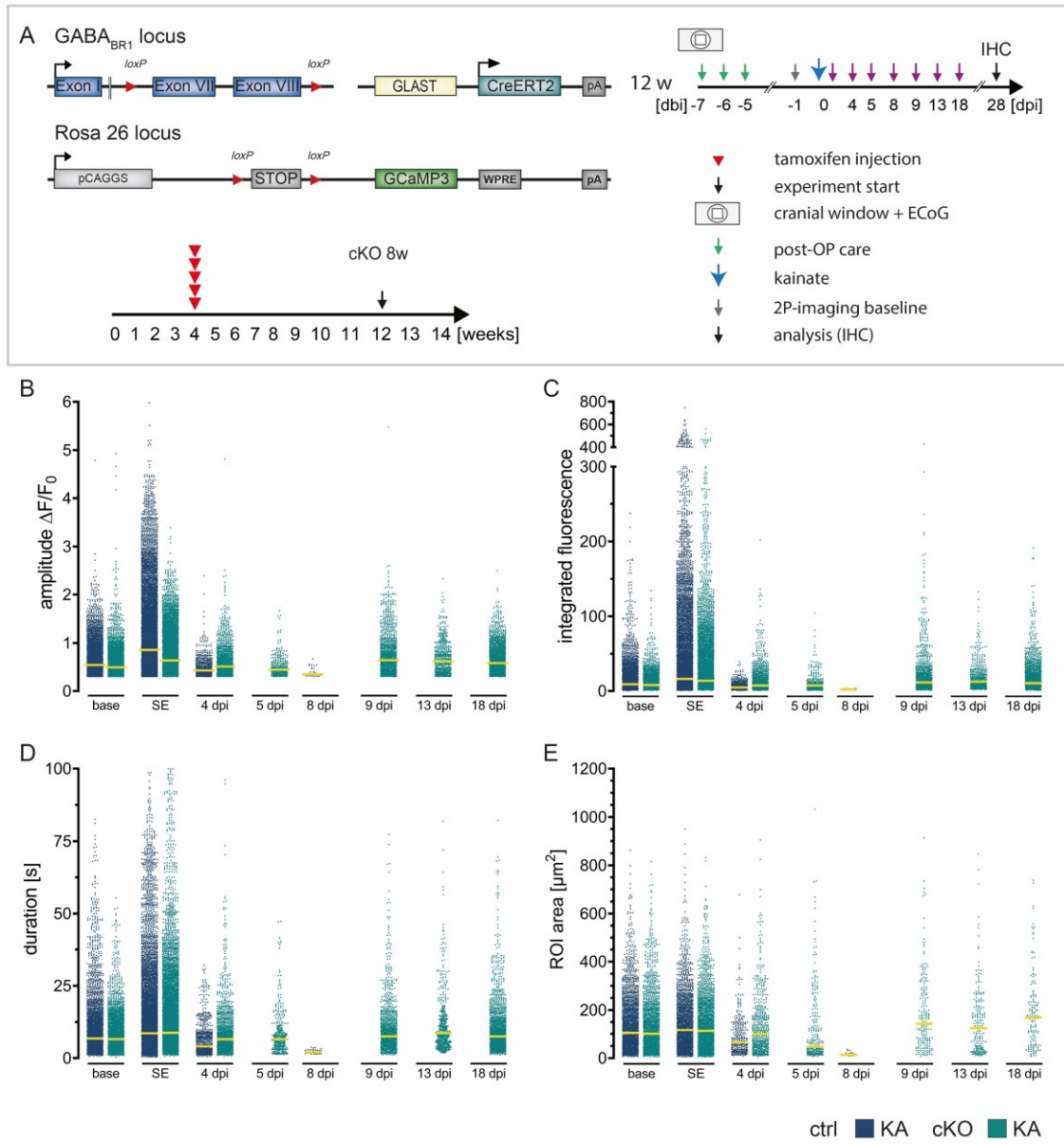
Stats: individual data points correspond to brain slices (n) and slices from the same animal (N) are colour coded. Saline ctrl N = 4, n = 12; ctrl N = 14, n = 41; cKO 4w N = 10, n = 29; cKO 8w N = 7, n = 19. Kruskal-Wallis test followed by uncorrected Dunn's post hoc test. * p < 0.05, ** p < 0.01, *** p < 0.001, **** p < 0.0001.



Suppl. figure 4 Overview of individual Ca^{2+} signals during baseline and kainate-induced SE four weeks post tamoxifen.

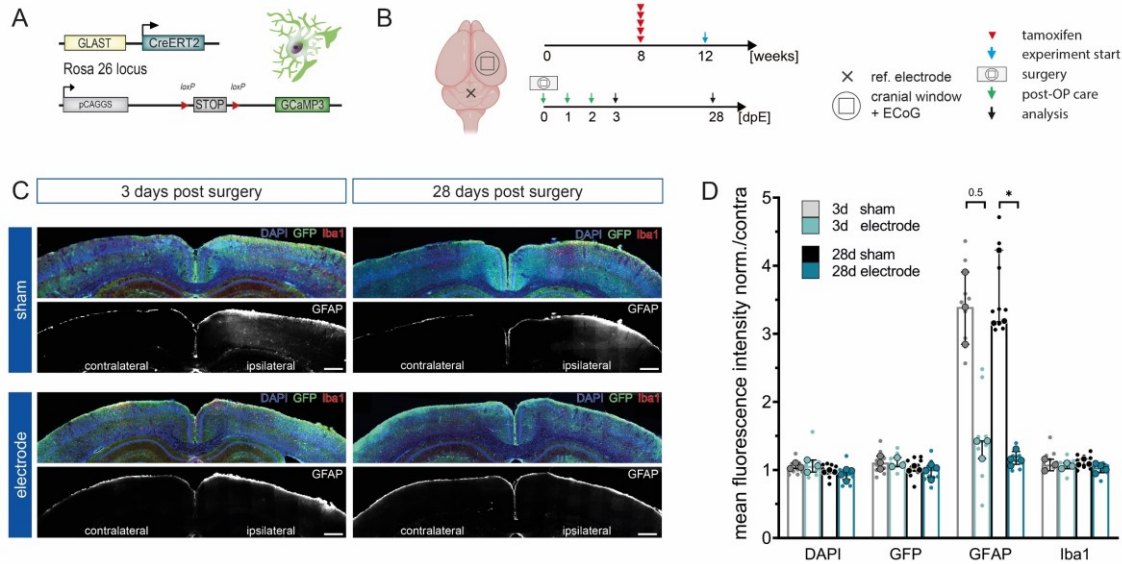


Suppl. figure 5 Overview of individual Ca²⁺ signals at various time points post saline injection in the prolonged receptor deletion protocol.



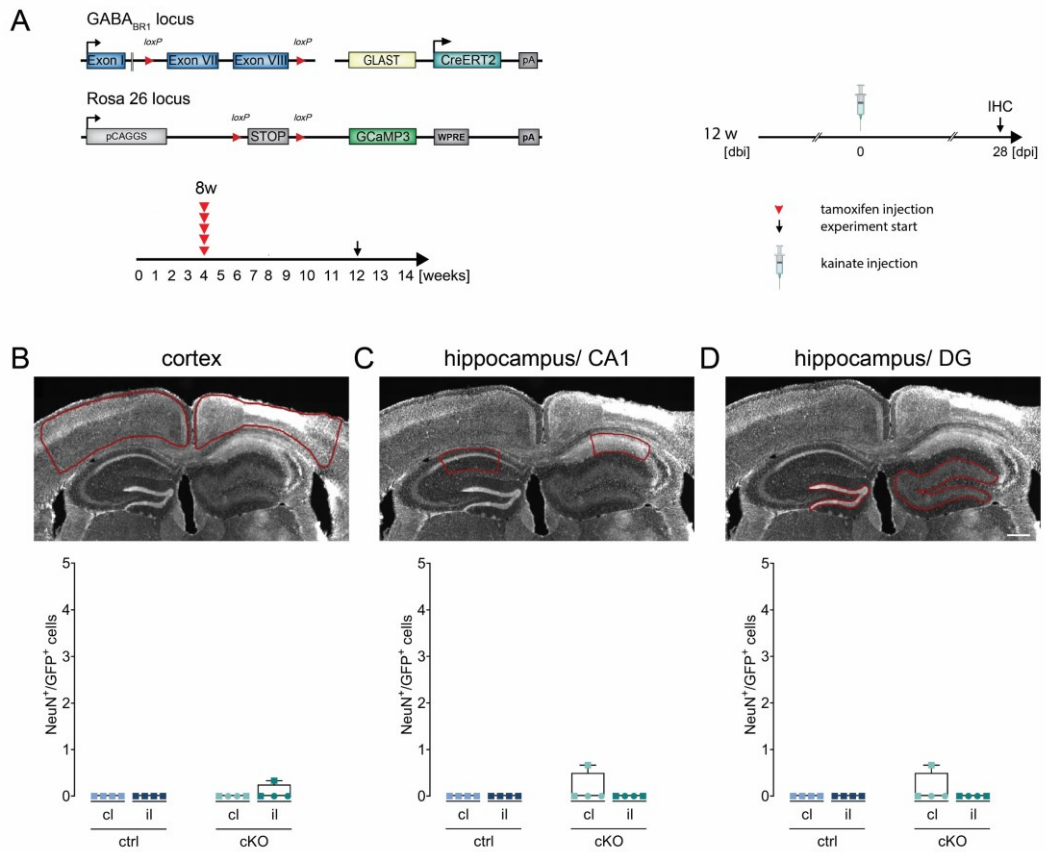
Suppl. figure 6 Overview of individual Ca^{2+} signals at various time points post kainate injection in the prolonged receptor deletion protocol.

Appendix



Suppl. figure 7 LCP cortical surface electrodes are long-term biocompatible *in vivo*.

A The biocompatibility study was carried out on transgenic mice with tamoxifen induced, astrocyte-specific GCaMP3 expression. **B** 8-week-old animals were administered five consecutive i.p. injections of tamoxifen to induce GCaMP3 expression in astrocytes. At 12 weeks of age, animals underwent cranial window surgery with or without (sham) surface electrode implantation and immunohistochemical analysis was carried out 3 or 28 days post surgery. **C** Activation of microglia (Iba1) and astrocytes (GFAP) was assessed by immunohistochemical staining of coronal slices. GCaMP3 expression was revealed with GFP staining. Ipsilateral: surgery side, contralateral: control side. Scale bars indicate 500 μ m. **D** Astroglial GFAP reactivity was increased in sham groups compared to electrode implanted groups both 3 and 28 days post surgery, while the electrode implanted groups itself were only minimally increased, indicating high biocompatibility and an additional stabilizing effect of the LCP cortical surface electrode. Ipsilateral fluorescence intensity values were normalized to the contralateral side. Statistics: Kruskal-Wallis test followed by Dunn's multiples comparisons test * $p < 0.05$. Data are displayed as median with IQR. Larger data points correspond to the average of slices from the same animal, smaller data points indicate individual slices. 3 d sham N(animal)=3, n(slice)=9; 3 d electrode N=3, n=9; 28 d sham N=3, n=9; 28 d electrode N=4, n=12. Modified from Schweigmann, Caudal et al., in press, *Frontiers in Cellular Neuroscience*.



Suppl. figure 8 Unspecific recombination of mature neurons in the GLAST-Cre^{ERT2} line is negligible in cortex and hippocampus four weeks post kainate.

A GABA_BR control and mutant mice were injected with tamoxifen at four weeks. Intracortical kainate injection followed eight weeks later and immunohistochemical analysis was performed four weeks post kainate. **B-C** Quantification of NeuN⁺/GFP⁺ (GCaMP3)⁺ cells in cortex (**B**, 2 mm²), hippocampal CA1 (**C**, 0.5 mm²) and dentate gyrus (**D**) revealed insignificant numbers of recombined, mature neurons in the GLAST-Cre^{ERT2} mouse line. Scale bar = 200 μm.

11. REFERENCES

- Abbott NJ, Rönnbäck L, Hansson E (2006) Astrocyte-endothelial interactions at the blood-brain barrier. *Nat Rev Neurosci* 7:41-53.
- Abudara V, Retamal MA, Del Rio R, Orellana JA (2018) Synaptic Functions of Hemichannels and Pannexons: A Double-Edged Sword. *Front Mol Neurosci* 11:435.
- Accardi MV, Huang H, Authier S (2018) Seizure liability assessments using the hippocampal tissue slice: Comparison of non-clinical species. *J Pharmacol Toxicol Methods* 93:59-68.
- Agarwal A, Wu PH, Hughes EG, Fukaya M, Tischfield MA, Langseth AJ, Wirtz D, Bergles DE (2017) Transient Opening of the Mitochondrial Permeability Transition Pore Induces Microdomain Calcium Transients in Astrocyte Processes. *Neuron* 93:587-605.e587.
- Allen NJ, Barres BA (2009) Neuroscience: Glia - more than just brain glue. *Nature* 457:675-677.
- Allen NJ, Eroglu C (2017) Cell Biology of Astrocyte-Synapse Interactions. *Neuron* 96:697-708.
- Anderson CM, Swanson RA (2000) Astrocyte glutamate transport: review of properties, regulation, and physiological functions. *Glia* 32:1-14.
- Anderson CM, Bergher JP, Swanson RA (2004) ATP-induced ATP release from astrocytes. *J Neurochem* 88:246-256.
- Andriezen WL (1893) The Neuroglia Elements in the Human Brain. *Br Med J* 2:227-230.
- Angulo MC, Kozlov AS, Charpak S, Audinat E (2004) Glutamate released from glial cells synchronizes neuronal activity in the hippocampus. *J Neurosci* 24:6920-6927.
- Angulo MC, Le Meur K, Kozlov AS, Charpak S, Audinat E (2008) GABA, a forgotten gliotransmitter. *Prog Neurobiol* 86:297-303.
- Anthony TE, Klein C, Fishell G, Heintz N (2004) Radial glia serve as neuronal progenitors in all regions of the central nervous system. *Neuron* 41:881-890.
- Araque A, Parpura V, Sanzgiri RP, Haydon PG (1999) Tripartite synapses: glia, the unacknowledged partner. *Trends Neurosci* 22:208-215.
- Araque A, Carmignoto G, Haydon PG, Oliet SHR, Robitaille R, Volterra A (2014) Gliotransmitters Travel in Time and Space. *Neuron* 81:728-739.
- Arizono M, Inavalli VVGK, Panatier A, Pfeiffer T, Angibaud J, Levet F, Ter Veer MJT, Stobart J, Bellocchio L, Mikoshiba K, Marsicano G, Weber B, Oliet SHR, Nägerl UV (2020) Structural basis of astrocytic Ca. *Nat Commun* 11:1906.
- Aronica E, Gorter JA (2007) Gene expression profile in temporal lobe epilepsy. *Neuroscientist* 13:100-108.
- Asadi-Pooya AA, Stewart GR, Abrams DJ, Sharan A (2017) Prevalence and Incidence of Drug-Resistant Mesial Temporal Lobe Epilepsy in the United States. *World Neurosurg* 99:662-666.
- Attwell D, Buchan AM, Charpak S, Lauritzen M, Macvicar BA, Newman EA (2010) Glial and neuronal control of brain blood flow. *Nature* 468:232-243.
- Augustinaite S, Kuhn B (2020) Chronic Cranial Window for Imaging Cortical Activity in Head-Fixed Mice. *STAR Protoc* 1:100194.
- Avoli M, Jefferys JG (2016) Models of drug-induced epileptiform synchronization in vitro. *J Neurosci Methods* 260:26-32.
- Ayata C, Lauritzen M (2015) Spreading Depression, Spreading Depolarizations, and the Cerebral Vasculature. *Physiol Rev* 95:953-993.
- Azevedo FA, Carvalho LR, Grinberg LT, Farfel JM, Ferretti RE, Leite RE, Jacob Filho W, Lent R, Herculano-Houzel S (2009) Equal numbers of neuronal and nonneuronal cells make the human brain an isometrically scaled-up primate brain. *J Comp Neurol* 513:532-541.
- Balasubramanian S, Fam SR, Hall RA (2007) GABAB receptor association with the PDZ scaffold Mupp1 alters receptor stability and function. *J Biol Chem* 282:4162-4171.
- Barker-Haliski M, Steve White H (2020) Validated animal models for antiseizure drug (ASD) discovery: Advantages and potential pitfalls in ASD screening. *Neuropharmacology* 167:107750.
- Beckner ME (2020) A roadmap for potassium buffering/dispersion via the glial network of the CNS. *Neurochem Int* 136:104727.

References

- Bedner P, Dupper A, Hüttmann K, Müller J, Herde MK, Dublin P, Deshpande T, Schramm J, Häussler U, Haas CA, Henneberger C, Theis M, Steinhäuser C (2015) Astrocyte uncoupling as a cause of human temporal lobe epilepsy. *Brain* 138:1208-1222.
- Bennett MV, Contreras JE, Bukauskas FF, Sáez JC (2003) New roles for astrocytes: gap junction hemichannels have something to communicate. *Trends Neurosci* 26:610-617.
- Berger TC, Vigeland MD, Hjorthaug HS, Nome CG, Taubøll E, Selmer KK, Heuser K (2020) Differential Glial Activation in Early Epileptogenesis-Insights From Cell-Specific Analysis of DNA Methylation and Gene Expression in the Contralateral Hippocampus. *Front Neurol* 11:573575.
- Bernard C (2015) Spreading depression: epilepsy's wave of death. *Sci Transl Med* 7:282fs214.
- Bernstein M, Lyons SA, Möller T, Kettenmann H (1996) Receptor-mediated calcium signalling in glial cells from mouse corpus callosum slices. *J Neurosci Res* 46:152-163.
- Bezzi P, Gundersen V, Galbete JL, Seifert G, Steinhäuser C, Pilati E, Volterra A (2004) Astrocytes contain a vesicular compartment that is competent for regulated exocytosis of glutamate. *Nat Neurosci* 7:613-620.
- Bezzi P, Domercq M, Brambilla L, Galli R, Schols D, De Clercq E, Vescovi A, Bagetta G, Kollias G, Meldolesi J, Volterra A (2001) CXCR4-activated astrocyte glutamate release via TNF α : amplification by microglia triggers neurotoxicity. *Nat Neurosci* 4:702-710.
- Bignami A, Eng LF, Dahl D, Uyeda CT (1972) Localization of the glial fibrillary acidic protein in astrocytes by immunofluorescence. *Brain Res* 43:429-435.
- Binder DK, Nagelhus EA, Ottersen OP (2012) Aquaporin-4 and epilepsy. *Glia* 60:1203-1214.
- Bindocci E, Savtchouk I, Liaudet N, Becker D, Carriero G, Volterra A (2017) Three-dimensional Ca(2+) imaging advances understanding of astrocyte biology. *Science* 356.
- Bjørnsen LP, Eid T, Holmseth S, Danbolt NC, Spencer DD, de Lanerolle NC (2007) Changes in glial glutamate transporters in human epileptogenic hippocampus: inadequate explanation for high extracellular glutamate during seizures. *Neurobiol Dis* 25:319-330.
- Blümcke I, Kistner I, Clusmann H, Schramm J, Becker AJ, Elger CE, Bien CG, Merschhemke M, Meencke HJ, Lehmann T, Buchfelder M, Weigel D, Buslei R, Stefan H, Pauli E, Hildebrandt M (2009) Towards a clinico-pathological classification of granule cell dispersion in human mesial temporal lobe epilepsies. *Acta Neuropathol* 117:535-544.
- Boddum K, Jensen TP, Magloire V, Kristiansen U, Rusakov DA, Pavlov I, Walker MC (2016) Astrocytic GABA transporter activity modulates excitatory neurotransmission. *Nat Commun* 7:13572.
- Borges K, Gearing M, McDermott DL, Smith AB, Almonte AG, Wainer BH, Dingledine R (2003) Neuronal and glial pathological changes during epileptogenesis in the mouse pilocarpine model. *Exp Neurol* 182:21-34.
- Bovolenta R, Zucchini S, Paradiso B, Rodi D, Merigo F, Navarro Mora G, Osculati F, Berto E, Marconi P, Marzola A, Fabene PF, Simonato M (2010) Hippocampal FGF-2 and BDNF overexpression attenuates epileptogenesis-associated neuroinflammation and reduces spontaneous recurrent seizures. *J Neuroinflammation* 7:81.
- Buckmaster PS, Zhang GF, Yamawaki R (2002) Axon sprouting in a model of temporal lobe epilepsy creates a predominantly excitatory feedback circuit. *J Neurosci* 22:6650-6658.
- Buckmaster PS, Abrams E, Wen X (2017) Seizure frequency correlates with loss of dentate gyrus GABAergic neurons in a mouse model of temporal lobe epilepsy. *J Comp Neurol* 525:2592-2610.
- Burda JE, Sofroniew MV (2014) Reactive Gliosis and the Multicellular Response to CNS Damage and Disease. *Neuron* 81:229-248.
- Bushong EA, Martone ME, Jones YZ, Ellisman MH (2002) Protoplasmic astrocytes in CA1 stratum radiatum occupy separate anatomical domains. *J Neurosci* 22:183-192.
- Butt AM, Kalsi A (2006) Inwardly rectifying potassium channels (Kir) in central nervous system glia: a special role for Kir4.1 in glial functions. *J Cell Mol Med* 10:33-44.
- Buzsáki G, Wang XJ (2012) Mechanisms of gamma oscillations. *Annu Rev Neurosci* 35:203-225.
- Bélanger M, Allaman I, Magistretti PJ (2011) Brain energy metabolism: focus on astrocyte-neuron metabolic cooperation. *Cell Metab* 14:724-738.
- Cahoy JD, Emery B, Kaushal A, Foo LC, Zamanian JL, Christopherson KS, Xing Y, Lubischer JL, Krieg PA, Krupenko SA, Thompson WJ, Barres BA (2008) A transcriptome database for astrocytes, neurons, and oligodendrocytes: a new resource for understanding brain development and function. *J Neurosci* 28:264-278.
- Carafoli E (2002) Calcium signaling: a tale for all seasons. *Proc Natl Acad Sci U S A* 99:1115-1122.
- Carmignoto G, Haydon PG (2012) Astrocyte calcium signaling and epilepsy. *Glia* 60:1227-1233.

- Castel-Branco MM, Alves GL, Figueiredo IV, Falcão AC, Caramona MM (2009) The maximal electroshock seizure (MES) model in the preclinical assessment of potential new antiepileptic drugs. *Methods Find Exp Clin Pharmacol* 31:101-106.
- Caudal LC, Gobbo D, Scheller A, Kirchhoff F (2020) The Paradox of Astroglial Ca²⁺ + Signals at the Interface of Excitation and Inhibition. *Frontiers in Cellular Neuroscience* 14.
- Cavelier P, Attwell D (2005) Tonic release of glutamate by a DIDS-sensitive mechanism in rat hippocampal slices. *J Physiol* 564:397-410.
- Cavus I, Kasoff WS, Cassaday MP, Jacob R, Gueorguieva R, Sherwin RS, Krystal JH, Spencer DD, Abi-Saab WM (2005) Extracellular metabolites in the cortex and hippocampus of epileptic patients. *Ann Neurol* 57:226-235.
- Cendes F, Sakamoto AC, Spreafico R, Bingaman W, Becker AJ (2014) Epilepsies associated with hippocampal sclerosis. *Acta Neuropathol* 128:21-37.
- Charles AC, Baca SM (2013) Cortical spreading depression and migraine. *Nat Rev Neurol* 9:637-644.
- Charles KJ, Deuchars J, Davies CH, Pangalos MN (2003) GABA B receptor subunit expression in glia. *Mol Cell Neurosci* 24:214-223.
- Chen SD, Wang YL, Liang SF, Shaw FZ (2016) Rapid Amygdala Kindling Causes Motor Seizure and Comorbidity of Anxiety- and Depression-Like Behaviors in Rats. *Front Behav Neurosci* 10:129.
- Collaborators GE (2019) Global, regional, and national burden of epilepsy, 1990-2016: a systematic analysis for the Global Burden of Disease Study 2016. *Lancet Neurol* 18:357-375.
- Conley JM, Radhakrishnan S, Valentino SA, Tantama M (2017) Imaging extracellular ATP with a genetically-encoded, ratiometric fluorescent sensor. *PLoS One* 12:e0187481.
- Cope DW, Hughes SW, Crunelli V (2005) GABA_A receptor-mediated tonic inhibition in thalamic neurons. *J Neurosci* 25:11553-11563.
- Cornell-Bell AH, Finkbeiner SM, Cooper MS, Smith SJ (1990) Glutamate induces calcium waves in cultured astrocytes: long-range glial signaling. *Science* 247:470-473.
- Cossart R, Bernard C, Ben-Ari Y (2005) Multiple facets of GABAergic neurons and synapses: multiple fates of GABA signalling in epilepsies. *Trends Neurosci* 28:108-115.
- Coulter DA, Eid T (2012) Astrocytic regulation of glutamate homeostasis in epilepsy. *Glia* 60:1215-1226.
- Couve A, Calver AR, Fairfax B, Moss SJ, Pangalos MN (2004) Unravelling the unusual signalling properties of the GABA(B) receptor. *Biochem Pharmacol* 68:1527-1536.
- Covelo A, Araque A (2018) Neuronal activity determines distinct gliotransmitter release from a single astrocyte. *Elife* 7.
- Crunelli V, Carmignoto G (2013) New vistas on astroglia in convulsive and non-convulsive epilepsy highlight novel astrocytic targets for treatment. *J Physiol* 591:775-785.
- Crunelli V, Carmignoto G, Steinhäuser C (2015) Novel astrocyte targets: new avenues for the therapeutic treatment of epilepsy. *Neuroscientist* 21:62-83.
- Cupido A, Catalin B, Steffens H, Kirchhoff F (2014) Surgical procedures to study microglial motility in the brain and in the spinal cord by in vivo two-photon laser-scanning microscopy. In: *Confocal and Multiphoton Laser-Scanning Microscopy of Neuronal Tissue: Applications and Quantitative Image Analysis* (Bakota L, Brandt R, eds), pp 37-50: Springer.
- Curia G, Longo D, Biagini G, Jones RS, Avoli M (2008) The pilocarpine model of temporal lobe epilepsy. *J Neurosci Methods* 172:143-157.
- da Silva LF, Pereira P, Elisabetsky E (1998) A neuropharmacological analysis of PTZ-induced kindling in mice. *Gen Pharmacol* 31:47-50.
- Das A, Wallace GC, Holmes C, McDowell ML, Smith JA, Marshall JD, Bonilha L, Edwards JC, Glazier SS, Ray SK, Banik NL (2012) Hippocampal tissue of patients with refractory temporal lobe epilepsy is associated with astrocyte activation, inflammation, and altered expression of channels and receptors. *Neuroscience* 220:237-246.
- De Pittà M, Brunel N, Volterra A (2016) Astrocytes: Orchestrating synaptic plasticity? *Neuroscience* 323:43-61.
- De Simoni MG, Perego C, Ravizza T, Moneta D, Conti M, Marchesi F, De Luigi A, Garattini S, Vezzani A (2000) Inflammatory cytokines and related genes are induced in the rat hippocampus by limbic status epilepticus. *Eur J Neurosci* 12:2623-2633.

References

- DeCarolis NA, Mechanic M, Petrik D, Carlton A, Ables JL, Malhotra S, Bachoo R, Götz M, Lagace DC, Eisch AJ (2013) In vivo contribution of nestin- and GLAST-lineage cells to adult hippocampal neurogenesis. *Hippocampus* 23:708-719.
- Del Bigio MR (2010) Ependymal cells: biology and pathology. *Acta Neuropathol* 119:55-73.
- Delorenzo RJ, Sun DA, Deshpande LS (2005) Cellular mechanisms underlying acquired epilepsy: the calcium hypothesis of the induction and maintenance of epilepsy. *Pharmacol Ther* 105:229-266.
- Denise A, Garcia R, Doan NB, Imura T, Bush TG, Sofroniew MV (2004) GFAP-expressing progenitors are the principal source of constitutive neurogenesis in adult mouse forebrain. *Nature Neuroscience* 7:1233-1241.
- Dermietzel R, Hertberg EL, Kessler JA, Spray DC (1991) Gap junctions between cultured astrocytes: immunocytochemical, molecular, and electrophysiological analysis. *J Neurosci* 11:1421-1432.
- Derouiche A, Frotscher M (1991) Astroglial processes around identified glutamatergic synapses contain glutamine synthetase: evidence for transmitter degradation. *Brain Res* 552:346-350.
- Deshpande T, Li T, Henning L, Wu Z, Müller J, Seifert G, Steinhäuser C, Bedner P (2020) Constitutive deletion of astrocytic connexins aggravates kainate-induced epilepsy. *Glia* 68:2136-2147.
- Deshpande T, Li T, Herde MK, Becker A, Vatter H, Schwarz MK, Henneberger C, Steinhäuser C, Bedner P (2017) Subcellular reorganization and altered phosphorylation of the astrocytic gap junction protein connexin43 in human and experimental temporal lobe epilepsy. *Glia* 65:1809-1820.
- Devinsky O, Vezzani A, Najjar S, De Lanerolle NC, Rogawski MA (2013) Glia and epilepsy: excitability and inflammation. *Trends Neurosci* 36:174-184.
- Dhir A (2012) Pentylentetrazol (PTZ) kindling model of epilepsy. *Curr Protoc Neurosci* Chapter 9:Unit9.37.
- Di Castro MA, Chuquet J, Liaudet N, Bhaukaurally K, Santello M, Bouvier D, Tiret P, Volterra A (2011) Local Ca²⁺ detection and modulation of synaptic release by astrocytes. *Nat Neurosci* 14:1276-1284.
- Diaz Verdugo C, Myren-Svelstad S, Aydin E, Van Hoeymissen E, Deneubourg C, Vanderhaeghe S, Vancraeynest J, Pelgrims R, Cosacak MI, Muto A, Kizil C, Kawakami K, Jurisch-Yaksi N, Yaksi E (2019) Glia-neuron interactions underlie state transitions to generalized seizures. *Nat Commun* 10:3830.
- Dimou L, Gallo V (2015) NG2-glia and their functions in the central nervous system. *Glia* 63:1429-1451.
- Ding F, O'Donnell J, Thrane AS, Zeppenfeld D, Kang H, Xie L, Wang F, Nedergaard M (2013) alpha(1)-Adrenergic receptors mediate coordinated Ca²⁺ signaling of cortical astrocytes in awake, behaving mice. *Cell Calcium* 54:387-394.
- Ding S, Fellin T, Zhu Y, Lee S-Y, Auberson YP, Meaney DF, Coulter DA, Carmignoto G, Haydon PG (2007) Enhanced astrocytic Ca²⁺ signals contribute to neuronal excitotoxicity after status epilepticus. *Journal of Neuroscience* 27:10674-10684.
- Dityatev A, Rusakov DA (2011) Molecular signals of plasticity at the tetrapartite synapse. *Curr Opin Neurobiol* 21:353-359.
- Doetsch F (2003) The glial identity of neural stem cells. *Nat Neurosci* 6:1127-1134.
- Domercq M, Brambilla L, Pilati E, Marchaland J, Volterra A, Bezzi P (2006) P2Y1 receptor-evoked glutamate exocytosis from astrocytes: control by tumor necrosis factor-alpha and prostaglandins. *J Biol Chem* 281:30684-30696.
- Dreier JP (2011) The role of spreading depression, spreading depolarization and spreading ischemia in neurological disease. *Nat Med* 17:439-447.
- During MJ, Spencer DD (1993) Extracellular hippocampal glutamate and spontaneous seizure in the conscious human brain. *Lancet* 341:1607-1610.
- Durkee CA, Covelo A, Lines J, Kofuji P, Aguilar J, Araque A (2019) G. *Glia* 67:1076-1093.
- Dürmüller N, Porsolt RD (2003) Electrical amygdala kindling. *Curr Protoc Pharmacol* Chapter 5:Unit5.33.
- Egawa K, Yamada J, Furukawa T, Yanagawa Y, Fukuda A (2013) Cl⁻ homeodynamics in gap junction-coupled astrocytic networks on activation of GABAergic synapses. *J Physiol* 591:3901-3917.
- Eid T, Thomas MJ, Spencer DD, Rundén-Pran E, Lai JC, Malthankar GV, Kim JH, Danbolt NC, Ottersen OP, de Lanerolle NC (2004) Loss of glutamine synthetase in the human epileptogenic hippocampus: possible mechanism for raised extracellular glutamate in mesial temporal lobe epilepsy. *Lancet* 363:28-37.
- El-Brolosy MA, Stainier DYR (2017) Genetic compensation: A phenomenon in search of mechanisms. *PLoS Genet* 13:e1006780.

References

- Fabricius M, Fuhr S, Willumsen L, Dreier JP, Bhatia R, Boutelle MG, Hartings JA, Bullock R, Strong AJ, Lauritzen M (2008) Association of seizures with cortical spreading depression and peri-infarct depolarisations in the acutely injured human brain. *Clin Neurophysiol* 119:1973-1984.
- Fahrner A, Kann G, Flubacher A, Heinrich C, Freiman TM, Zentner J, Frotscher M, Haas CA (2007) Granule cell dispersion is not accompanied by enhanced neurogenesis in temporal lobe epilepsy patients. *Exp Neurol* 203:320-332.
- Fairfax BP, Pitcher JA, Scott MG, Calver AR, Pangalos MN, Moss SJ, Couve A (2004) Phosphorylation and chronic agonist treatment atypically modulate GABAB receptor cell surface stability. *J Biol Chem* 279:12565-12573.
- Falcicchia C, Paolone G, Emerich DF, Lovisari F, Bell WJ, Fradet T, Wahlberg LU, Simonato M (2018) Seizure-Suppressant and Neuroprotective Effects of Encapsulated BDNF-Producing Cells in a Rat Model of Temporal Lobe Epilepsy. *Mol Ther Methods Clin Dev* 9:211-224.
- Feil R, Wagner J, Metzger D, Chambon P (1997) Regulation of Cre recombinase activity by mutated estrogen receptor ligand-binding domains. *Biochem Biophys Res Commun* 237:752-757.
- Feil S, Valcheva N, Feil R (2009) Inducible Cre mice. *Methods Mol Biol* 530:343-363.
- Fellin T, Pascual O, Haydon PG (2006) Astrocytes coordinate synaptic networks: Balanced excitation and inhibition. *Physiology* 21:208-215.
- Fellin T, Pascual O, Gobbo S, Pozzan T, Haydon PG, Carmignoto G (2004) Neuronal synchrony mediated by astrocytic glutamate through activation of extrasynaptic NMDA receptors. *Neuron* 43:729-743.
- Fiacco TA, McCarthy KD (2006) Astrocyte calcium elevations: properties, propagation, and effects on brain signaling. *Glia* 54:676-690.
- Fisher RS, van Emde Boas W, Blume W, Elger C, Genton P, Lee P, Engel J (2005) Epileptic seizures and epilepsy: definitions proposed by the International League Against Epilepsy (ILAE) and the International Bureau for Epilepsy (IBE). *Epilepsia* 46:470-472.
- Fraser DD, Mudrick-Donnon LA, MacVicar BA (1994) Astrocytic GABA receptors. *Glia* 11:83-93.
- Freeman MR, Rowitch DH (2013) Evolving concepts of gliogenesis: a look way back and ahead to the next 25 years. *Neuron* 80:613-623.
- Friedman HV, Bresler T, Garner CC, Ziv NE (2000) Assembly of new individual excitatory synapses: time course and temporal order of synaptic molecule recruitment. *Neuron* 27:57-69.
- Fritzus T, Bettler B (2020) The organizing principle of GABA. *Basic Clin Pharmacol Toxicol* 126 Suppl 6:25-34.
- Frotscher M, Chai X, Bock HH, Haas CA, Förster E, Zhao S (2009) Role of Reelin in the development and maintenance of cortical lamination. *J Neural Transm (Vienna)* 116:1451-1455.
- Fujii Y, Maekawa S, Morita M (2017) Astrocyte calcium waves propagate proximally by gap junction and distally by extracellular diffusion of ATP released from volume-regulated anion channels. *Sci Rep* 7:13115.
- Giaume C, Koulakoff A, Roux L, Holcman D, Rouach N (2010) Astroglial networks: a step further in neuroglial and gliovascular interactions. *Nat Rev Neurosci* 11:87-99.
- Gobbo D, Scheller A, Kirchhoff F (2021) From Physiology to Pathology of Cortico-Thalamo-Cortical Oscillations: Astroglia as a Target for Further Research. *Frontiers in Neurology* 12.
- Goldberg EM, Coulter DA (2013) Mechanisms of epileptogenesis: a convergence on neural circuit dysfunction. *Nat Rev Neurosci* 14:337-349.
- Golovina VA, Blaustein MP (2000) Unloading and refilling of two classes of spatially resolved endoplasmic reticulum Ca(2+) stores in astrocytes. *Glia* 31:15-28.
- Gramp T, Notz V, Broll I, Fischer N, Benke D (2008) Constitutive, agonist-accelerated, recycling and lysosomal degradation of GABA(B) receptors in cortical neurons. *Mol Cell Neurosci* 39:628-637.
- Guerra-Gomes S, Sousa N, Pinto L, Oliveira JF (2017) Functional Roles of Astrocyte Calcium Elevations: From Synapses to Behavior. *Front Cell Neurosci* 11:427.
- Guo ZV, Hires SA, Li N, O'Connor DH, Komiyama T, Ophir E, Huber D, Bonardi C, Morandell K, Gutnisky D, Peron S, Xu NL, Cox J, Svoboda K (2014) Procedures for behavioral experiments in head-fixed mice. *PLoS One* 9:e88678.
- Guthrie PB, Knappenberger J, Segal M, Bennett MV, Charles AC, Kater SB (1999) ATP released from astrocytes mediates glial calcium waves. *J Neurosci* 19:520-528.
- Gómez-Gonzalo M, Losi G, Chiavegato A, Zonta M, Cammarota M, Brondi M, Vetri F, Uva L, Pozzan T, de Curtis M, Ratto GM, Carmignoto G (2010) An excitatory loop with astrocytes contributes to drive neurons to seizure threshold. *PLoS Biol* 8:e1000352.

References

- Haas CA, Frotscher M (2010) Reelin deficiency causes granule cell dispersion in epilepsy. *Exp Brain Res* 200:141-149.
- Halassa MM, Fellin T, Haydon PG (2007a) The tripartite synapse: roles for gliotransmission in health and disease. *Trends in Molecular Medicine* 13:54-63.
- Halassa MM, Fellin T, Takano H, Dong J-H, Haydon PG (2007b) Synaptic islands defined by the territory of a single astrocyte. *Journal of Neuroscience* 27:6473-6477.
- Haller C, Casanova E, Müller M, Vacher CM, Vigot R, Doll T, Barbieri S, Gassmann M, Bettler B (2004) Floxed allele for conditional inactivation of the GABAB(1) gene. *Genesis* 40:125-130.
- Hamad MIK, Jbara A, Rabaya O, Petrova P, Daoud S, Melliti N, Meseke M, Lutz D, Petrasch-Parwez E, Schwitalla JC, Mark MD, Herlitz S, Reiss G, Herz J, Förster E (2021) Reelin signaling modulates GABA. *J Neurochem* 156:589-603.
- Hamilton DL, Abremski K (1984) Site-specific recombination by the bacteriophage P1 lox-Cre system. Cre-mediated synapsis of two lox sites. *J Mol Biol* 178:481-486.
- Hamilton SE, Loose MD, Qi M, Levey AI, Hille B, McKnight GS, Idzerda RL, Nathanson NM (1997) Disruption of the m1 receptor gene ablates muscarinic receptor-dependent M current regulation and seizure activity in mice. *Proc Natl Acad Sci U S A* 94:13311-13316.
- Hattingen E, Enkirch SJ, Jurcoane A, Kruse M, Delev D, Grote A, Becker A (2018) Hippocampal "gliosis only" on MR imaging represents a distinct entity in epilepsy patients. *Neuroradiology* 60:161-168.
- Haustein MD, Kracun S, Lu XH, Shih T, Jackson-Weaver O, Tong X, Xu J, Yang XW, O'Dell TJ, Marvin JS, Ellisman MH, Bushong EA, Looger LL, Khakh BS (2014) Conditions and constraints for astrocyte calcium signaling in the hippocampal mossy fiber pathway. *Neuron* 82:413-429.
- Heinrich C, Lähteinen S, Suzuki F, Anne-Marie L, Huber S, Häussler U, Haas C, Larmet Y, Castren E, Depaulis A (2011) Increase in BDNF-mediated TrkB signaling promotes epileptogenesis in a mouse model of mesial temporal lobe epilepsy. *Neurobiol Dis* 42:35-47.
- Heinrich C, Nitta N, Flubacher A, Müller M, Fahrner A, Kirsch M, Freiman T, Suzuki F, Depaulis A, Frotscher M, Haas CA (2006) Reelin deficiency and displacement of mature neurons, but not neurogenesis, underlie the formation of granule cell dispersion in the epileptic hippocampus. *J Neurosci* 26:4701-4713.
- Heller JP, Rusakov DA (2017) The Nanoworld of the Tripartite Synapse: Insights from Super-Resolution Microscopy. *Front Cell Neurosci* 11:374.
- Henneberger C, Papouin T, Oliet SH, Rusakov DA (2010) Long-term potentiation depends on release of D-serine from astrocytes. *Nature* 463:232-236.
- Henning L, Steinhäuser C, Bedner P (2021) Initiation of Experimental Temporal Lobe Epilepsy by Early Astrocyte Uncoupling Is Independent of TGFβR1/ALK5 Signaling. *Front Neurol* 12:660591.
- Herculano-Houzel S (2014) The glia/neuron ratio: how it varies uniformly across brain structures and species and what that means for brain physiology and evolution. *Glia* 62:1377-1391.
- Hesdorffer DC, Logroscino G, Benn EK, Katri N, Cascino G, Hauser WA (2011) Estimating risk for developing epilepsy: a population-based study in Rochester, Minnesota. *Neurology* 76:23-27.
- Heuser K, Nome CG, Pettersen KH, Åbjørsbråten KS, Jensen V, Tang W, Sprengel R, Taubøll E, Nagelhus EA, Enger R (2018) Ca²⁺ Signals in Astrocytes Facilitate Spread of Epileptiform Activity. *Cereb Cortex* 28:4036-4048.
- Hinterkeuser S, Schröder W, Hager G, Seifert G, Blümcke I, Elger CE, Schramm J, Steinhäuser C (2000) Astrocytes in the hippocampus of patients with temporal lobe epilepsy display changes in potassium conductances. *Eur J Neurosci* 12:2087-2096.
- Hirase H, Qian L, Barthó P, Buzsáki G (2004) Calcium dynamics of cortical astrocytic networks in vivo. *PLoS Biol* 2:E96.
- Hirono M, Yoshioka T, Konishi S (2001) GABA(B) receptor activation enhances mGluR-mediated responses at cerebellar excitatory synapses. *Nat Neurosci* 4:1207-1216.
- Hirrlinger PG, Scheller A, Braun C, Hirrlinger J, Kirchhoff F (2006) Temporal control of gene recombination in astrocytes by transgenic expression of the tamoxifen-inducible DNA recombinase variant CreERT2. *Glia* 54:11-20.
- Hirrlinger PG, Scheller A, Braun C, Quintela-Schneider M, Fuss B, Hirrlinger J, Kirchhoff F (2005) Expression of reef coral fluorescent proteins in the central nervous system of transgenic mice. *Mol Cell Neurosci* 30:291-303.

- Hoeller AA, de Carvalho CR, Franco PLC, Formolo DA, Imthön AK, Dos Santos HR, Eidt I, Souza GR, Constantino LC, Ferreira CL, Prediger RD, Bainy Leal R, Walz R (2017) Behavioral and Neurochemical Consequences of Pentylentetrazol-Induced Kindling in Young and Middle-Aged Rats. *Pharmaceuticals* (Basel) 10.
- Holtmaat A, Bonhoeffer T, Chow DK, Chuckowree J, De Paola V, Hofer SB, Hübener M, Keck T, Knott G, Lee WC, Mostany R, Mrsic-Flogel TD, Nedivi E, Portera-Cailliau C, Svoboda K, Trachtenberg JT, Wilbrecht L (2009) Long-term, high-resolution imaging in the mouse neocortex through a chronic cranial window. *Nat Protoc* 4:1128-1144.
- Houser CR (1990) Granule cell dispersion in the dentate gyrus of humans with temporal lobe epilepsy. *Brain Res* 535:195-204.
- Huusko N, Römer C, Nnode-Ekane XE, Lukasiuk K, Pitkänen A (2015) Loss of hippocampal interneurons and epileptogenesis: a comparison of two animal models of acquired epilepsy. *Brain Struct Funct* 220:153-191.
- Héja L, Barabás P, Nyitrai G, Kékesi KA, Lasztóczy B, Toke O, Tárkányi G, Madsen K, Schousboe A, Dobolyi A, Palkovits M, Kardos J (2009) Glutamate uptake triggers transporter-mediated GABA release from astrocytes. *PLoS One* 4:e7153.
- Ishibashi M, Egawa K, Fukuda A (2019) Diverse Actions of Astrocytes in GABAergic Signaling. *Int J Mol Sci* 20.
- Isomura Y, Sugimoto M, Fujiwara-Tsukamoto Y, Yamamoto-Muraki S, Yamada J, Fukuda A (2003) Synaptically activated Cl⁻ accumulation responsible for depolarizing GABAergic responses in mature hippocampal neurons. *J Neurophysiol* 90:2752-2756.
- Jahn HM, Scheller A, Kirchhoff F (2015) Genetic control of astrocyte function in neural circuits. *Front Cell Neurosci* 9:310.
- Jahn HM, Kasakow CV, Helfer A, Michely J, Verkhatsky A, Maurer HH, Scheller A, Kirchhoff F (2018) Refined protocols of tamoxifen injection for inducible DNA recombination in mouse astroglia. *Sci Rep* 8:5913.
- Janz P, Schwaderlapp N, Heining K, Häussler U, Korvink JG, von Elverfeldt D, Hennig J, Egert U, LeVan P, Haas CA (2017) Early tissue damage and microstructural reorganization predict disease severity in experimental epilepsy. *Elife* 6.
- Jen JC, Wan J, Palos TP, Howard BD, Baloh RW (2005) Mutation in the glutamate transporter EAAT1 causes episodic ataxia, hemiplegia, and seizures. *Neurology* 65:529-534.
- Jiang R, Diaz-Castro B, Looger LL, Khakh BS (2016) Dysfunctional Calcium and Glutamate Signaling in Striatal Astrocytes from Huntington's Disease Model Mice. *J Neurosci* 36:3453-3470.
- Jobst BC, Williamson PD, Neuschwander TB, Darcey TM, Thadani VM, Roberts DW (2001) Secondarily generalized seizures in mesial temporal epilepsy: clinical characteristics, lateralizing signs, and association with sleep-wake cycle. *Epilepsia* 42:1279-1287.
- Johnson AM, Sugo E, Barreto D, Hiew CC, Lawson JA, Connolly AM, Somerville E, Hasic E, Bye AM, Cunningham AM (2016) The Severity of Gliosis in Hippocampal Sclerosis Correlates with Pre-Operative Seizure Burden and Outcome After Temporal Lobectomy. *Mol Neurobiol* 53:5446-5456.
- Jungblut M, Tiveron MC, Barral S, Abrahamsen B, Knöbel S, Pennartz S, Schmitz J, Perraut M, Pfrieger FW, Stoffel W, Cremer H, Bosio A (2012) Isolation and characterization of living primary astroglial cells using the new GLAST-specific monoclonal antibody ACSA-1. *Glia* 60:894-907.
- Kanemaru K, Sekiya H, Xu M, Satoh K, Kitajima N, Yoshida K, Okubo Y, Sasaki T, Moritoh S, Hasuwa H, Mimura M, Horikawa K, Matsui K, Nagai T, Iino M, Tanaka KF (2014) In vivo visualization of subtle, transient, and local activity of astrocytes using an ultrasensitive Ca²⁺ indicator. *Cell Rep* 8:311-318.
- Kang J, Jiang L, Goldman SA, Nedergaard M (1998) Astrocyte-mediated potentiation of inhibitory synaptic transmission. *Nat Neurosci* 1:683-692.
- Kang M, Othmer HG (2009) Spatiotemporal characteristics of calcium dynamics in astrocytes. *Chaos* 19:037116.
- Kantamneni S (2015) Cross-talk and regulation between glutamate and GABA_B receptors. *Front Cell Neurosci* 9:135.
- Kettenmann H, Backus KH, Schachner M (1987) gamma-Aminobutyric acid opens Cl⁻ channels in cultured astrocytes. *Brain Res* 404:1-9.
- Kettenmann H, Kirchhoff F, Verkhratsky A (2013) Microglia: new roles for the synaptic stripper. *Neuron* 77:10-18.
- Khakh BS, Sofroniew MV (2015) Diversity of astrocyte functions and phenotypes in neural circuits. *Nat Neurosci* 18:942-952.
- Khalilov I, Le Van Quyen M, Gozlan H, Ben-Ari Y (2005) Epileptogenic actions of GABA and fast oscillations in the developing hippocampus. *Neuron* 48:787-796.

References

- Kimelberg HK, Goderie SK, Higman S, Pang S, Waniewski RA (1990) Swelling-induced release of glutamate, aspartate, and taurine from astrocyte cultures. *J Neurosci* 10:1583-1591.
- Kirchhoff F (2017) Analysis of Functional NMDA Receptors in Astrocytes. *Methods Mol Biol* 1677:241-251.
- Kislin M, Mugantseva E, Molotkov D, Kuleshkaya N, Khirug S, Kirilkin I, Pryazhnikov E, Kolikova J, Toptunov D, Yuryev M, Giniatullin R, Voikar V, Rivera C, Rauvala H, Khiroug L (2014) Flat-floored air-lifted platform: a new method for combining behavior with microscopy or electrophysiology on awake freely moving rodents. *J Vis Exp*:e51869.
- Kivi A, Lehmann TN, Kovács R, Eilers A, Jauch R, Meeneke HJ, von Deimling A, Heinemann U, Gabriel S (2000) Effects of barium on stimulus-induced rises of $[K^+]_o$ in human epileptic non-sclerotic and sclerotic hippocampal area CA1. *Eur J Neurosci* 12:2039-2048.
- Kuchibhotla KV, Lattarulo CR, Hyman BT, Bacskaï BJ (2009) Synchronous hyperactivity and intercellular calcium waves in astrocytes in Alzheimer mice. *Science* 323:1211-1215.
- Köhler S, Winkler U, Hirrlinger J (2019) Heterogeneity of Astrocytes in Grey and White Matter. *Neurochem Res*.
- Lalo U, Pankratov Y, Kirchhoff F, North RA, Verkhratsky A (2006) NMDA receptors mediate neuron-to-glia signaling in mouse cortical astrocytes. *J Neurosci* 26:2673-2683.
- Lalo U, Palygin O, Rasooli-Nejad S, Andrew J, Haydon PG, Pankratov Y (2014) Exocytosis of ATP from astrocytes modulates phasic and tonic inhibition in the neocortex. *PLoS Biol* 12:e1001747.
- Le Meur K, Mendizabal-Zubiaga J, Grandes P, Audinat E (2012) GABA release by hippocampal astrocytes. *Front Comput Neurosci* 6:59.
- Lee HS, Ghetti A, Pinto-Duarte A, Wang X, Dziewczapolski G, Galimi F, Huitron-Resendiz S, Piña-Crespo JC, Roberts AJ, Verma IM, Sejnowski TJ, Heinemann SF (2014) Astrocytes contribute to gamma oscillations and recognition memory. *Proc Natl Acad Sci U S A* 111:E3343-3352.
- Lee S, Yoon BE, Berglund K, Oh SJ, Park H, Shin HS, Augustine GJ, Lee CJ (2010) Channel-mediated tonic GABA release from glia. *Science* 330:790-796.
- Lee S, Kang BM, Kim JH, Min J, Kim HS, Ryu H, Park H, Bae S, Oh D, Choi M, Suh M (2018) Real-time in vivo two-photon imaging study reveals decreased cerebro-vascular volume and increased blood-brain barrier permeability in chronically stressed mice. *Sci Rep* 8:13064.
- Leybaert L, Sanderson MJ (2012) Intercellular Ca^{2+} waves: mechanisms and function. *Physiol Rev* 92:1359-1392.
- Li D, Li P, He Z, Cen D, Meng Z, Liang L, Luo X (2012a) Human intravenous immunoglobulins suppress seizure activities and inhibit the activation of GFAP-positive astrocytes in the hippocampus of picrotoxin-kindled rats. *Int J Neurosci* 122:200-208.
- Li T, Lytle N, Lan JQ, Sandau US, Boison D (2012b) Local disruption of glial adenosine homeostasis in mice associates with focal electrographic seizures: a first step in epileptogenesis? *Glia* 60:83-95.
- Lia A, Henriques VJ, Zonta M, Chiavegato A, Carmignoto G, Gómez-Gonzalo M, Losi G (2021) Calcium Signals in Astrocyte Microdomains, a Decade of Great Advances. *Front Cell Neurosci* 15:673433.
- Liddel SA et al. (2017) Neurotoxic reactive astrocytes are induced by activated microglia. *Nature*.
- Liu JH, Li ZL, Liu YS, Chu HD, Hu NY, Wu DY, Huang L, Li SJ, Li XW, Yang JM, Gao TM (2020) Astrocytic GABA. *Neurosci Bull* 36:705-718.
- Livet J, Weissman TA, Kang H, Draft RW, Lu J, Bennis RA, Sanes JR, Lichtman JW (2007) Transgenic strategies for combinatorial expression of fluorescent proteins in the nervous system. *Nature* 450:56-62.
- Loonen ICM, Jansen NA, Cain SM, Schenke M, Voskuyl RA, Yung AC, Bohnet B, Kozłowski P, Thijs RD, Ferrari MD, Snutch TP, van den Maagdenberg AMJM, Tolner EA (2019) Brainstem spreading depolarization and cortical dynamics during fatal seizures in *Cacna1a* S218L mice. *Brain* 142:412-425.
- Losi G, Mariotti L, Carmignoto G (2014) GABAergic interneuron to astrocyte signalling: a neglected form of cell communication in the brain. *Philos Trans R Soc Lond B Biol Sci* 369:20130609.
- Losi G, Marcon I, Mariotti L, Sessolo M, Chiavegato A, Carmignoto G (2016) A brain slice experimental model to study the generation and the propagation of focally-induced epileptiform activity. *J Neurosci Methods* 260:125-131.
- Lévesque M, Avoli M (2013) The kainic acid model of temporal lobe epilepsy. *Neurosci Biobehav Rev* 37:2887-2899.
- Lévesque M, Avoli M, Bernard C (2016) Animal models of temporal lobe epilepsy following systemic chemoconvulsant administration. *J Neurosci Methods* 260:45-52.

References

- Lévesque M, Langlois JM, Lema P, Courtemanche R, Bilodeau GA, Carmant L (2009) Synchronized gamma oscillations (30-50 Hz) in the amygdalo-hippocampal network in relation with seizure propagation and severity. *Neurobiol Dis* 35:209-218.
- Löscher W (2002) Animal models of epilepsy for the development of antiepileptogenic and disease-modifying drugs. A comparison of the pharmacology of kindling and post-status epilepticus models of temporal lobe epilepsy. *Epilepsy Res* 50:105-123.
- Löscher W, Schmidt D (2011) Modern antiepileptic drug development has failed to deliver: ways out of the current dilemma. *Epilepsia* 52:657-678.
- MacVicar BA, Newman EA (2015) Astrocyte regulation of blood flow in the brain. *Cold Spring Harb Perspect Biol* 7.
- MacVicar BA, Tse FW, Crichton SA, Kettenmann H (1989) GABA-activated Cl⁻ channels in astrocytes of hippocampal slices. *J Neurosci* 9:3577-3583.
- Mahmoud S, Gharagozloo M, Simard C, Gris D (2019) Astrocytes Maintain Glutamate Homeostasis in the CNS by Controlling the Balance between Glutamate Uptake and Release. *Cells* 8.
- Malarkey EB, Ni Y, Parpura V (2008) Ca²⁺ entry through TRPC1 channels contributes to intracellular Ca²⁺ dynamics and consequent glutamate release from rat astrocytes. *Glia* 56:821-835.
- Malatesta P, Hack MA, Hartfuss E, Kettenmann H, Klinkert W, Kirchhoff F, Gotz M (2003) Neuronal or glial progeny: Regional differences in radial glia fate. *Neuron* 37:751-764.
- Marina N, Turovsky E, Christie IN, Hosford PS, Hadjihambi A, Korsak A, Ang R, Mastitskaya S, Sheikhabaev S, Theparambil SM, Gourine AV (2018) Brain metabolic sensing and metabolic signaling at the level of an astrocyte. *Glia* 66:1185-1199.
- Mariotti L, Losi G, Sessolo M, Marcon I, Carmignoto G (2016) The inhibitory neurotransmitter GABA evokes long-lasting Ca²⁺ oscillations in cortical astrocytes. *Glia* 64:363-373.
- Mariotti L, Losi G, Lia A, Melone M, Chiavegato A, Gómez-Gonzalo M, Sessolo M, Bovetti S, Forli A, Zonta M, Reque LM, Marcon I, Pugliese A, Viollet C, Bettler B, Fellin T, Conti F, Carmignoto G (2018) Interneuron-specific signaling evokes distinctive somatostatin-mediated responses in adult cortical astrocytes. *Nat Commun* 9:82.
- Marshall FH, Jones KA, Kaupmann K, Bettler B (1999) GABAB receptors - the first 7TM heterodimers. *Trends Pharmacol Sci* 20:396-399.
- Marx M, Haas CA, Häussler U (2013) Differential vulnerability of interneurons in the epileptic hippocampus. *Front Cell Neurosci* 7:167.
- Matos M, Bosson A, Riebe I, Reynell C, Vallée J, Laplante I, Panatier A, Robitaille R, Lacaille JC (2018) Astrocytes detect and upregulate transmission at inhibitory synapses of somatostatin interneurons onto pyramidal cells. *Nat Commun* 9:4254.
- Matyash V, Kettenmann H (2010) Heterogeneity in astrocyte morphology and physiology. *Brain Res Rev* 63:2-10.
- Mederos S, Perea G (2019) GABAergic-astrocyte signaling: A refinement of inhibitory brain networks. *Glia* 67:1842-1851.
- Mederos S, González-Arias C, Perea G (2018) Astrocyte-Neuron Networks: A Multilane Highway of Signaling for Homeostatic Brain Function. *Front Synaptic Neurosci* 10:45.
- Mederos S, Sánchez-Puelles C, Esparza J, Valero M, Ponomarenko A, Perea G (2021) GABAergic signaling to astrocytes in the prefrontal cortex sustains goal-directed behaviors. *Nat Neurosci* 24:82-92.
- Meier SD, Kafitz KW, Rose CR (2008) Developmental profile and mechanisms of GABA-induced calcium signaling in hippocampal astrocytes. *Glia* 56:1127-1137.
- Messing A, Brenner M, Feany MB, Nedergaard M, Goldman JE (2012) Alexander Disease. *Journal of Neuroscience* 32:5017-5023.
- Mori T, Tanaka K, Buffo A, Wurst W, Kühn R, Götz M (2006) Inducible gene deletion in astroglia and radial glia--a valuable tool for functional and lineage analysis. *Glia* 54:21-34.
- Murphy-Royal C, Dupuis J, Groc L, Olié SHR (2017) Astroglial glutamate transporters in the brain: Regulating neurotransmitter homeostasis and synaptic transmission. *J Neurosci Res* 95:2140-2151.
- Müller J (2018) Preservation of Astrocytic Coupling Prevents Epileptogenesis (PhD Thesis). In: Bonn: Rheinische Friedrich-Wilhelms-Universität.
- Müller J, Timmermann A, Henning L, Müller H, Steinhäuser C, Bedner P (2020) Astrocytic GABA Accumulation in Experimental Temporal Lobe Epilepsy. *Front Neurol* 11:614923.

References

- Nagai J, Rajbhandari AK, Gangwani MR, Hachisuka A, Coppola G, Masmanidis SC, Fanselow MS, Khakh BS (2019) Hyperactivity with Disrupted Attention by Activation of an Astrocyte Synaptogenic Cue. *Cell* 177:1280-1292.e1220.
- Nagelhus EA, Ottersen OP (2013) Physiological roles of aquaporin-4 in brain. *Physiol Rev* 93:1543-1562.
- Navarrete M, Araque A (2010) Endocannabinoids potentiate synaptic transmission through stimulation of astrocytes. *Neuron* 68:113-126.
- Nett WJ, Oloff SH, McCarthy KD (2002) Hippocampal astrocytes in situ exhibit calcium oscillations that occur independent of neuronal activity. *J Neurophysiol* 87:528-537.
- Nielsen S, Nagelhus EA, Amiry-Moghaddam M, Bourque C, Agre P, Ottersen OP (1997) Specialized membrane domains for water transport in glial cells: high-resolution immunogold cytochemistry of aquaporin-4 in rat brain. *J Neurosci* 17:171-180.
- Nikolic L, Nobili P, Shen W, Audinat E (2020) Role of astrocyte purinergic signaling in epilepsy. *Glia* 68:1677-1691.
- Nikolic L, Shen W, Nobili P, Virenque A, Ulmann L, Audinat E (2018) Blocking TNF α -driven astrocyte purinergic signaling restores normal synaptic activity during epileptogenesis. *Glia* 66:2673-2683.
- Nimmerjahn A, Kirchhoff F, Helmchen F (2005) Resting microglial cells are highly dynamic surveillants of brain parenchyma in vivo. *Science* 308:1314-1318.
- Nimmerjahn A, Mukamel EA, Schnitzer MJ (2009) Motor behavior activates Bergmann glial networks. *Neuron* 62:400-412.
- Nolte C, Matyash M, Pivneva T, Schipke CG, Ohlemeyer C, Hanisch UK, Kirchhoff F, Kettenmann H (2001) GFAP promoter-controlled EGFP-expressing transgenic mice: a tool to visualize astrocytes and astrogliosis in living brain tissue. *Glia* 33:72-86.
- Noè F, Cattalini A, Vila Verde D, Alessi C, Colciaghi F, Figini M, Zucca I, de Curtis M (2019) Epileptiform activity contralateral to unilateral hippocampal sclerosis does not cause the expression of brain damage markers. *Epilepsia* 60:1184-1199.
- Ogata K, Kosaka T (2002) Structural and quantitative analysis of astrocytes in the mouse hippocampus. *Neuroscience* 113:221-233.
- Oheim M, Schmidt E, Hirrlinger J (2017) Local energy on demand: Are 'spontaneous' astrocytic Ca(2+)-microdomains the regulatory unit for astrocyte-neuron metabolic cooperation? *Brain Res Bull*.
- Orr AG, Hsiao EC, Wang MM, Ho K, Kim DH, Wang X, Guo W, Kang J, Yu GQ, Adame A, Devizde N, Dubal DB, Masliah E, Conklin BR, Mucke L (2015) Astrocytic adenosine receptor A2A and Gs-coupled signaling regulate memory. *Nat Neurosci* 18:423-434.
- Ortinski PI, Dong J, Mungenast A, Yue C, Takano H, Watson DJ, Haydon PG, Coulter DA (2010) Selective induction of astrocytic gliosis generates deficits in neuronal inhibition. *Nat Neurosci* 13:584-591.
- Pandit S, Neupane C, Woo J, Sharma R, Nam MH, Lee GS, Yi MH, Shin N, Kim DW, Cho H, Jeon BH, Kim HW, Lee CJ, Park JB (2020) Bestrophin1-mediated tonic GABA release from reactive astrocytes prevents the development of seizure-prone network in kainate-injected hippocampi. *Glia* 68:1065-1080.
- Pandolfo M (2011) Genetics of epilepsy. *Semin Neurol* 31:506-518.
- Pankratov Y, Lalo U (2015) Role for astroglial α 1-adrenoreceptors in gliotransmission and control of synaptic plasticity in the neocortex. *Front Cell Neurosci* 9:230.
- Pannasch U, Vargová L, Reingruber J, Ezan P, Holcman D, Giaume C, Syková E, Rouach N (2011) Astroglial networks scale synaptic activity and plasticity. *Proc Natl Acad Sci U S A* 108:8467-8472.
- Park H, Oh SJ, Han KS, Woo DH, Mannaioni G, Traynelis SF, Lee CJ (2009) Bestrophin-1 encodes for the Ca²⁺-activated anion channel in hippocampal astrocytes. *J Neurosci* 29:13063-13073.
- Parpura V, Basarsky TA, Liu F, Jęftinija K, Jęftinija S, Haydon PG (1994) GLUTAMATE-MEDIATED ASTROCYTE NEURON SIGNALING. *Nature* 369:744-747.
- Parri HR, Gould TM, Crunelli V (2001) Spontaneous astrocytic Ca²⁺ oscillations in situ drive NMDAR-mediated neuronal excitation. *Nat Neurosci* 4:803-812.
- Pascual O, Casper KB, Kubera C, Zhang J, Revilla-Sanchez R, Sul JY, Takano H, Moss SJ, McCarthy K, Haydon PG (2005) Astrocytic purinergic signaling coordinates synaptic networks. *Science* 310:113-116.
- Paukert M, Agarwal A, Cha J, Doze VA, Kang JU, Bergles DE (2014) Norepinephrine controls astroglial responsiveness to local circuit activity. *Neuron* 82:1263-1270.
- Pavlov I, Walker MC (2013) Tonic GABA(A) receptor-mediated signalling in temporal lobe epilepsy. *Neuropharmacology* 69:55-61.

References

- Pekny M, Pekna M, Messing A, Steinhäuser C, Lee JM, Parpura V, Hol EM, Sofroniew MV, Verkhratsky A (2016) Astrocytes: a central element in neurological diseases. *Acta Neuropathol* 131:323-345.
- Pelvig DP, Pakkenberg H, Stark AK, Pakkenberg B (2008) Neocortical glial cell numbers in human brains. *Neurobiol Aging* 29:1754-1762.
- Perea G, Araque A (2007) Astrocytes potentiate transmitter release at single hippocampal synapses. *Science* 317:1083-1086.
- Perea G, Navarrete M, Araque A (2009) Tripartite synapses: astrocytes process and control synaptic information. *Trends Neurosci* 32:421-431.
- Perea G, Gómez R, Mederos S, Covelo A, Ballesteros JJ, Schlosser L, Hernández-Vivanco A, Martín-Fernández M, Quintana R, Rayan A, Díez A, Fuenzalida M, Agarwal A, Bergles DE, Bettler B, Manahan-Vaughan D, Martín ED, Kirchhoff F, Araque A (2016) Activity-dependent switch of GABAergic inhibition into glutamatergic excitation in astrocyte-neuron networks. *Elife* 5.
- Pestana F, Edwards-Faret G, Belgard TG, Martirosyan A, Holt MG (2020) No Longer Underappreciated: The Emerging Concept of Astrocyte Heterogeneity in Neuroscience. *Brain Sci* 10.
- Pierce KL, Premont RT, Lefkowitz RJ (2002) Seven-transmembrane receptors. *Nat Rev Mol Cell Biol* 3:639-650.
- Pin JP, Bettler B (2016) Organization and functions of mGlu and GABAB receptor complexes. *Nature* 540:60-68.
- Pinto DJ, Patrick SL, Huang WC, Connors BW (2005) Initiation, propagation, and termination of epileptiform activity in rodent neocortex in vitro involve distinct mechanisms. *J Neurosci* 25:8131-8140.
- Pirttimäki T, Parri HR, Crunelli V (2013) Astrocytic GABA transporter GAT-1 dysfunction in experimental absence seizures. *J Physiol* 591:823-833.
- Pitkänen A, Lukasiuk K, Dudek FE, Staley KJ (2015) Epileptogenesis. *Cold Spring Harb Perspect Med* 5.
- Plata A, Lebedeva A, Denisov P, Nosova O, Postnikova TY, Pimashkin A, Brazhe A, Zaitsev AV, Rusakov DA, Semyanov A (2018) Astrocytic Atrophy Following. *Front Mol Neurosci* 11:215.
- Podor B, Hu YL, Ohkura M, Nakai J, Croll R, Fine A (2015) Comparison of genetically encoded calcium indicators for monitoring action potentials in mammalian brain by two-photon excitation fluorescence microscopy. *Neurophotonics* 2:021014.
- Pologruto TA, Sabatini BL, Svoboda K (2003) ScanImage: flexible software for operating laser scanning microscopes. *Biomed Eng Online* 2:13.
- Porter JT, McCarthy KD (1996) Hippocampal astrocytes in situ respond to glutamate released from synaptic terminals. *J Neurosci* 16:5073-5081.
- Prosser HM et al. (2001) Epileptogenesis and enhanced prepulse inhibition in GABA(B1)-deficient mice. *Mol Cell Neurosci* 17:1059-1070.
- Puttachary S, Sharma S, Tse K, Beamer E, Sexton A, Crutison J, Thippeswamy T (2015) Immediate Epileptogenesis after Kainate-Induced Status Epilepticus in C57BL/6J Mice: Evidence from Long Term Continuous Video-EEG Telemetry. *PLoS One* 10:e0131705.
- Racine RJ (1972) Modification of seizure activity by electrical stimulation. II. Motor seizure. *Electroencephalogr Clin Neurophysiol* 32:281-294.
- Rassendren F, Audinat E (2016) Purinergic signaling in epilepsy. *J Neurosci Res* 94:781-793.
- Represa A, Jorquera I, Le Gal La Salle G, Ben-Ari Y (1993) Epilepsy induced collateral sprouting of hippocampal mossy fibers: does it induce the development of ectopic synapses with granule cell dendrites? *Hippocampus* 3:257-268.
- Robel S (2017) Astroglial Scarring and Seizures: A Cell Biological Perspective on Epilepsy. *Neuroscientist* 23:152-168.
- Robel S, Buckingham SC, Boni JL, Campbell SL, Danbolt NC, Riedemann T, Sutor B, Sontheimer H (2015) Reactive astrogliosis causes the development of spontaneous seizures. *J Neurosci* 35:3330-3345.
- Rogawski MA, Löscher W (2004) The neurobiology of antiepileptic drugs. *Nat Rev Neurosci* 5:553-564.
- Rossi DJ, Oshima T, Attwell D (2000) Glutamate release in severe brain ischaemia is mainly by reversed uptake. *Nature* 403:316-321.
- Rouach N, Koulakoff A, Abudara V, Willecke K, Giaume C (2008) Astroglial metabolic networks sustain hippocampal synaptic transmission. *Science* 322:1551-1555.
- Rusakov DA (2015) Disentangling calcium-driven astrocyte physiology. *Nat Rev Neurosci* 16:226-233.
- Río-Hortega DP (1928) Tercera aportacion al conocimiento morfologico e interpretacion funcional de la oligodendroglia.

References

- Río-Hortega P (1932) Microglia. In: Cytology and cellular pathology of the nervous system, pp 483-534. New York, N.Y.: P.B. Hoeber, inc.
- Saab AS, Neumeyer A, Jahn HM, Cupido A, Šimek AA, Boele HJ, Scheller A, Le Meur K, Götz M, Monyer H, Sprengel R, Rubio ME, Deitmer JW, De Zeeuw CI, Kirchhoff F (2012) Bergmann glial AMPA receptors are required for fine motor coordination. *Science* 337:749-753.
- Saab AS et al. (2016) Oligodendroglial NMDA Receptors Regulate Glucose Import and Axonal Energy Metabolism. *Neuron*.
- Sano F, Shigetomi E, Shinozaki Y, Tsuzukiyama H, Saito K, Mikoshiba K, Horiuchi H, Cheung DL, Nabekura J, Sugita K, Aihara M, Koizumi S (2021) Reactive astrocyte-driven epileptogenesis is induced by microglia initially activated following status epilepticus. *JCI Insight* 6.
- Sanon N, Carmant L, Emond M, Congar P, Lacaille JC (2005) Short-term effects of kainic acid on CA1 hippocampal interneurons differentially vulnerable to excitotoxicity. *Epilepsia* 46:837-848.
- Santello M, Bezzi P, Volterra A (2011) TNF α controls glutamatergic gliotransmission in the hippocampal dentate gyrus. *Neuron* 69:988-1001.
- Sarac S, Afzal S, Broholm H, Madsen FF, Ploug T, Laursen H (2009) Excitatory amino acid transporters EAAT-1 and EAAT-2 in temporal lobe and hippocampus in intractable temporal lobe epilepsy. *APMIS* 117:291-301.
- Sasaki T, Ishikawa T, Abe R, Nakayama R, Asada A, Matsuki N, Ikegaya Y (2014) Astrocyte calcium signalling orchestrates neuronal synchronization in organotypic hippocampal slices. *J Physiol* 592:2771-2783.
- Sato Y, Wong SM, Iimura Y, Ochi A, Doesburg SM, Otsubo H Spatiotemporal changes in regularity of gamma oscillations contribute to focal ictogenesis.
- Scemes E, Giaume C (2006) Astrocyte calcium waves: what they are and what they do. *Glia* 54:716-725.
- Scharfman HE, Goodman JH, Sollas AL, Croll SD (2002) Spontaneous limbic seizures after intrahippocampal infusion of brain-derived neurotrophic factor. *Exp Neurol* 174:201-214.
- Scheffer IE, Berkovic S, Capovilla G, Connolly MB, French J, Guilhoto L, Hirsch E, Jain S, Mathern GW, Moshé SL, Nordli DR, Perucca E, Tomson T, Wiebe S, Zhang YH, Zuberi SM (2017) ILAE classification of the epilepsies: Position paper of the ILAE Commission for Classification and Terminology. *Epilepsia* 58:512-521.
- Scheller A, Kirchhoff F (2016) Endocannabinoids and Heterogeneity of Glial Cells in Brain Function. *Front Integr Neurosci* 10:24.
- Schuler V et al. (2001) Epilepsy, hyperalgesia, impaired memory, and loss of pre- and postsynaptic GABA(B) responses in mice lacking GABA(B1). *Neuron* 31:47-58.
- Schwarz Y, Zhao N, Kirchhoff F, Bruns D (2017) Astrocytes control synaptic strength by two distinct v-SNARE-dependent release pathways. *Nat Neurosci* 20:1529-1539.
- Seidel JL, Escartin C, Ayata C, Bonvento G, Shuttleworth CW (2016) Multifaceted roles for astrocytes in spreading depolarization: A target for limiting spreading depolarization in acute brain injury? *Glia* 64:5-20.
- Seifert G, Steinhäuser C (1995) Glial cells in the mouse hippocampus express AMPA receptors with an intermediate Ca²⁺ permeability. *Eur J Neurosci* 7:1872-1881.
- Seifert G, Steinhäuser C (2018) Heterogeneity and function of hippocampal macroglia. *Cell Tissue Res* 373:653-670.
- Seifert G, Hüttmann K, Binder DK, Hartmann C, Wyczynski A, Neusch C, Steinhäuser C (2009) Analysis of astroglial K⁺ channel expression in the developing hippocampus reveals a predominant role of the Kir4.1 subunit. *J Neurosci* 29:7474-7488.
- Semyanov A (2019) Spatiotemporal pattern of calcium activity in astrocytic network. *Cell Calcium* 78:15-25.
- Serrano A, Haddjeri N, Lacaille JC, Robitaille R (2006) GABAergic network activation of glial cells underlies hippocampal heterosynaptic depression. *J Neurosci* 26:5370-5382.
- Sharma S, Puttachary S, Thippeswamy A, Kanthasamy AG, Thippeswamy T (2018) Status Epilepticus: Behavioral and Electroencephalography Seizure Correlates in Kainate Experimental Models. *Front Neurol* 9:7.
- Shen W, Nikolic L, Meunier C, Pfrieger F, Audinat E (2017) An autocrine purinergic signaling controls astrocyte-induced neuronal excitation. *Sci Rep* 7:11280.
- Shibata T, Yamada K, Watanabe M, Ikenaka K, Wada K, Tanaka K, Inoue Y (1997) Glutamate transporter GLAST is expressed in the radial glia-astrocyte lineage of developing mouse spinal cord. *J Neurosci* 17:9212-9219.
- Shigetomi E, Patel S, Khakh BS (2016) Probing the Complexities of Astrocyte Calcium Signaling. *Trends Cell Biol* 26:300-312.

References

- Shigetomi E, Kracun S, Sofroniew MV, Khakh BS (2010) A genetically targeted optical sensor to monitor calcium signals in astrocyte processes. *Nature Neuroscience* 13:759-U143.
- Shigetomi E, Saito K, Sano F, Koizumi S (2019) Aberrant Calcium Signals in Reactive Astrocytes: A Key Process in Neurological Disorders. *Int J Mol Sci* 20.
- Shigetomi E, Tong X, Kwan KY, Corey DP, Khakh BS (2011) TRPA1 channels regulate astrocyte resting calcium and inhibitory synapse efficacy through GAT-3. *Nat Neurosci* 15:70-80.
- Shimada T, Yamagata K (2018) Pentylentetrazole-Induced Kindling Mouse Model. *J Vis Exp*.
- Simard M, Nedergaard M (2004) The neurobiology of glia in the context of water and ion homeostasis. *Neuroscience* 129:877-896.
- Sofroniew MV (2014) Astrogliosis. *Cold Spring Harb Perspect Biol* 7:a020420.
- Sofroniew MV, Vinters HV (2010) Astrocytes: biology and pathology. *Acta Neuropathol* 119:7-35.
- Somjen GG (2001) Mechanisms of spreading depression and hypoxic spreading depression-like depolarization. *Physiol Rev* 81:1065-1096.
- Steinhäuser C, Grunnet M, Carmignoto G (2016) Crucial role of astrocytes in temporal lobe epilepsy. *Neuroscience* 323:157-169.
- Steinmetz NA et al. (2017) Aberrant Cortical Activity in Multiple GCaMP6-Expressing Transgenic Mouse Lines. *eNeuro* 4.
- Sternberg N, Hamilton D (1981) Bacteriophage P1 site-specific recombination. I. Recombination between loxP sites. *J Mol Biol* 150:467-486.
- Stopper L (2018) Complexity of Ca²⁺ signals in astrocytes : Contribution of astroglial GABA_B receptors (PhD Thesis). In. Homburg Saar: Universität des Saarlandes.
- Tabata T, Araishi K, Hashimoto K, Hashimoto Y, van der Putten H, Bettler B, Kano M (2004) Ca²⁺ activity at GABA_B receptors constitutively promotes metabotropic glutamate signaling in the absence of GABA. *Proc Natl Acad Sci U S A* 101:16952-16957.
- Takata N, Hirase H (2008) Cortical layer 1 and layer 2/3 astrocytes exhibit distinct calcium dynamics in vivo. *PLoS One* 3:e2525.
- Tasic B et al. (2018) Shared and distinct transcriptomic cell types across neocortical areas. *Nature* 563:72-78.
- Teive HA, Kowacs PA, Maranhão Filho P, Piovesan EJ, Werneck LC (2005) Leao's cortical spreading depression: from experimental "artifact" to physiological principle. *Neurology* 65:1455-1459.
- Thom M (2014) Review: Hippocampal sclerosis in epilepsy: a neuropathology review. *Neuropathol Appl Neurobiol* 40:520-543.
- Thom M, Martinian L, Williams G, Stoeber K, Sisodiya SM (2005) Cell proliferation and granule cell dispersion in human hippocampal sclerosis. *J Neuropathol Exp Neurol* 64:194-201.
- Thrane AS, Rangroo Thrane V, Zeppenfeld D, Lou N, Xu Q, Nagelhus EA, Nedergaard M (2012) General anesthesia selectively disrupts astrocyte calcium signaling in the awake mouse cortex. *Proc Natl Acad Sci U S A* 109:18974-18979.
- Tian GF, Azmi H, Takano T, Xu QW, Peng WG, Lin J, Oberheim N, Lou NH, Wang XH, Zielke HR, Kang J, Nedergaard M (2005a) An astrocytic basis of epilepsy. *Nature Medicine* 11:973-981.
- Tian GF, Azmi H, Takano T, Xu Q, Peng W, Lin J, Oberheim N, Lou N, Wang X, Zielke HR, Kang J, Nedergaard M (2005b) An astrocytic basis of epilepsy. *Nat Med* 11:973-981.
- Tian L, Hires SA, Mao T, Huber D, Chiappe ME, Chalasani SH, Petreanu L, Akerboom J, McKinney SA, Schreier ER, Bargmann CI, Jayaraman V, Svoboda K, Looger LL (2009) Imaging neural activity in worms, flies and mice with improved GCaMP calcium indicators. *Nat Methods* 6:875-881.
- Treiman DM (2001) GABAergic mechanisms in epilepsy. *Epilepsia* 42 Suppl 3:8-12.
- Trevelyan AJ, Sussillo D, Watson BO, Yuste R (2006) Modular propagation of epileptiform activity: evidence for an inhibitory veto in neocortex. *J Neurosci* 26:12447-12455.
- Twele F, Schidlitzki A, Töllner K, Löscher W (2017) The intrahippocampal kainate mouse model of mesial temporal lobe epilepsy: Lack of electrographic seizure-like events in sham controls. *Epilepsia Open* 2:180-187.
- Umpierre AD, West PJ, White JA, Wilcox KS (2019) Conditional Knock-out of mGluR5 from Astrocytes during Epilepsy Development Impairs High-Frequency Glutamate Uptake. *J Neurosci* 39:727-742.
- Upadhyay D, Kodali M, Gitai D, Castro OW, Zanirati G, Upadhyay R, Attaluri S, Mitra E, Shuai B, Hattiangady B, Shetty AK (2019) A Model of Chronic Temporal Lobe Epilepsy Presenting Constantly Rhythmic and Robust Spontaneous Seizures, Co-morbidities and Hippocampal Neuropathology. *Aging Dis* 10:915-936.

References

- Uva L, Avoli M, de Curtis M (2009) Synchronous GABA-receptor-dependent potentials in limbic areas of the in-vitro isolated adult guinea pig brain. *Eur J Neurosci* 29:911-920.
- van der Hel WS, Notenboom RG, Bos IW, van Rijen PC, van Veelen CW, de Graan PN (2005) Reduced glutamine synthetase in hippocampal areas with neuron loss in temporal lobe epilepsy. *Neurology* 64:326-333.
- Ventura R, Harris KM (1999) Three-dimensional relationships between hippocampal synapses and astrocytes. *J Neurosci* 19:6897-6906.
- Verhoog QP, Holtman L, Aronica E, van Vliet EA (2020) Astrocytes as Guardians of Neuronal Excitability: Mechanisms Underlying Epileptogenesis. *Front Neurol* 11:591690.
- Verkhatsky A, Nedergaard M (2014) Astroglial cradle in the life of the synapse. *Philos Trans R Soc Lond B Biol Sci* 369:20130595.
- Verkhatsky A, Nedergaard M (2018) Physiology of Astroglia. *Physiol Rev* 98:239-389.
- Verkhatsky A, Verkhatsky A, Krishtal OA, Burnstock G (2009) Purinoceptors on neuroglia. *Mol Neurobiol* 39:190-208.
- Verkhatsky A, Matteoli M, Parpura V, Mothet JP, Zorec R (2016) Astrocytes as secretory cells of the central nervous system: idiosyncrasies of vesicular secretion. *EMBO J* 35:239-257.
- Vezzani A, Balosso S, Ravizza T (2008) The role of cytokines in the pathophysiology of epilepsy. *Brain Behav Immun* 22:797-803.
- Vezzani A, French J, Bartfai T, Baram TZ (2011) The role of inflammation in epilepsy. *Nat Rev Neurol* 7:31-40.
- Vezzani A, Moneta D, Conti M, Richichi C, Ravizza T, De Luigi A, De Simoni MG, Sperk G, Andell-Jonsson S, Lundkvist J, Iverfeldt K, Bartfai T (2000) Powerful anticonvulsant action of IL-1 receptor antagonist on intracerebral injection and astrocytic overexpression in mice. *Proc Natl Acad Sci U S A* 97:11534-11539.
- Vélez-Fort M, Audinat E, Angulo MC (2012) Central role of GABA in neuron-glia interactions. *Neuroscientist* 18:237-250.
- Walker MC (2015) Hippocampal Sclerosis: Causes and Prevention. *Semin Neurol* 35:193-200.
- Wallraff A, Köhling R, Heinemann U, Theis M, Willecke K, Steinhäuser C (2006) The impact of astrocytic gap junctional coupling on potassium buffering in the hippocampus. *J Neurosci* 26:5438-5447.
- Walls AB, Waagepetersen HS, Bak LK, Schousboe A, Sonnewald U (2015) The glutamine-glutamate/GABA cycle: function, regional differences in glutamate and GABA production and effects of interference with GABA metabolism. *Neurochem Res* 40:402-409.
- Wang F, Smith NA, Xu Q, Goldman S, Peng W, Huang JH, Takano T, Nedergaard M (2013) Photolysis of Caged Ca²⁺ But Not Receptor-Mediated Ca²⁺ Signaling Triggers Astrocytic Glutamate Release. *Journal of Neuroscience* 33:17404-17412.
- Wang Y, Toprani S, Tang Y, Vrabcic T, Durand DM (2014) Mechanism of highly synchronized bilateral hippocampal activity. *Exp Neurol* 251:101-111.
- Weiergräber M, Henry M, Hescheler J, Smyth N, Schneider T (2005) Electroencephalographic and deep intracerebral EEG recording in mice using a telemetry system. *Brain Res Brain Res Protoc* 14:154-164.
- Woo DH, Han KS, Shim JW, Yoon BE, Kim E, Bae JY, Oh SJ, Hwang EM, Marmorstein AD, Bae YC, Park JY, Lee CJ (2012) TREK-1 and Best1 channels mediate fast and slow glutamate release in astrocytes upon GPCR activation. *Cell* 151:25-40.
- Wu DC, Chen RY, Cheng TC, Chiang YC, Shen ML, Hsu LL, Zhou N (2018) Spreading Depression Promotes Astrocytic Calcium Oscillations and Enhances Gliotransmission to Hippocampal Neurons. *Cereb Cortex* 28:3204-3216.
- Xin W, Bonci A (2018) Functional Astrocyte Heterogeneity and Implications for Their Role in Shaping Neurotransmission. *Front Cell Neurosci* 12:141.
- Yang Y, Vidensky S, Jin L, Jie C, Lorenzini I, Frankl M, Rothstein JD (2011) Molecular comparison of GLT1+ and ALDH1L1+ astrocytes in vivo in astroglial reporter mice. *Glia* 59:200-207.
- Yang Y, Liu N, He Y, Liu Y, Ge L, Zou L, Song S, Xiong W, Liu X (2018) Improved calcium sensor GCaMP-X overcomes the calcium channel perturbations induced by the calmodulin in GCaMP. *Nat Commun* 9:1504.
- Ye L, Haroon MA, Salinas A, Paukert M (2017) Comparison of GCaMP3 and GCaMP6f for studying astrocyte Ca²⁺ dynamics in the awake mouse brain. *PLoS One* 12:e0181113.
- Ye ZC, Wyeth MS, Baltan-Tekkok S, Ransom BR (2003) Functional hemichannels in astrocytes: a novel mechanism of glutamate release. *J Neurosci* 23:3588-3596.
- Yoon BE, Woo J, Justin Lee C (2012) Astrocytes as GABA-ergic and GABA-ceptive Cells. *Neurochem Res*.

References

- Zeisel A, Muñoz-Manchado AB, Codeluppi S, Lönnerberg P, La Manno G, Juréus A, Marques S, Munguba H, He L, Betsholtz C, Rolny C, Castelo-Branco G, Hjerling-Leffler J, Linnarsson S (2015) Brain structure. Cell types in the mouse cortex and hippocampus revealed by single-cell RNA-seq. *Science* 347:1138-1142.
- Zeng W, Mak DO, Li Q, Shin DM, Foskett JK, Muallem S (2003) A new mode of Ca²⁺ signaling by G protein-coupled receptors: gating of IP₃ receptor Ca²⁺ release channels by Gbetagamma. *Curr Biol* 13:872-876.
- Zhang X, Qiao Z, Liu N, Gao L, Wei L, Liu A, Ma Z, Wang F, Hou S, Li J, Shen H (2019) Stereotypical patterns of epileptiform calcium signal in hippocampal CA1, CA3, dentate gyrus and entorhinal cortex in freely moving mice. *Sci Rep* 9:4518.
- Zhang Y, Barres BA (2010) Astrocyte heterogeneity: an underappreciated topic in neurobiology. *Curr Opin Neurobiol* 20:588-594.
- Zhang Y, Chen K, Sloan SA, Bennett ML, Scholze AR, O'Keefe S, Phatnani HP, Guarnieri P, Caneda C, Ruderisch N, Deng S, Liddelow SA, Zhang C, Daneman R, Maniatis T, Barres BA, Wu JQ (2014) An RNA-Sequencing Transcriptome and Splicing Database of Glia, Neurons, and Vascular Cells of the Cerebral Cortex. *J Neurosci* 34:11929-11947.
- Zorec R, Araque A, Carmignoto G, Haydon PG, Verkhratsky A, Parpura V (2012) Astroglial excitability and gliotransmission: an appraisal of Ca²⁺ as a signalling route. *ASN Neuro* 4.
- Zur Nieden R, Deitmer JW (2006) The role of metabotropic glutamate receptors for the generation of calcium oscillations in rat hippocampal astrocytes in situ. *Cereb Cortex* 16:676-687.
- Álvarez-Ferradas C, Morales JC, Wellmann M, Nualart F, Roncagliolo M, Fuenzalida M, Bonansco C (2015) Enhanced astroglial Ca²⁺ signaling increases excitatory synaptic strength in the epileptic brain. *Glia* 63:1507-1521.

12. ACKNOWLEDGEMENT

Firstly, I would like to extend my gratitude and appreciation to my supervisor Prof. Frank Kirchhoff for entrusting me with this challenging and exciting PhD project. Your guidance paired with the ambition to let us experience science from Tokyo to Saõ Paolo has been pivotal for my scientific and personal development.

I thank Dr. Etienne Audinat for scientific discussions during our EU-Glia PhD meetings and accepting to review my thesis.

I am thankful to the European Union's Horizon 2020 Research and Innovation Programme for funding this project (Marie Skłodowska-Curie grant agreement No. 722053), along with the Deutsche Forschungsgemeinschaft DFG (SFB 894, SFB 1158, SPP 1757).

I am grateful to my collaborators Peter Bedner, Lukas Henning and Toni Berger for instrumental discussions about epilepsy models (including surgery course with Peter) and EEG analysis. Moreover, it was a pleasure to be a part of the EU-Glia PhD network and to represent my fellow ESRs. Thank you all for the great synergy. Being a speaker at our symposium at the XIV European Meeting on Glial Cells in Health and Disease in Porto was a highlight during my PhD.

I want to thank all current and former members of the Kirchhoff lab for a pleasant working atmosphere, exceptional team spirit, and scientific exchange. A special thank you in this regard goes to Fei (Wenhui Huang), Qilin Guo, Qing Liu, Daniel Schauenburg, Frank Rhode, Bogdan Cătălin, Luciana Politti Cartarozzi, Erika Meyer, Mariza Bortolanza, Elisa Damo, Na Zhao, and Arne Blickle.

My sincere thanks also goes to Anja Scheller, for always lending a sympathetic ear and solution-driven support. You have contributed to my scientific and personal progress during this incredible adventure. My deep gratitude and admiration go to Cai (Xianshu Bai). Thank you for teaching me since my master student times. Your support has been invaluable. Michael Schweigmann, thank you for providing the surface electrodes and the epic imaging sessions. Lipao Fang, thanks a lot for supporting me with additional experiments for the publication of this work. Emeline Buttigieg, ma chère compatriote, thank you for accompanying me through the ups and downs of PhD life! Davide Gobbo and Phillip Rieder, my favorite passageiros, thank you for the "hammer" times in the lab and around the world (one day we will make it to Curitiba)! Gebhard Stopper, thank you for providing MSparkles for Ca²⁺ signal/ ECoG analysis and being open to all refining requests. Your excellent sense of humour and support in all circumstances were highly appreciated!

Carmen Kasakow and Laura Stopper, thank you for welcoming me in the lab at the very beginning of this journey. I will always cherish the memories of the “glia girls” times with you two, Cai and your families. Furthermore, I am especially grateful to Julia Müller for exceptional scientific and personal advice.

A heartfelt thanks goes to my closest friends and spikey confidant who offered wonderful support, especially throughout the last two years.

Lastly, I address my deepest gratitude to my family for always encouraging me and being present.

I dedicate this thesis to my parents, who have enabled this achievement with their unconditional support.

Ich widme diese Arbeit meinen Eltern, welche diese Leistung durch ihre bedingungslose Unterstützung ermöglicht haben.

Je dédie cette thèse à mes parents, qui m'ont permis de réaliser ce travail grâce à leur soutien inconditionnel.

13. CURRICULUM VITAE AND LIST OF PUBLICATIONS

The curriculum vitae was removed from the electronic version of the doctoral thesis for reasons of data protection.

PUBLICATIONS

- Caudal LC***, Gobbo D*, Scheller A & Kirchhoff F (2020). The paradox of astroglial Ca²⁺ signals at the interface of excitation and inhibition. *Frontiers in Cellular Neuroscience* 14:399.
- Schweigmann M*, **Caudal LC***, Scheller A, Koch KP, Kirchhoff F (in press). Versatile LCP surface micro-electrodes for combining electrophysiology and *in vivo* 2P-imaging in the murine CNS. *Frontiers in Cellular Neuroscience*.
- Fang L, Zhao N, **Caudal LC**, Zhao R, Lin C-H, Chang H-F, Hainz N, Meier C, Bettler B, Huang W, Scheller A, Kirchhoff F & Bai X. (in revision). Impaired bidirectional communication between interneurons and oligodendrocyte precursor cells affects cognitive behavior. *Nature communications* (bioRxiv 2021.2005.2004.442422).
- Müller FE, Cherkas V, Stopper G, **Caudal LC**, Stopper L, Kirchhoff F, Henneberger C, Ponimaskin EG & Zeug A. (in revision). Deciphering spatio-temporal fluorescence changes using multi-threshold event detection (MTED). *Glia* (bioRxiv 2020.2012.2006.413492).
- Laporte MH, Chi KI, Rolland M, **Caudal LC**, Martinez-Hernandez J, Martineau M, Chatellard C, Denarier E, Mercier V, Lemaître F, Blot B, Moutaux E, Cazorla M, Buisson A, Perrais D, Fraboulet S, Lanté F, Kirchhoff F, Hemming FJ & Sadoul R. (submitted to Review Commons by EMBO Press). ALG-2 interacting protein-X (Alix) is required for activity-dependent bulk endocytosis at brain synapses. *bioRxiv*, 2020.07.20.211854.
- Bai X, Zhao N, Huang W, **Caudal LC**, Zhao R, Hirrlinger J, Walz W, Kirchhoff F & Scheller A. (2021). After traumatic brain injury oligodendrocytes regain a plastic phenotype and can become astrocytes. *bioRxiv*, 2021.2006.2018.448919.
- Caudal LC**, Fang L, Stopper G, Schweigmann M, Schwarz Y, Scheller A, Bruns D, Kirchhoff F (in preparation). Astroglial GABA_B receptor deletion attenuates epileptic network function *in vivo*.
- Stopper G, **Caudal LC**, Felix L, Stopper L, Everaerts K, Rose CR, Scheller A, Kirchhoff F (in preparation). MSparkles – An open-source tool to visualize and analyze fluorescent microscopy image sequences.
- Scheller A, Kasakow CV, Stopper L, **Caudal LC**, Price AM, Linder S, Guo Q, Fang L, Ponciano Da Silva Moraes RA, Qing L, Bortolanza M, Bai X, Stopper G, Huang W & Kirchhoff F. (in preparation). Tamoxifen independent recombination of DNA (TIReD) in various glial CreERT2 transgenic mouse lines.

PRESENTATIONS AT INTERNATIONAL CONFERENCES

- Caudal LC**, Stopper G, Schweigmann M, Bedner P, Steinhäuser C, Scheller A and Kirchhoff F (2019). In vivo contributions of astroglial GABA_B receptors to pathological network function in temporal lobe epilepsy. CAPES DAAD COFECUB Symposium “Brazil Glia Network: The Magic and Mystery of Glia”, University of São Paulo, Ribeirão Preto. (Oral presentation)
- Caudal LC**, Stopper G, Schweigmann M, Bedner P, Steinhäuser C, Scheller A and Kirchhoff F (2019). In vivo contributions of astroglial GABA_B receptors to pathological network function in temporal lobe epilepsy. Young Glia meeting, Québec. (Oral presentation)
- Caudal LC**, Stopper G, Schweigmann M, Bedner P, Steinhäuser C, Scheller A and Kirchhoff F (2019). In vivo contributions of astroglial GABA_B receptors to pathological network function in temporal lobe epilepsy. XIV European Meeting on Glial Cells in Health and Disease, Porto. (Oral presentation)
- Caudal LC**, Stopper G, Kasakow CV, Scheller A and Kirchhoff F (2018). Contribution of glial transmitter receptors to pathological network function in mouse models of epilepsy. Young Glia meeting, Tokyo. (Poster presentation)
- Caudal LC**, Bai X, Schlosser L, Bohn CV, Stopper G, Schweigmann M, Scheller A and Kirchhoff F (2017). Contribution of glial transmitter receptors to pathological network function in mouse models of epilepsy. XIII European Meeting on Glial Cells in Health and Disease, Edinburgh. (Poster presentation)